DYNAMIC RESPONSE OF CIRCULAR PLATES SUBJECTED TO MOVING MASSIVE LOADS

Thesis by
Karl John Stahl

In Partial Fulfillment of the Requirements
for the Degree of
Doctor of Philosophy

California Institute of Technology
Pasadena, California
1971

(Submitted May 25, 1971)

ACKNOWLEDGEMENTS

The author wishes to express his sincere appreciation to Professor W. D. Iwan for his guidance and constant encouragement throughout this investigation. The assistance of the faculty in the Applied Mechanics Department is also gratefully appreciated.

The author is further indebted to the R. C. Baker Foundation, the Burroughs Corporation, the California Institute of Technology, the National Aeronautics and Space Administration, and the National Science Foundation for their financial aid.

The author also wishes to thank his wife, Patti, for her encouragement throughout the years of graduate study.

ABSTRACT

Techniques are presented for studying the dynamic response of circular disks excited by moving loads. The loading system, consisting of a mass, spring, and dashpot, travels in a circular path concentric with the disk at constant angular velocity. For cases involving elastically-supported rigid disks, the equations of motion for the disk and moving load may be written as a set of coupled Hill-Mathieu equations, typical of moving mass problems. By applying relatively simple transformations, the equations may be rewritten as a set of coupled linear differential equations with constant coefficients. The problem is then reduced to solving an ordinary eigenvalue problem.

When the eigenvalues are pure imaginary numbers, they correspond to the frequency components in the motion of the moving mass, and describe the disk motion as well. In certain regions the eigenvalues have positive real parts, corresponding to motions which are unbounded in time. There are three distinct regions of instability which appear in the rigid disk problem. A stiffness instability region occurs immediately above the critical speed of the disk, and is caused by load stiffness. At higher speeds, a region of instability due to modal coupling appears. Finally, if the load speed exceeds a certain terminal velocity (determined primarily by the mass of the load), an unstable solution will always exist.

The dynamic response of circular elastic disks with similar loading is investigated using the conventional eigenfunction expansion technique. The system of coupled Hill-Mathieu equations obtained by applying this method reduces to an ordinary eigenvalue problem when certain transformations are made. Thus, many modes may be included in the solution, although it is generally sufficient to consider only a few modes. Solutions to the eigenvalue problem reveal regions of instability directly analogous to those observed in the rigid disk examples.

TABLE OF CONTENTS

I. INTRODUCTION

The dynamic response of structures subjected to moving loads has been of interest to engineers and applied theoreticians for many years. Often, the load applied to a structure is due to a traveling mass, whose inertia is neglected for simplicity. There are clearly many problems of physical importance in which load inertia is not negligible and may alter the dynamic behavior of a system significantly. The mathematics describing the response of systems with moving massive loads involves equations which are sufficiently complex that many assumptions are generally made before a solution is attempted. One such assumption is that the velocity of the moving mass is much less than the critical velocities of the structure. This assumption is generally useful for the kinds of physical problems which have attracted interest in the past, but with the development of machinery operating at higher speeds, the assumption is often violated. The dynamics of such systems appears to be poorly understood.

In the computer industry, disk file memory units are often used for storage of large amounts of data when core storage space is insufficient and magnetic tape storage is too slow. A typical disk memory unit consists of a thin metal disk (circular plate), spinning at high speed, upon which data are recorded by means of a magnetic recording head.

Generally, an air bearing separates the recording head from the disk, and the head is fastened to a supporting frame by a spring restraint mount of some type. The stiffness of this restraint is kept low to decrease the transverse force applied to the disk if the disk deflects. Because the stiffness of the air bearing is much greater than that of the restraint, the displacement of the head can usually be assumed to be equal to the transverse deflection of the disk. In a reference frame fixed with respect to the spinning disk, the recording head would appear as a massive load moving around the disk in a circular path, with constant angular velocity equal to the disk rotation speed.

In many applications involving rotating machinery, it is desirable to achieve the highest possible speeds. In computer applications this corresponds to the highest possible information transfer rate. When rotation speeds approach the lowest critical speeds of the disk, the low speed assumption often made in moving mass problems must be abandoned.

Many types of rotating machinery involve structural interactions similar to those in disk memory systems. The effects of load inertia and stiffness are often involved in problems of this type. The analytic techniques necessary for understanding these effects are developed in this thesis. The class of problems dealt with here relates to the dynamics of stationary rigid and elastic disks subjected to mass-spring

loads traveling in concentric circular paths. By considering stationary disks, the complication of rotational inertia effects on the disk is eliminated. Thus, the problem is reduced to investigating the effects of the inertia and stiffness of the loading system.

The literature related to the free and forced vibration of circular plates is quite extensive, and the references cited should be considered as a representative sample of available literature, by no means complete. The most helpful in connection with this thesis are the papers by Southwell [1], McLeod and Bishop [2], and Weiner [3], as well as the numerous papers by Tobias [4]-[6]. Many of the techniques developed for the analysis of the vibration of circular plates are utilized within this thesis to study the effects of moving load inertia and stiffness. These techniques are primarily used in the chapters dealing with elastic disks, but have been valuable in providing insight into the rigid disk problems of the earlier chapters.

While there are some papers dealing with the response of circular plates subjected to moving forces, such as that by Weiner, there appears to be no literature regarding moving massive loads on circular plates. In fact, the literature on moving massive loads interacting with any structure is relatively sparse, although such problems have been of interest for many years.

Todhunter and Pearson[7] have documented the early history (pre-1900) of moving mass problems very well. These problems were motivated by fears of railway bridge failures due to the passage of heavy moving trains, and therefore were of considerable interest. Willis[8], in 1849, derived an approximate ordinary differential equation for the trajectory of a heavy particle traveling with constant velocity along a beam with negligible inertia. This equation was of sufficient difficulty that Willis felt compelled to request his friend G. G. Stokes[9] to undertake the analysis. Stokes was able to solve the equation by means of a convergent series, and thus provided a solution for the limiting case in which the mass of the load far exceeded the mass of the beam. Although valuable at the time, the inertia of most bridges could not really be considered negligible, and thus other investigators began to consider more complicated cases. The developments in the period 1850-1880 appear to be marred by numerous errors, which were rectified by Saint-Venant[10] in 1883. His analysis was based on Bernoulli-Euler beam theory as was the previous research, and followed a perturbation technique which was based on the assumption of relatively low velocity. This assumption was certainly valid for all physically meaningful problems of the time, and evidently was enough to satisfy bridge designers for the next 50 years, for further literature until 1934 appears very sparse.

In 1934 a book was written by C. E. Inglis [11], which presented a significant amount of material relating to the vibration of railway bridges, and including the most comprehensive study of the effects of load inertia until that time. The major assumption of Inglis was that the beam (as usual, a Bernoulli-Euler beam) vibrated in its fundamental mode shape, and thus the influence of higher modes was neglected. This assumption led to an ordinary differential equation with the complication of time-dependent coefficients, for which Inglis obtained an approximate solution in series form. The fundamental mode assumption has been utilized by others such as Piszczek [12], Bolotin [13], and Raske and Joung [14]. This assumption generally leads to Mathieu-Hill type equations which are known to possess regions of unstable solutions. [15] However, since higher modes are neglected in the analysis, it cannot be claimed that the system is actually unstable in such regions (note the word "possibility" in the title of Reference 12).

In order to avoid making single-mode assumptions, other authors [16], [17] have tried various forms of series solutions, and still others [18] proceed with a direct numerical integration approach. The disadvantage of these procedures is that it is difficult to make generalizations from the results of the analysis. It is interesting to note that despite the formidable problems encountered in the early

research, the trend in current research has been to complicate the problem by considering more complex loading systems (e. g., the vehicle structure of Reference 18, and the variable mass velocity of Reference 14) or to replace the simpler beam structure by a more complicated one (e. g., the orthotropic plate of Reference 17).

To develop methods for understanding the behavior of circular plates with traveling inertial loads, it is helpful to consider the simplest systems first. The problems studied in Chapters 2 and 3 involve elastically supported rigid disks subjected to moving mass-spring loads. The nonlinear equations of motion for these systems are derived using Lagrange's equations, and by suitable transformation are shown to be similar to the equations often derived using the fundamental mode assumption on elastic systems [12]-[14]. That is, they are of the Mathieu-Hill type, involving time-dependent coefficients. It is shown that a simple transformation can be made which reduces this set of coupled Mathieu-Hill equations to an equivalent set of equations with coefficients which are constant in time. Thus, the problem can be reformulated as an ordinary eigenvalue problem. An exact solution to the equations can be obtained, giving the frequencies of vibration for steady-state oscillations when the eigenvalues are pure imaginary, and indicating regions of unstable behavior when the eigenvalues have

positive real parts. In addition, the exact solution for transient motions can be obtained for any initial conditions of the system. No assumptions are necessary on mass ratios or load speed.

The solutions presented in Chapters 2 and 3 reveal that there are three distinct types of instability which occur in systems of this type. They are attributable to the inertia of the moving load, the stiffness of the load, and modal coupling. This information is helpful in understanding the more complicated behavior of elastic disks, discussed in detail in Chapters 4 and 5.

In the analysis of elastic disks in Chapters 4 and 5, the eigenfunction expansion technique commonly used by others [12], [14] is employed. By using the same transformation techniques as in Chapters 2 and 3, it is shown that the equations may be written as an equivalent set with constant coefficients. Thus, if the eigenfunction series is truncated, an ordinary eigenvalue problem is obtained. This permits a large number of modes to be used in the expansion if necessary. As many as 12 modes have been used in some examples, but generally far fewer modes are necessary to understand the disk behavior. If a one mode approximation is used, the equations reduce to those of Chapter 2, and if a two mode approximation is used, the equations resemble those of Chapter 3. Thus, understanding the behavior of the rigid disks in Chapters 2 and 3 is valuable in interpreting the results in the later chapters.

II. TWO DEGREE OF FREEDOM RIGID DISK

2.1 Introduction

The dynamic response of circular elastic plates subjected to moving massive loads involves the study of systems of coupled differential equations which are, in general, very complex. In order to understand the behavior of the solutions for systems of this type, it is helpful to begin with a mathematically simple case which retains the important physical features. The equations of motion describing the displacement of a rigid disk on an elastic foundation, subjected to a moving massive load, are of the same type as those found in elastic disk problems. The rigid disk equations, though highly nonlinear and with periodic coefficients, can be solved exactly using techniques that are directly applicable to the more complicated elastic disk equations. Further, the solutions to the rigid disk problems illustrate the same types of behavior encountered in the elastic disk problems, making it easier to understand the dynamic behavior of elastic disks.

In this chapter, the dynamic response of a two degree of freedom rigid disk subjected to a moving load consisting of a mass, spring, and dashpot will be studied. An exact solution for the problem is obtained by transforming the nonlinear equations of motion (having periodic coefficients) into an equivalent set of linear equations with

constant coefficients. The result is an ordinary eigenvalue problem, permitting the direct study of steady-state response, transient response, and stability.

2.2 Formulation of Equations of Motion

Consider the motion of a rigid disk, simply supported at the center and constrained against rotation about the z-axis as shown in Figure 1. The equilibrium position of the disk is in the horizontal plane, and the position of the disk at any time may be specified by the Euler angles α and β indicated in the figure. The angle α is the angle between the disk and the horizontal plane, and β is the angle between the x-axis ($\theta = 0°$) and the nodal diameter (sometimes called the line of nodes). Motion away from the equilibrium position is opposed by a restoring torque linear in α , and with no preferential direction in θ. This can be provided by several arrangements, one of which is the Winkler foundation, which provides a restoring force at a point proportional to the deflection of that point. If the angle α is small, the resultant torque provided by the Winkler foundation will be linear in α. The elastic foundation modulus k for the Winkler foundation has units $(F/L)/L^2$.

Defining $u(r, \theta, t)$ to be the deflection of the disk at the point (r, θ) and at the time t, the disk deflection for small α is:

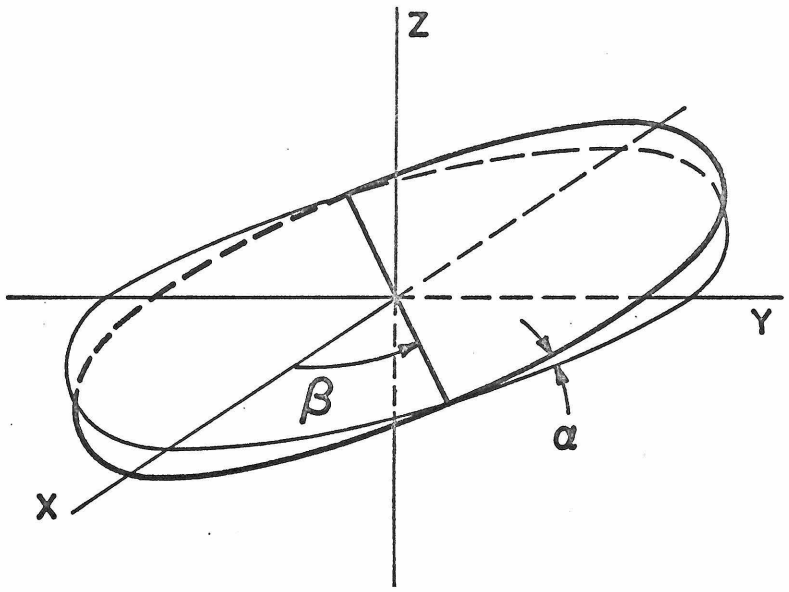

Fig. 1: Euler angles for the rigid circular disk.

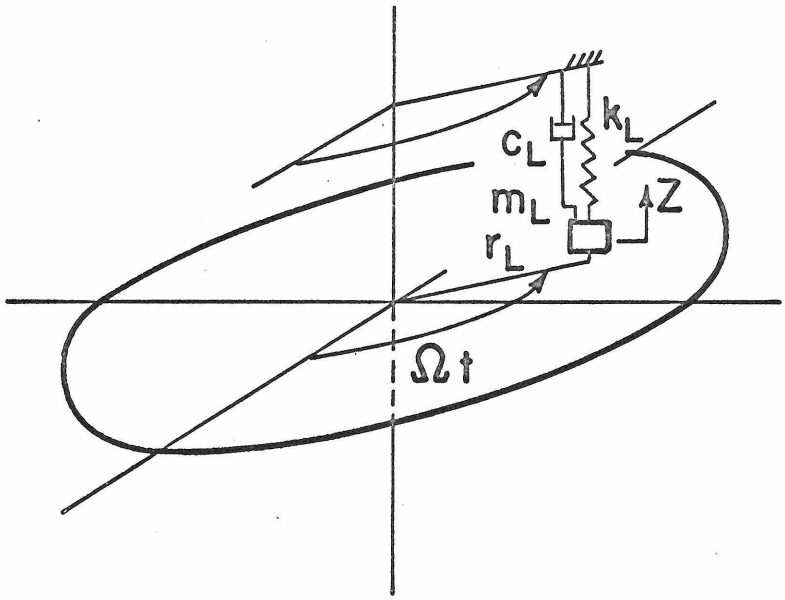

Fig. 2: Circular disk with moving load system

$$u(r, \theta, t) = r \cdot \alpha(t) \cdot \sin[\theta - \beta(t)] \tag{2.1}$$

The kinetic energy of the disk is given by:

$$T_D = \int_0^a \int_0^{2\pi} \frac{1}{2} \rho(2h) \cdot \left(\frac{\partial u}{\partial t}\right)^2 r\,dr\,d\theta \tag{2.2}$$

$$= \frac{1}{4}\pi\rho h a^4 \left[\dot{\alpha}^2 + \alpha^2 \dot{\beta}^2\right] \tag{2.3}$$

The potential energy of the foundation is:

$$V_D = \int_0^a \int_0^{2\pi} \frac{1}{2} k(u)^2 r\,dr\,d\theta \tag{2.4}$$

$$= \frac{1}{8}\pi k a^4 [\alpha^2] \tag{2.5}$$

Further, the foundation is assumed to include viscous dissipation c per unit area (units $\frac{F/(L/T)}{L^2}$), so that a dissipation function F_D may be defined as:

$$F_D = \int_0^a \int_0^{2\pi} \frac{1}{2} c \left(\frac{\partial u}{\partial t}\right)^2 r\,dr\,d\theta \tag{2.6}$$

$$= \frac{1}{8}\pi c a^4 \left[\dot{\alpha}^2 + \alpha^2 \dot{\beta}^2\right] \tag{2.7}$$

Attached to the disk, and moving around the disk with constant angular velocity Ω at fixed radius r_L, is a spring-mass-dashpot system as shown in Figure 2. The displacement of the mass, z(t), is

assumed to be equal to the deflection of the disk at the point $r = r_L$, $\theta = \Omega t$:

$$z(t) = \left[u(r, \theta, t)\right]\Big|_{\substack{r=r_L \\ \theta=\Omega t}} \tag{2.8}$$

Similarly, the velocity and acceleration of the mass are equal to the first and second total derivatives (sometimes called material derivatives) of the displacement at the point $r=r_L$, $\theta = \Omega t$:

$$\frac{dz}{dt} = \frac{d}{dt}\left\{\left[u(r,\theta,t)\right]\Big|_{\substack{r=r_L \\ \theta=\Omega t}}\right\} \tag{2.9}$$

$$= \left[\frac{\partial u}{\partial t} + \Omega\frac{\partial u}{\partial \theta}\right]\Big|_{\substack{r=r_L \\ \theta=\Omega t}} \tag{2.10}$$

$$\frac{d^2z}{dt^2} = \frac{d^2}{dt^2}\left\{\left[u(r,\theta,t)\right]\Big|_{\substack{r=r_L \\ \theta=\Omega t}}\right\} \tag{2.11}$$

$$= \left[\frac{\partial^2 u}{\partial t^2} + 2\Omega\frac{\partial^2 u}{\partial t\partial\theta} + \Omega^2\frac{\partial^2 u}{\partial\theta^2}\right]\Big|_{\substack{r=r_L \\ \theta=\Omega t}} \tag{2.12}$$

The kinetic energy of the load mass m_L is then:

$$T_L = \frac{1}{2}m_L\left(\frac{dz}{dt}\right)^2 \tag{2.13}$$

$$= \frac{1}{2}m_L\left[u_t(r_L, \Omega t, t) + \Omega u_\theta(r_L, \Omega t, t)\right]^2 \tag{2.14}$$

Substituting $u(r, \theta, t) = r\cdot\alpha(t)\cdot\sin(\theta - \beta(t))$, this becomes

$$T_L = \frac{1}{2}m_L r_L^2\left[\dot{\alpha}^2\sin^2(\Omega t-\beta) + \alpha^2(\Omega-\dot{\beta})^2\cos^2(\Omega t-\beta)\right. \tag{2.15}$$

$$+2\alpha\dot{\alpha}(\Omega-\dot{\beta})\sin(\Omega t-\beta)\cos(\Omega t-\beta)\Big]\Big\} \quad (2.15)\ \text{cont.}$$

The potential energy of the load spring (spring constant k_L) is:

$$V_L=\frac{1}{2}k_L z^2 \quad (2.16)$$

$$=\frac{1}{2}k_L\Big[u(r_L,\Omega t,t)\Big]^2 \quad (2.17)$$

$$=\frac{1}{2}k_L r_L^2\alpha^2\sin^2(\Omega t-\beta) \quad (2.18)$$

Finally, the dissipation function associated with the load dashpot (damping constant c_L) is:

$$F_L=\frac{1}{2}c_L\left(\frac{dz}{dt}\right)^2 \quad (2.19)$$

$$=\frac{1}{2}c_L\Big[u_t(r_L,\Omega t,t)+\Omega u_\theta(r_L,\Omega t,t)\Big]^2 \quad (2.20)$$

$$=\frac{1}{2}c_L\cdot r_L^2\Big[\dot{\alpha}^2\sin^2(\Omega t-\beta)+\alpha^2(\Omega-\dot{\beta})^2\cos^2(\Omega t-\beta) +2\alpha\dot{\alpha}(\Omega-\dot{\beta})\sin(\Omega t-\beta)\cos(\Omega t-\beta)\Big] \quad (2.21)$$

The Lagrangian and dissipation functions for the system consisting of the disk and moving spring, mass, and dashpot are:

$$L=T-V=(T_D+T_L)-(V_D+V_L) \quad (2.22)$$

$$F=F_D+F_L \quad (2.23)$$

where T_D, V_D and F_D are given by (2.3), (2.5), and (2.7) respectively, and T_L, V_L and F_L are given by (2.15), (2.18), and (2.21) respectively.

Using Lagrange's equations:

$$\frac{d}{dt}\frac{\partial L}{\partial \dot{q}_i} - \frac{\partial L}{\partial q_i} + \frac{\partial F}{\partial \dot{q}_i} = 0 \qquad (2.24)$$

where $q_1=\alpha$, $q_2=\beta$ represent the generalized coordinates of the problem, a set of two coupled nonlinear equations with periodic coefficients can be obtained. These are:

$$\begin{aligned}
&\ddot{\alpha} - \alpha\dot{\beta}^2 + p^2\alpha + \frac{c}{2\rho h}\dot{\alpha} + \Delta\frac{k_L}{M}\cdot\alpha\cdot\sin^2(\Omega t-\beta) \\
&+\Delta\frac{m_L}{M}\Big\{\Big[\ddot{\alpha} - \alpha(\Omega-\dot{\beta})^2\Big]\sin^2(\Omega t-\beta) \\
&\qquad +\Big[2\dot{\alpha}(\Omega-\dot{\beta}) - \alpha\ddot{\beta}\Big]\sin(\Omega t-\beta)\cos(\Omega t-\beta)\Big\} \\
&+\Delta\frac{c_L}{M}\Big\{\dot{\alpha}\sin^2(\Omega t-\beta) + (\Omega-\dot{\beta})\alpha\sin(\Omega t-\beta)\cos(\Omega t-\beta)\Big\} = 0
\end{aligned} \qquad (2.25)$$

$$\begin{aligned}
&\alpha^2\ddot{\beta} + 2\alpha\dot{\alpha}\dot{\beta} + \frac{c}{2\rho h}\alpha^2\dot{\beta} - \Delta\frac{k_L}{M}\alpha^2\sin(\Omega t-\beta)\cos(\Omega t-\beta) \\
&+\Delta\frac{m_L}{M}\Big\{\Big[\alpha^2\ddot{\beta} - 2\alpha\dot{\alpha}(\Omega-\dot{\beta})\Big]\cos^2(\Omega t-\beta) \\
&\qquad +\Big[\alpha^2(\Omega-\dot{\beta})^2 - \alpha\ddot{\alpha}\Big]\sin(\Omega t-\beta)\cos(\Omega t-\beta)\Big\} \\
&-\Delta\frac{c_L}{M}\Big\{\alpha^2(\Omega-\dot{\beta})\cos^2(\Omega t-\beta) + \alpha\dot{\alpha}\sin(\Omega t-\beta)\cos(\Omega t-\beta)\Big\} = 0
\end{aligned} \qquad (2.26)$$

where

$$\Delta = \left(\frac{2r_L}{a}\right)^2 \quad , \quad M = 2\rho h \pi a^2, \; p^2 = \frac{k}{2\rho h} \tag{2.27}$$

Equations (2.25) and (2.26) are coupled second-order nonlinear differential equations for $\alpha(t)$ and $\beta(t)$, having time-dependent coefficients. The equations may be transformed to a linear set of equations by introducing time-dependent functions C(t) and D(t) related to $\alpha(t)$ and $\beta(t)$ by:

$$\begin{aligned} C(t) &= -\alpha(t)\,\sin\beta(t) \\ D(t) &= \alpha(t)\cos\beta(t) \end{aligned} \tag{2.28}$$

The corresponding inverse transformations are:

$$\begin{aligned} \alpha^2(t) &= C^2(t) + D^2(t) \\ \beta(t) &= \mathrm{Tan}^{-1}\left[\frac{-C(t)}{D(t)}\right] \end{aligned} \tag{2.29}$$

Using these relations, a set of coupled second-order linear differential equations are found for C(t) and D(t), still having time-dependent periodic coefficients. The new equations are:

$$\left.\begin{aligned} &\left[\left(1+\Delta\frac{m_L}{2M}\right)+\Delta\frac{m_L}{2M}\cos 2\Omega t\right]\ddot{C} + \left[\Delta\frac{m_L}{2M}\sin 2\Omega t\right]\ddot{D} \\ &+\left[\left(\frac{c}{2\rho h}+\Delta\frac{c_L}{2M}\right)+\Delta\frac{c_L}{2M}\cos 2\Omega t - 2\Omega\Delta\frac{m_L}{2M}\sin 2\Omega t\right]\dot{C} \\ &+\left[\left(2\Omega\Delta\frac{m_L}{2M}\right)+2\Omega\Delta\frac{m_L}{2M}\cos 2\Omega t+\Delta\frac{c_L}{2M}\sin 2\Omega t\right]\dot{D} \end{aligned}\right\} \tag{2.30}$$

$$+\left[\left(p^2+\Delta\frac{k_L}{2M}-\Omega^2\Delta\frac{m_L}{2M}\right)+\left(\Delta\frac{k_L}{2M}-\Omega^2\Delta\frac{m_L}{2M}\right)\cos 2\Omega t - \Omega\Delta\frac{c_L}{2M}\sin 2\Omega t\right] C$$

$$+\left[\left(\Omega\Delta\frac{c_L}{2M}\right)+\left(\Omega\Delta\frac{c_L}{2M}\right)\cos 2\Omega t+\left(\Delta\frac{k_L}{2M}-\Omega^2\Delta\frac{m_L}{2M}\right)\sin 2\Omega t\right]D=0 \Bigg\} \text{(2.30) cont.}$$

$$\left[\Delta\frac{m_L}{2M}\sin 2\Omega t\right]\ddot{C}+\left[\left(1+\Delta\frac{m_L}{2M}\right)-\Delta\frac{m_L}{2M}\cos 2\Omega t\right]\ddot{D}$$

$$+\left[\left(-2\Omega\Delta\frac{m_L}{2M}\right)+2\Omega\Delta\frac{m_L}{2M}\cos 2\Omega t+\Delta\frac{c_L}{2M}\sin 2\Omega t\right]\dot{C}$$

$$+\left[\left(\frac{c}{2\rho h}+\Delta\frac{c_L}{2M}\right)-\Delta\frac{c_L}{2M}\cos 2\Omega t+2\Omega\Delta\frac{m_L}{2M}\sin 2\Omega t\right]\dot{D} \qquad (2.31)$$

$$+\left[\left(-\Omega\Delta\frac{c_L}{2M}\right)+\Omega\Delta\frac{c_L}{2M}\cos 2\Omega t+\left(\Delta\frac{k_L}{2M}-\Omega^2\Delta\frac{m_L}{2M}\right)\sin 2\Omega t\right]C$$

$$+\left[\left(p^2+\Delta\frac{k_L}{2M}-\Omega^2\Delta\frac{m_L}{2M}\right)-\left(\Delta\frac{k_L}{2M}-\Omega^2\Delta\frac{m_L}{2M}\right)\cos 2\Omega t+\Omega\Delta\frac{c_L}{2M}\sin 2\Omega t\right]D=0$$

The transformation (2.28) is equivalent to writing the deflection $u(r,\theta,t)$ as $u(r,\theta,t)=r\cdot\left[C(t)\cos\theta+D(t)\sin\theta\right]$, rewriting the Lagrangian L and dissipation function F as functions of C and D, and using Lagrange's equations to deduce equations for C(t) and D(t). The result of this procedure is of course the same as by the direct transformation (2.28), namely, equations (2.30) and (2.31).

Equations (2.30) and (2.31) are coupled equations of the Hill-Mathieu type, similar to equations that are encountered in other moving mass problems. Usually, in problems having a fixed boundary, only one of the two equations (2.30) or (2.31) is obtained. Such would be the case here if the line of nodes were fixed; in that event, C(t) would vanish and only one equation would result for D(t). Remarkably,

the coupled set of equations is more readily solved than one equation alone. In fact, by making one more transformation an exact solution to this problem may be found. Let A(t) and B(t) be related to C(t) and D(t) by:

$$\begin{aligned} A(t) &= C(t)\cos\Omega t + D(t)\sin\Omega t \\ B(t) &= -C(t)\sin\Omega t + D(t)\cos\Omega t \end{aligned} \tag{2.32}$$

with the inverse relations:

$$\begin{aligned} C(t) &= A(t)\cos\Omega t - B(t)\sin\Omega t \\ D(t) &= A(t)\sin\Omega t + B(t)\cos\Omega t \end{aligned} \tag{2.33}$$

Making use of this transformation gives the following coupled second-order linear differential equations for A(t) and B(t). Note that the coefficients are now all constant in time:

$$\left(1+\Delta\frac{m_L}{M}\right)\ddot{A}+\left(\frac{c}{2\rho h}+\Delta\frac{c_L}{M}\right)\dot{A}-2\Omega\dot{B}+\left(p^2+\Delta\frac{k_L}{M}-\Omega^2\right)A-\frac{c}{2\rho h}\Omega B=0 \tag{2.34}$$

$$\ddot{B}+2\Omega\dot{A}+\frac{c}{2\rho h}\dot{B}+\frac{c}{2\rho h}\Omega A+\left(p^2-\Omega^2\right)B=0 \tag{2.35}$$

This transformation corresponds to a change from a fixed reference frame to a reference frame rotating with angular velocity Ω. In the rotating frame, the disk reflection will be $u'(r, \Phi, t) = r\cdot\left[A(t)\cos\Phi + B(t)\sin\Phi\right]$, where $\Phi = \theta - \Omega t$. Thus in the rotating frame the angular position of the moving mass is a constant, at $\Phi = 0$. Equations (2.34) and (2.35) can be derived by writing the Lagrangian

in the rotating frame, but some care must be taken when using this method, since $\frac{\partial u'}{\partial t}(r, \Phi, t)$ no longer gives the actual velocity of the disk at the point (r, Φ). This is due to the fact Φ depends on time, and thus the point r = constant, Φ = constant in the rotating frame does not correspond to a fixed mass point of the disk.

Since the equations for A(t) and B(t) have constant coefficients, conventional methods may be used to solve for A(t) and B(t). The inverse transformations (2. 33) and (2. 29) may then be used to determine $\alpha(t)$ and $\beta(t)$ exactly. First, Equations (2. 34) and (2. 35) may be written in dimensionless form as follows:

$$\tau = pt \ , \ \bar{m} = \frac{m_L}{M} \ , \ \bar{k} = \frac{1}{p^2} \cdot \frac{k_L}{M}$$

$$\bar{c}_L = \frac{1}{p} \frac{c_L}{M} \ , \ \bar{c} = \frac{1}{p} \cdot \frac{c}{2\rho h} \ , \ \bar{s} = \frac{\Omega}{p} \qquad (2.36)$$

With the above substitutions, Equations (2. 34) and (2. 35) become:

$$(1+\Delta\bar{m})\frac{d^2A}{d\tau^2} + \left(\bar{c} + \Delta\bar{c}_L\right)\frac{dA}{d\tau} - 2\bar{s}\frac{dB}{d\tau} + \left(1 + \Delta\bar{k} - \bar{s}^2\right)A - \bar{s}\bar{c}B = 0 \qquad (2.37)$$

$$\frac{d^2B}{d\tau^2} + 2\bar{s}\frac{dA}{d\tau} + \bar{c}\frac{dB}{d\tau} + \bar{s}\bar{c}A + \left(1 - \bar{s}^2\right)B = 0 \qquad (2.38)$$

2.3 Solution of the Equations of Motion

Equations (2.37) and (2.38) may be rewritten as a matrix differential equation as follows:

$$P\frac{d\underline{x}}{d\tau} = Q\underline{x} \quad , \quad \underline{x}(0) = \underline{f} \tag{2.39}$$

where $\underline{x}$ is a four element column vector and P and Q are four by four matrices:

$$\underline{x} = \begin{Bmatrix} A \\ B \\ \frac{dA}{d\tau} \\ \frac{dB}{d\tau} \end{Bmatrix} \qquad P = \begin{bmatrix} 1 & 0 & 0 & 0 \\ 0 & 1 & 0 & 0 \\ 0 & 0 & 1+\Delta\bar{m} & 0 \\ 0 & 0 & 0 & 1 \end{bmatrix} \tag{2.40}$$

$$Q = \begin{bmatrix} 0 & 0 & 1 & 0 \\ 0 & 0 & 0 & 1 \\ -(1+\Delta\bar{k}-\bar{s}^2) & \bar{s}\,\bar{c} & -(\bar{c}+\Delta\bar{c}_L) & 2\bar{s} \\ -\bar{s}\,\bar{c} & -(1-\bar{s}^2) & -2\bar{s} & -\bar{c} \end{bmatrix}$$

Premultiplying by P^{-1}, the first of Equations (2.39) becomes:

$$\frac{d\underline{x}}{dt} = P^{-1}Q\underline{x} \tag{2.41}$$

Assuming a solution of the form

$$\underline{x} = e^{\lambda\tau}\underline{\Phi} \tag{2.42}$$

where $\underline{\Phi}$ is a constant vector, (2.41) becomes:

$$(P^{-1}Q-\lambda I)\underline{\Phi} = 0 \tag{2.43}$$

For a nontrivial solution, the determinant of $(P^{-1}Q-\lambda I)$ must vanish:

$$|P^{-1}Q-\lambda I| = 0$$

$$\begin{vmatrix} -\lambda & 0 & 1 & 0 \\ 0 & -\lambda & 0 & 1 \\ -\frac{1+\Delta\bar{k}-\bar{s}^2}{1+\Delta\bar{m}} & \frac{\bar{s}\,\bar{c}}{1+\Delta\bar{m}} & -\frac{\bar{c}+\Delta\bar{c}_L}{1+\Delta\bar{m}}-\lambda & \frac{2\,\bar{s}}{1+\Delta\bar{m}} \\ -\bar{s}\,\bar{c} & -(1-\bar{s}^2) & -2\,\bar{s} & -\bar{c}-\lambda \end{vmatrix} = 0 \tag{2.44}$$

Expanding this determinant, a fourth order polynomical for λ is obtained:

$$a_0+a_1\lambda+a_2\lambda^2+a_3\lambda^3+a_4\lambda^4 = 0$$

$$\begin{aligned} a_0 &= (1-\bar{s}^2)(1+\Delta\bar{k}-\bar{s}^2)+\bar{s}^2\bar{c}^2 \\ a_1 &= (2\bar{c}+\Delta\bar{c}_L)+(2\bar{c}-\Delta\bar{c}_L)\bar{s}^2+\Delta\bar{c}\,\bar{k} \\ a_2 &= (2+\Delta\bar{m})+(2-\Delta\bar{m})\bar{s}^2+\Delta\bar{k}+\bar{c}(\bar{c}+\Delta\bar{c}_L) \\ a_3 &= (2+\Delta\bar{m})\bar{c}+\Delta\bar{c}_L \\ a_4 &= 1+\Delta\bar{m} \end{aligned} \tag{2.45}$$

2.4 Properties of the Solution of the Undamped Equations of Motion

When there is no foundation damping and no load dashpot ($\bar{c}=\bar{c}_L=0$), the fourth order equation for λ becomes a biquadratic equation, from which an exact analytic expression for λ^2 may be obtained. The polynomial in λ becomes:

$$(1+\Delta\bar{m})\lambda^4+\left[(2+\Delta\bar{m})+(2-\Delta\bar{m})\bar{s}^2+\Delta k\right]\lambda^2+(1-\bar{s}^2)(1+\Delta\bar{k}-\bar{s}^2)=0 \qquad (2.46)$$

This equation may be solved for λ^2 to give:

$$\lambda^2=-\frac{1}{2(1+\Delta\bar{m})}\left[(2+\Delta\bar{m})+\Delta\bar{k}+(2-\Delta\bar{m})\bar{s}^2\right] \qquad (2.47)$$
$$\pm\frac{1}{2(1+\Delta\bar{m})}\left\{\left[(2+\Delta\bar{m})+\Delta\bar{k}+(2-\Delta\bar{m})\bar{s}^2\right]^2-4(1+\Delta\bar{m})(1-\bar{s}^2)(1+\Delta\bar{k}-\bar{s}^2)\right\}^{\frac{1}{2}}$$

Case 1: $\bar{m}=\bar{k}=\bar{c}=\bar{c}_L=0$

This corresponds to the free vibration of the disk alone, with no attached spring or mass. In this case, Equation (2.47) reduces to:

$$\lambda^2=-(1+\bar{s})^2 \quad , \quad -(1-\bar{s})^2 \qquad (2.48)$$

$$\Rightarrow \quad \lambda=\pm i(1+\bar{s}) \quad , \quad \pm i(1-\bar{s}) \qquad (2.49)$$

Corresponding to these four eigenvalues are the four complex eigenvectors given below:

(2.50)

$$\underline{x}_1=\begin{Bmatrix}-1\\-i\\-i(1+\bar{s})\\1+\bar{s}\end{Bmatrix} \quad \underline{x}_2=\begin{Bmatrix}-1\\i\\i(1+\bar{s})\\1+\bar{s}\end{Bmatrix} \quad \underline{x}_3=\begin{Bmatrix}1\\-i\\i(1-\bar{s})\\1-\bar{s}\end{Bmatrix} \quad \underline{x}_4=\begin{Bmatrix}1\\i\\-i(1-\bar{s})\\1-\bar{s}\end{Bmatrix}$$

The above eigenvectors (which have not been normalized) are orthogonal by the usual definition of complex inner product. That is,

$$(\underline{x}_i, \underline{\tilde{x}}_j) = 0 \quad \text{if } i \neq j \tag{2.51}$$

where $\underline{\tilde{x}}_j$ denotes the complex conjugate of the vector $\underline{x}_j$.

The general solution will be of the form:

$$\begin{aligned} \underline{x}(\tau) = c_1 e^{i(1+\bar{s})\tau} \underline{x}_1 + c_2 e^{-i(1+\bar{s})\tau} \underline{x}_2 \\ + c_3 e^{i(1-\bar{s})\tau} \underline{x}_3 + c_4 e^{-i(1-\bar{s})\tau} \underline{x}_4 \end{aligned} \tag{2.52}$$

where the constants c_1, c_2, c_3, and c_4 are complex. It can be shown that if $\underline{x}(\tau)$ satisfies a real initial condition $\underline{x}(0) = \underline{f}$, where f_1, f_2, f_3 and f_4 are real constants, then $c_1 = \tilde{c}_2$, and $c_3 = \tilde{c}_4$. Further, $\underline{x}(\tau)$ will then be real for all τ. The constants c_i may be written:

$$\begin{aligned} c_1 &= d_1 + id_2 \quad , \quad c_3 = d_3 + id_4 \\ c_2 &= d_1 - id_2 \quad , \quad c_4 = d_3 - id_4 \end{aligned} \tag{2.53}$$

The expression for $\underline{x}(\tau)$ may then be written in real form as:

$$\underline{x}(\tau) = 2d_1 \underline{r}_1(\tau) + 2d_2 \underline{r}_2(\tau) + 2d_3 \underline{r}_3(\tau) + 2d_4 \underline{r}_4(\tau)$$

where:

$$\underline{r}_1(\tau) = \begin{Bmatrix} -\cos(1+\bar{s})\tau \\ \sin(1+\bar{s})\tau \\ (1+\bar{s})\sin(1+\bar{s})\tau \\ (1+\bar{s})\cos(1+\bar{s})\tau \end{Bmatrix} \quad , \quad \underline{r}_2(\tau) = \begin{Bmatrix} \sin(1+\bar{s})\tau \\ \cos(1+\bar{s})\tau \\ (1+\bar{s})\cos(1+\bar{s})\tau \\ -(1+\bar{s})\sin(1+\bar{s})\tau \end{Bmatrix}$$

$$\underline{r}_3(\tau)=\begin{Bmatrix}\cos(1-\bar{s})\tau\\ \sin(1-\bar{s})\tau\\ -(1-\bar{s})\sin(1-\bar{s})\tau\\ (1-\bar{s})\cos(1-\bar{s})\tau\end{Bmatrix},\quad \underline{r}_4(\tau)=\begin{Bmatrix}-\sin(1-\bar{s})\tau\\ \cos(1-\bar{s})\tau\\ -(1-\bar{s})\cos(1-\bar{s})\tau\\ -(1-\bar{s})\sin(1-\bar{s})\tau\end{Bmatrix} \tag{2.54}$$

In the discussion following Equation (2.35), it was pointed out that the transformation to the $A(\tau)$ and $B(\tau)$ coordinates corresponds to a transformation into a reference frame rotating with constant angular velocity Ω (corresponding to dimensionless angular velocity $\bar{s}$). With this in mind, some physical meaning can be attached to the eigenvalues and eigenvectors given by (2.49) and (2.54). Returning to the coordinates $\alpha(\tau)$ and $\beta(\tau)$, the normalized forms of the nonlinear differential equations (2.25) and (2.26) for the case $\Delta\bar{k}=\Delta\bar{m}=\bar{c}_L=\bar{c}=0$ are:

$$\frac{d^2\alpha}{d\tau^2}-\alpha\left(\frac{d\beta}{d\tau}\right)^2+\alpha=0 \tag{2.55}$$

$$\alpha^2\frac{d^2\beta}{d\tau^2}+2\alpha\frac{d\alpha}{d\tau}\frac{d\beta}{d\tau}=0 \tag{2.56}$$

Several solutions to Equations (2.55) and (2.56) may be found by inspection. If $\beta(\tau)=\beta_0$ is independent of time, (2.56) is immediately satisfied and (2.55) becomes

$$\frac{d^2\alpha}{d\tau^2}+\alpha=0 \tag{2.57}$$

Thus, one solution of the equations of motion is:

$$u(r,\theta,t) = r\cdot\alpha(t)\sin[\theta-\beta(t)]$$

$$= r\cdot\alpha_0\cos pt\cdot\sin(\theta-\beta_0) \qquad (2.58)$$

because $\tau = pt$. Physically, this is a harmonic oscillation of the disk about a nodal diameter whose position is $\theta = \beta_0$. The frequency of the oscillation is p.

A second solution can be obtained when $\alpha(\tau)=\alpha_0$ is a constant, and when $\beta(\tau)$ is a linear function of τ, so that $\frac{d^2\beta}{d\tau^2}$ vanishes. Again (2.56) is immediately satisfied, and (2.55) becomes:

$$\left(\frac{d\beta}{d\tau}\right)^2 = 1 \rightarrow \frac{d\beta}{d\tau} = \pm 1 \rightarrow \beta(\tau) = \tau \qquad (2.59)$$

Thus, other possible motions of the disk are:

$$u(r,\theta,t) = r\cdot\alpha_1\cdot\sin(\theta\pm pt) \qquad (2.60)$$

When the positive sign is chosen, the solution (2.60) corresponds to a wave (or wobbling) motion with a fixed angle to the horizontal, and a nodal diameter position given by $\theta = -pt$. The wave motion is then in the negative θ direction with angular velocity -p and is denoted as a backward traveling wave. When the negative sign in Equation (2.60) is chosen, the solution is a wave traveling in the positive θ direction with angular velocity +p and is denoted as a forward traveling wave. It is easy to show that when the forward and backward waves

given by (2.60) are superposed, the resulting motion is simply an oscillation about a fixed nodal diameter, given by Equation (2.58) with $\alpha_0 = 2\alpha_1$ and $\beta_0 = 0$.

If the wave motions (2.60) are viewed from a reference frame rotating with respect to the disk at a constant angular velocity Ω in the positive θ direction, the observed wave velocities will change. If Ω is less than p, the forward traveling wave will appear slowed down and will have velocity $p - \Omega$ in the rotating frame, whereas the backward traveling wave will appear speeded up and will have velocity $-p - \Omega$. The frequencies of vibration of a point fixed in the rotating frame will be $p - \Omega$ and $p + \Omega$ for the forward and backward waves, respectively. In normalized notation, the frequencies are divided by p to obtain $1-\bar{s}$ and $1+\bar{s}$ respectively, corresponding to the eigenvalues given in (2.49) and also as the frequencies in equation (2.54).

If the rotating frame angular velocity Ω is exactly equal to the wave velocity p, the forward traveling wave will appear to be stationary. This condition is known as the "critical speed" of the disk. A constant force traveling around the disk at this velocity will cause unbounded response.

If Ω is greater than p, the forward traveling wave appears with velocity $p - \Omega < 0$. Thus, the rotating frame is moving faster than the

forward wave. The observed frequencies of vibration of a point fixed in the rotating frame are given by $\Omega - p$ and $p + \Omega$ for the forward and backward traveling waves, respectively. These results are summarized in Figure 3, which is the so-called "frequency-speed" plot for the disk, giving the observed frequencies as a function of speed.

The time-dependent vectors $\underline{r}_1(\tau)$ and $\underline{r}_2(\tau)$ given by (2.54) are backward traveling waves, having nodal diameters located at $\theta = \pi/2$ and $\theta = 0$ at time $t=0$. Similarly, the vectors $\underline{r}_3(\tau)$ and $\underline{r}_4(\tau)$ given by (2.54) are forward traveling waves, having nodal diameters located at $\theta = \pi/2$ and $\theta = 0$ at $t=0$. The general solution to any initial value problem will be a linear combination of these four vectors.

Case 2: $\bar{m} \neq 0$, $\bar{k} \neq 0$, $\bar{c} = \bar{c}_L = 0$

For the case of an attached spring and mass, the expression for the eigenvalues is (repeating (2.47)):

$$\lambda^2 = -\frac{1}{2(1+\Delta\bar{m})}\left[(2+\Delta\bar{m})+\Delta\bar{k}+(2-\Delta\bar{m})\bar{s}^2\right] \pm \frac{1}{2(1+\Delta\bar{m})}\left\{\left[(2+\Delta\bar{m})+\Delta\bar{k}+(2-\Delta\bar{m})\bar{s}^2\right]^2 - 4(1+\Delta\bar{m})(1-\bar{s}^2)(1+\Delta\bar{k}-\bar{s}^2)\right\}^{\frac{1}{2}} \tag{2.47}$$

When the normalized load velocity $\bar{s}$ is zero, the expression for λ^2 becomes:

$$\lambda^2 = -1, -\frac{1+\Delta\bar{k}}{1+\Delta\bar{m}} \tag{2.61}$$

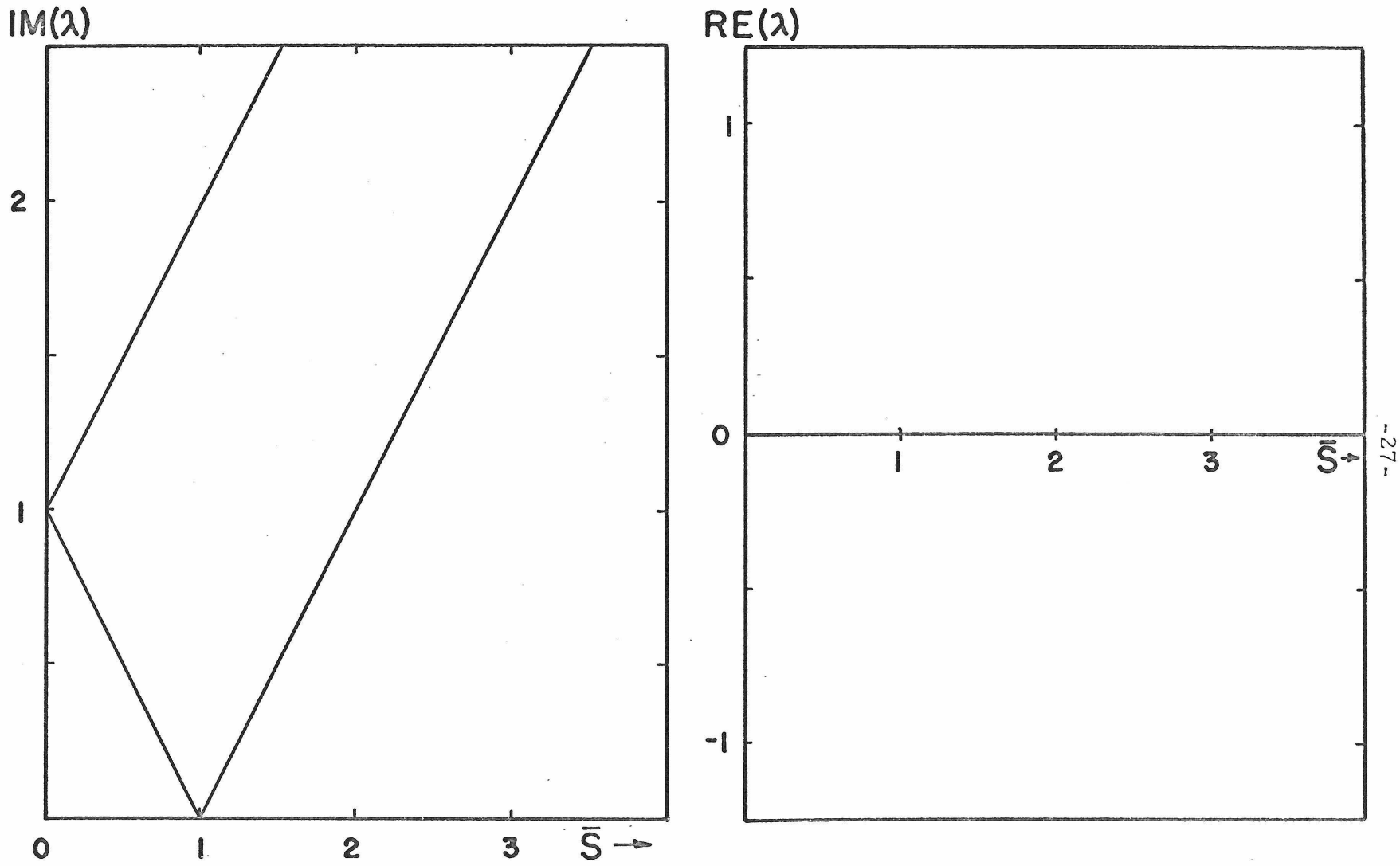

Fig. 3: Frequency-speed diagram for the disk alone $(\bar{m} = \bar{k} = \bar{c} = \bar{c}_L = 0)$.

The equations of motion for this case are very simple. Equations (2. 37) and (2. 38) uncouple for $\bar{s} = 0$, giving one equation for $B(\tau)$ and one for $A(\tau)$, with frequencies given by the first and second of (2. 61) respectively. For $\bar{s} = 0$, Equations (2. 33) show that $C(\tau) = A(\tau)$ and $D(\tau) = B(\tau)$. Further, Equations (2. 29) then imply that

$$\alpha^2(\tau) = C^2(\tau) + D^2(\tau) = A^2(\tau) + B^2(\tau)$$

$$\beta(\tau) = \mathrm{Tan}^{-1}\left[\frac{-C(\tau)}{D(\tau)}\right] = \mathrm{Tan}^{-1}\left[\frac{-A(\tau)}{B(\tau)}\right] \qquad (2.62)$$

Thus, when $\lambda^2 = -1$, or $\lambda = \pm i$, $B(\tau)$ will be nonzero but $A(\tau)$ will vanish. Then $\alpha(\tau)$ will have frequency 1 in the τ domain (frequency p in the t domain) and $\beta(\tau)$ will be zero. In other words, the attached spring-mass will be sitting on the nodal diameter and will have no effect on the disk frequency in this position.

The second eigenvalue corresponds to the case when the mass lies on a diameter perpendicular to the nodal diameter. Whether this frequency is greater than or less than 1 depends on the parameters $\Delta\bar{k}$ and $\Delta\bar{m}$. The analytic expression for this frequency may be easily verified by elementary methods.

For load speeds $0 \leq \bar{s} < 1$, an analysis of Equation (2. 47) reveals that since $4(1+\Delta\bar{m})(1-\bar{s}^2)(1+\Delta\bar{k}-\bar{s}^2) > 0$, the term under the radical sign will be less than the first quantity in (2. 47). Therefore, whichever sign is chosen in (2. 47), the resulting values of λ^2 will both be

negative, and hence all values of λ will be pure imaginary. The solution in the $A(\tau)$ and $B(\tau)$ coordinates will be simple linear combinations of the two frequencies, resulting in oscillatory behavior. The transformations to $C(\tau)$, $D(\tau)$ and $\alpha(\tau), \beta(\tau)$ give very complicated motions which will be discussed in greater detail in later sections. If the two values of λ^2 are denoted as $-\omega_L^2$ and $-\omega_u^2$ (the lower and upper frequencies) the general solution to the eigenvalue problem, analogous to Equation (2.52) is:

$$\underline{x}(\tau)=c_1 e^{i\omega_L \tau}\underline{x}_1+c_2 e^{-i\omega_L \tau}\underline{x}_2 + c_3 e^{i\omega_u \tau}\underline{x}_3+c_4 e^{-i\omega_u \tau}\underline{x}_4 \qquad (2.63)$$

where the constants c_1, c_2, c_3 and c_4 are complex. The new eigenvectors $\underline{x}_1, \underline{x}_2, \underline{x}_3$, and $\underline{x}_4$ correspond to the eigenvalues $i\omega_L$, $-i\omega_L$, $i\omega_u$, and $-i\omega_u$ respectively.

When $\bar{s}=1$, the lower of the two frequencies, ω_u, becomes zero. Then the $A(\tau)$ and $B(\tau)$ corresponding to this eigenvalue are constants. An inspection of the Equations of motion (2.37) and (2.38) reveals that (2.37) will be satisfied only if $A(\tau) = 0$, and that (2.38) will be satisfied if $B(\tau) = B_0$ is an arbitrary constant. Since the motion as viewed from the rotating frame has the form $u'(r, \Phi, t) = \left[A(t)\cos\Phi + B(t)\sin\Phi\right]$ where $\Phi = \theta - \Omega t$, this means that the spring and mass are riding on the nodal diameter of the forward traveling wave,

which appears stationary at $\Phi = 0$ in the rotating frame.

Immediately above the critical speed $\bar{s} = 1$, the nature of the solution will change considerably. Referring to the expression for λ^2, Equation (2.47), note that when the speed $\bar{s}$ lies in the range:

$$1 < \bar{s}^2 < 1 + \Delta\bar{k}, \tag{2.64}$$

the quantity $4(1+\Delta\bar{m})(1-\bar{s}^2)(1+\Delta\bar{k}-\bar{s}^2)$ will be negative. Thus, one value of λ^2 will be negative, but the other will be positive. That is, in this region the eigenvalues and solution of the problem are:

$$\lambda = \pm\mu, \pm i\omega_u \tag{2.65}$$

$$\underline{x}(\tau) = c_1 e^{\mu\tau}\underline{x}_1 + c_2 e^{-\mu\tau}\underline{x}_2 + c_3 e^{i\omega_u\tau}\underline{x}_3 + c_4 e^{-i\omega_u\tau}\underline{x}_4 \tag{2.66}$$

Thus, depending on initial conditions, the solution may be either oscillatory, exponentially decaying, exponentially growing or a combination of these. Because of the possibility of unbounded solutions on this region, and due to the fact that the region boundaries given by (2.64) depend only on the stiffness of the attached spring and not on the attached mass, this zone will be referred to as the "stiffness instability region". Note that as $\bar{k} \to 0$, the width of this region tends toward zero.

When $1 + \Delta\bar{k} < \bar{s}^2 < (\bar{s}^*)^2$, where $\bar{s}^*$ will be defined shortly, the

nature of the solution is much like that of the subcritical zone, with pure imaginary values of λ and hence oscillatory motion. The general solution in this region is of the type given by (2.63), although the eigenvectors are of course not the same.

As the load speed $\bar{s}$ continues to increase, there will be one more major change in the disk response. Equation (2.47) can be rearranged as:

$$\lambda^2 = \frac{-1}{2(1+\Delta\bar{m})}\cdot\left[(2+\Delta\bar{m})+\Delta\bar{k}+(2-\Delta\bar{m})\bar{s}^2\right] \pm \frac{1}{2(1+\Delta\bar{m})}\left\{\left[\Delta\bar{m}-\Delta\bar{k}\right]^2+\bar{s}^2\left[(16+8\Delta\bar{m}-2\Delta^2\bar{m}^2)+(8+2\Delta\bar{m})\Delta\bar{k}\right] - \bar{s}^4\left[\Delta\bar{m}(8-\Delta\bar{m})\right]\right\}^{\frac{1}{2}} \quad (2.67)$$

Hence, if $\Delta\bar{m} < 8$ (which is the case if the attached mass is no more than double the disk mass), the quantity under the radical sign will become negative for load speeds $\bar{s} > \bar{s}^*$. Thus, for speeds $\bar{s} > \bar{s}^*$, the values of λ^2 will be complex conjugates. The four corresponding values of λ are then:

$$\lambda = i\omega+\mu,\ i\omega-\mu,\ -i\omega+\mu,\ -i\omega-\mu \quad (2.68)$$

The general solution will then be of the form:

$$\underline{x}(\tau) = c_1 e^{\mu\tau} e^{i\omega\tau}\underline{x}_1 + c_2 e^{\mu t} e^{-i\omega\tau}\underline{x}_2 \quad (2.69)$$

$$+c_3 e^{-\mu\tau} e^{i\omega\tau} \underline{x}_3 + c_4 e^{-\mu\tau} e^{-i\omega\tau} \underline{x}_4 \Bigg\} \quad (2.69)\ \text{cont.}$$

where $\underline{x}_1, \underline{x}_2, \underline{x}_3$, and $\underline{x}_4$ are the corresponding eigenvectors. Solutions in this region are therefore oscillatory with a growing or decaying exponential envelope. The initial conditions determine whether or not the motion becomes unbounded in time. The region $\bar{s} > \bar{s}^*$ will be denoted as the "terminal instability zone", and $\bar{s}^*$ will be called the "terminal velocity".

These results are summarized in Table 1, and a typical frequency-speed plot is shown in Figure 4. Note that the parameters which are important in Equation (2.47) are $\Delta\bar{m}$ and $\Delta\bar{k}$. These quantities are assumed constant for any given plot. A given value of $\Delta\bar{m}$ may correspond to a wide variety of load positions and mass ratios, since

$$\Delta\bar{m} = \left(\frac{2r_L}{a}\right)^2 \cdot \frac{m_L}{M} \qquad (2.70)$$

Similarly, a given value of $\Delta\bar{k}$ may correspond to many spring stiffness and load positions, since

$$\Delta\bar{k} = \left(\frac{2r_L}{a}\right)^2 \cdot \frac{1}{2_p} \cdot \frac{k_L}{M} \qquad (2.71)$$

Figure 5 is a frequency-speed plot for the system with a moving mass only ($\bar{k}=0.$), for values of $\Delta\bar{m} = 0.0, 0.1, 0.5, 1.0$, and 5.0, representing many possible loading conditions. Figure 6 is a frequency-speed plot for the system with a moving spring only ($\bar{m}=0.$), for values of $\Delta\bar{k} = 0.0, 1.0$, and 4.0. Note that in the mass-only case the

Speed Range	Terminology	Possible Solutions	Stability*
$0 \le \bar{s} < 1$	Subcritical Speed	$e^{\pm i\omega_L \tau}$, $e^{\pm i\omega_u \tau}$	Stable
$\bar{s} = 1$	Critical Speed	e^{0t}, $e^{\pm i\omega_u \tau}$	Stable
$1 < \bar{s} < \sqrt{1+\Delta\bar{k}}$	Stiffness Instability Region	$e^{\mu\tau}$, $e^{-\mu\tau}$, $e^{\pm i\omega_u \tau}$	Unstable
$\sqrt{1+\Delta\bar{k}} \le \bar{s} \le \bar{s}^*$	Supercritical Stable Region	$e^{\pm i\omega_L \tau}$, $e^{\pm i\omega_u \tau}$	Stable
$\bar{s} > \bar{s}^*$	Terminal Instability Region	$e^{\pm\mu\tau \pm i\omega\tau}$	Unstable

*The system is said to be unstable if there exist initial conditions for which unbounded motions occur.

Table 1. Solution Behavior of the Undamped Two Degree of Freedom Disk with an Attached Moving Spring and Mass

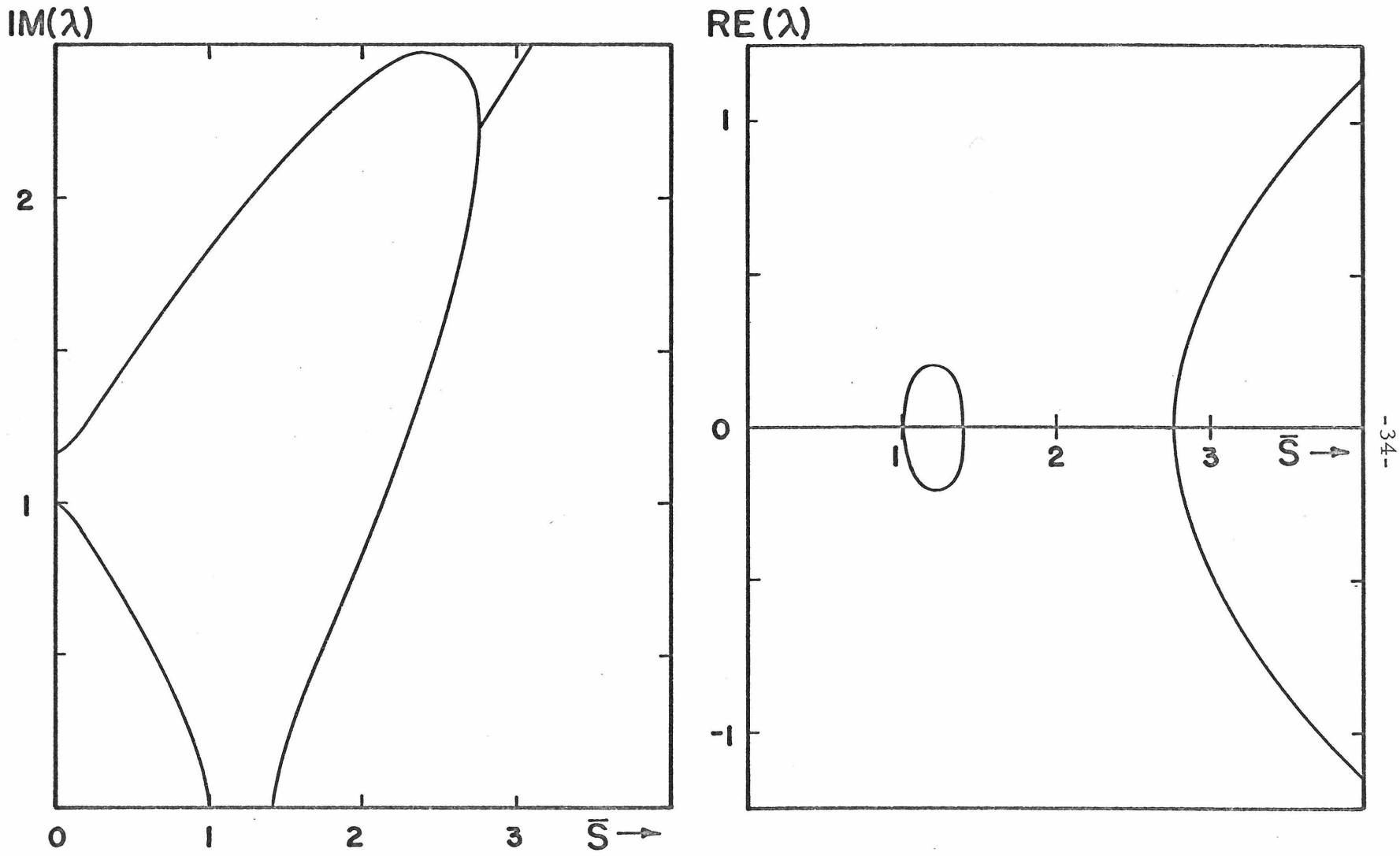

Fig. 4a: Typical frequency-speed diagram ($\Delta\bar{m} = 0.5$, $\Delta\bar{k} = 1.0$, $\bar{c} = \bar{c}_L = 0$) .

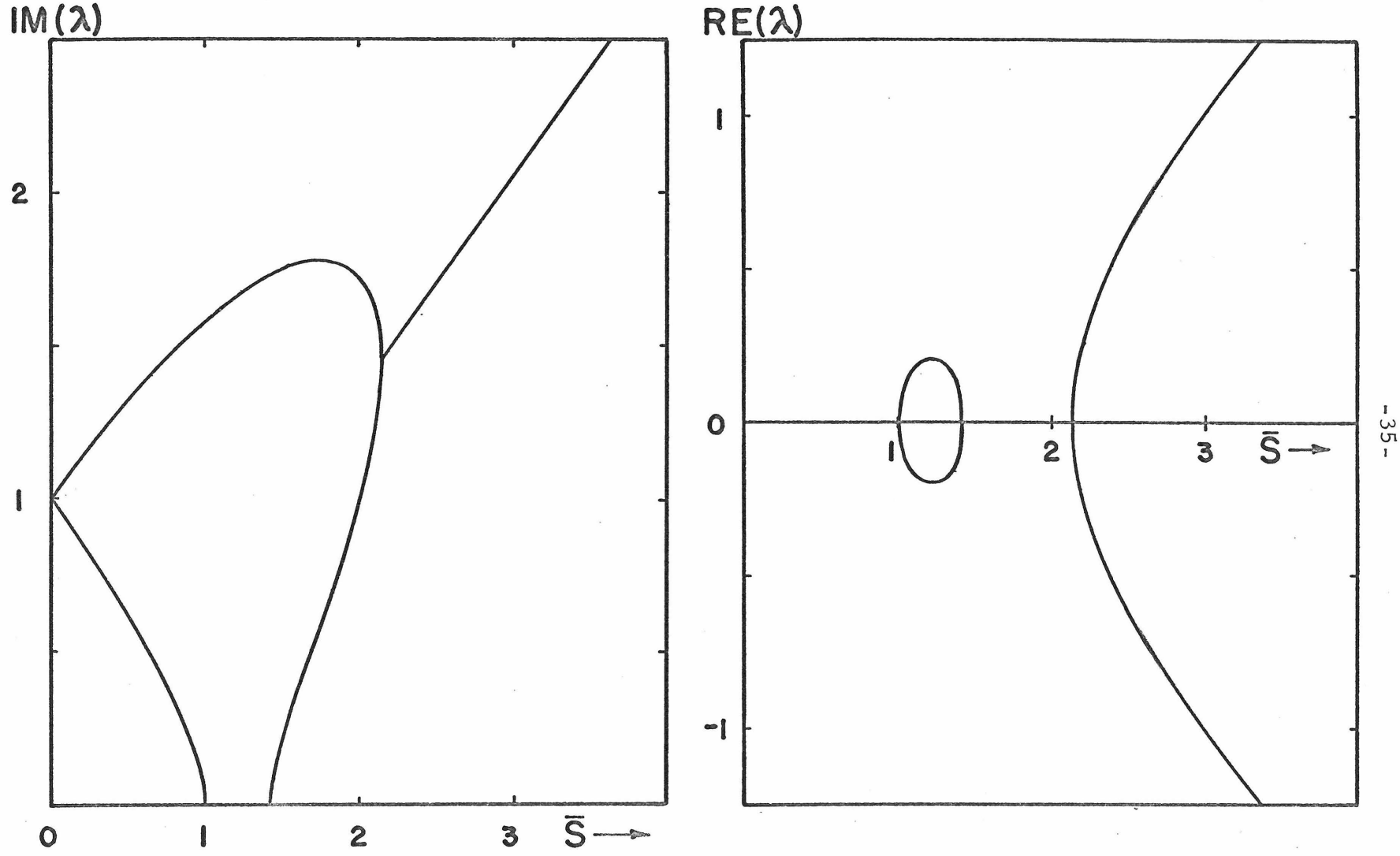

Fig. 4b: Typical frequency-speed diagram ($\Delta\bar{m} = 1.0$, $\Delta\bar{k} = 1.0$, $\bar{c} = \bar{c}_L = 0.0$)

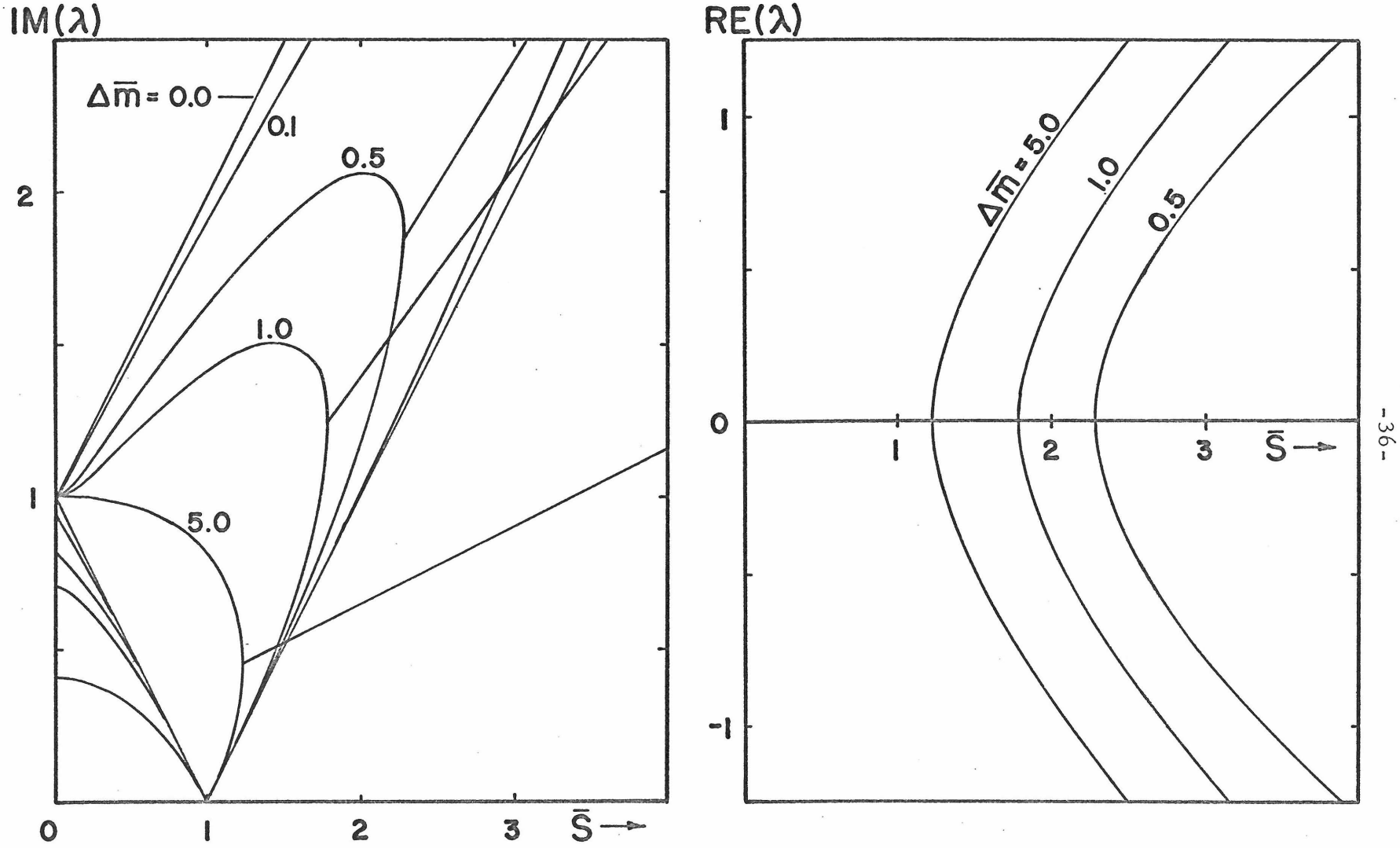

Fig 5: Frequency-speed diagrams for disk with moving mass only

($\Delta\bar{m} = 0.1, 0.5, 1.0, 5.0$, $\Delta\bar{k} = \bar{c} = \bar{c}_L = 0.0$)

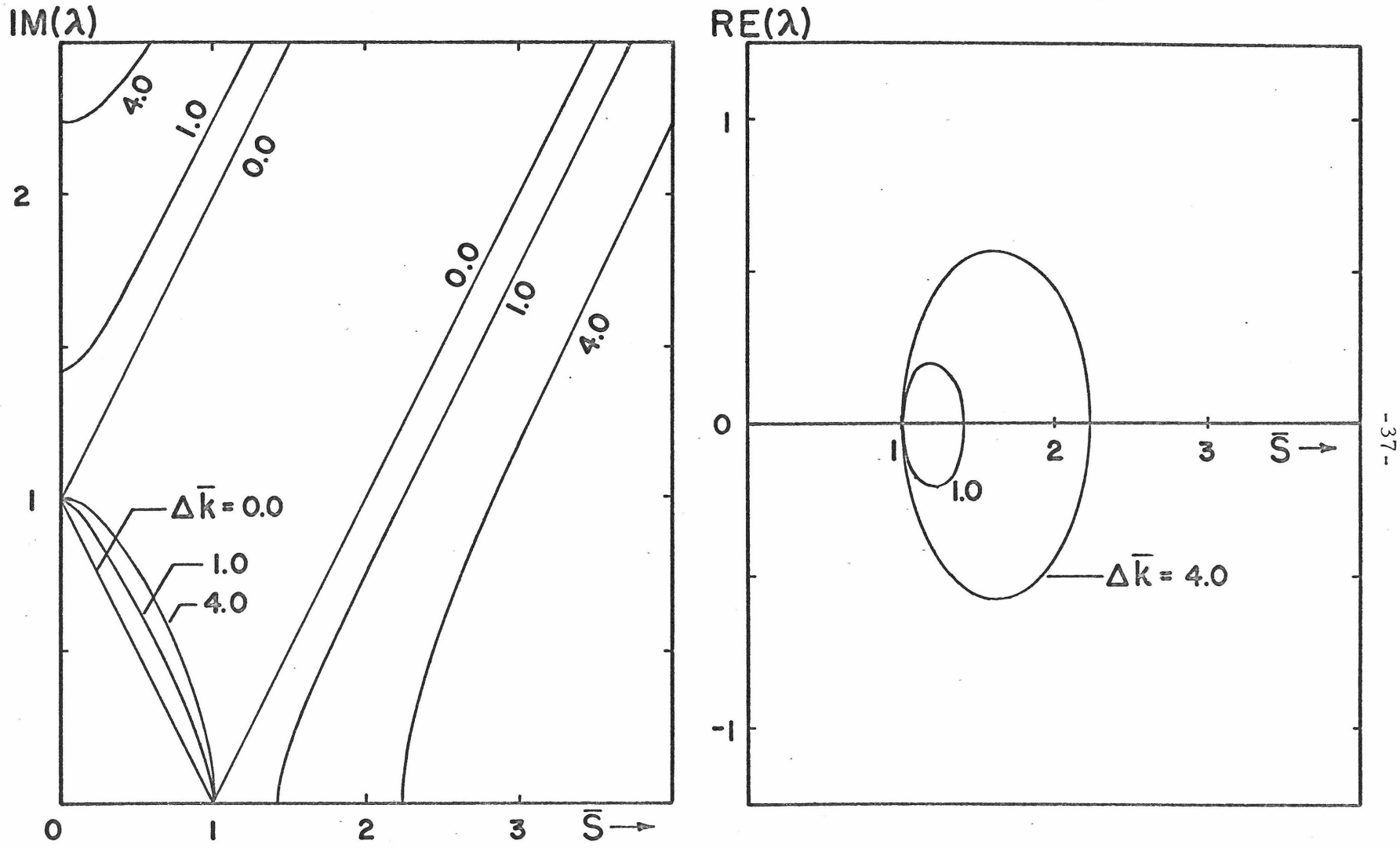

Fig. 6: Frequency-speed diagrams for disk with moving spring only.

$(\Delta\bar{k} = 1.0, 4.0, \ \Delta\bar{m} = \bar{c} = \bar{c}_L = 0.0)$

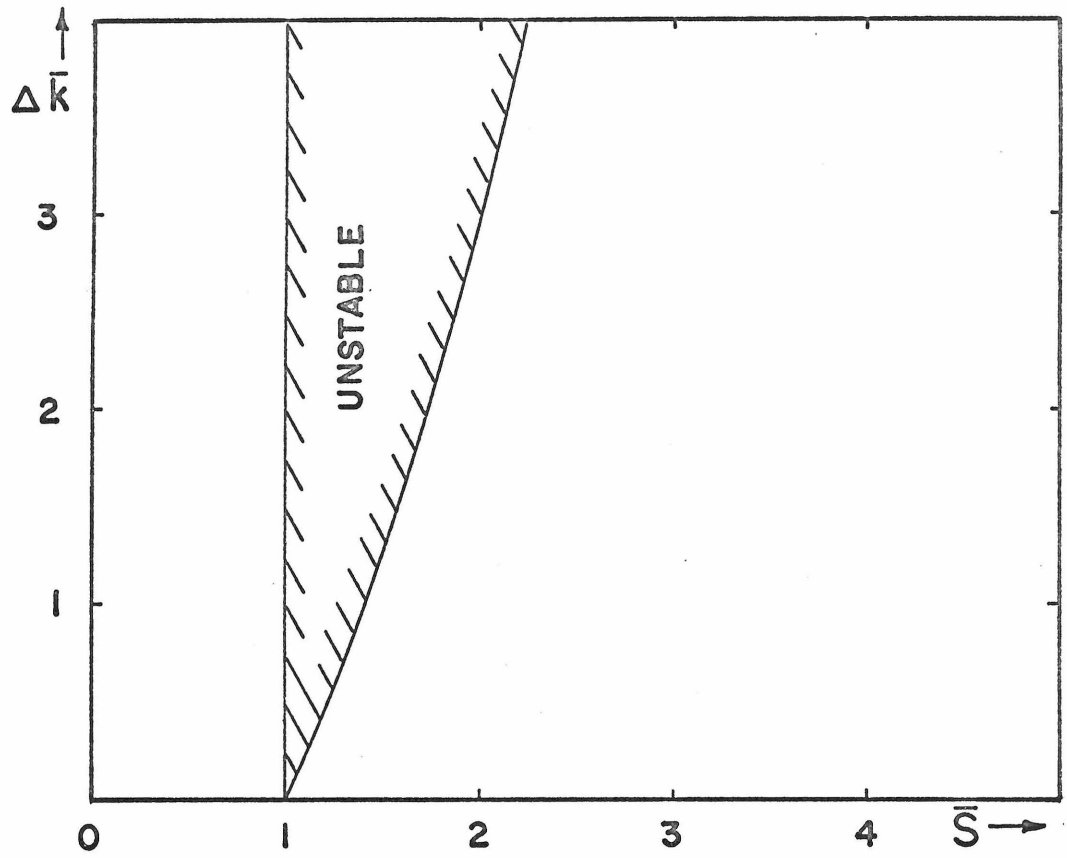

Fig. 7: Stiffness instability boundaries as a function of $\Delta\bar{k}$.

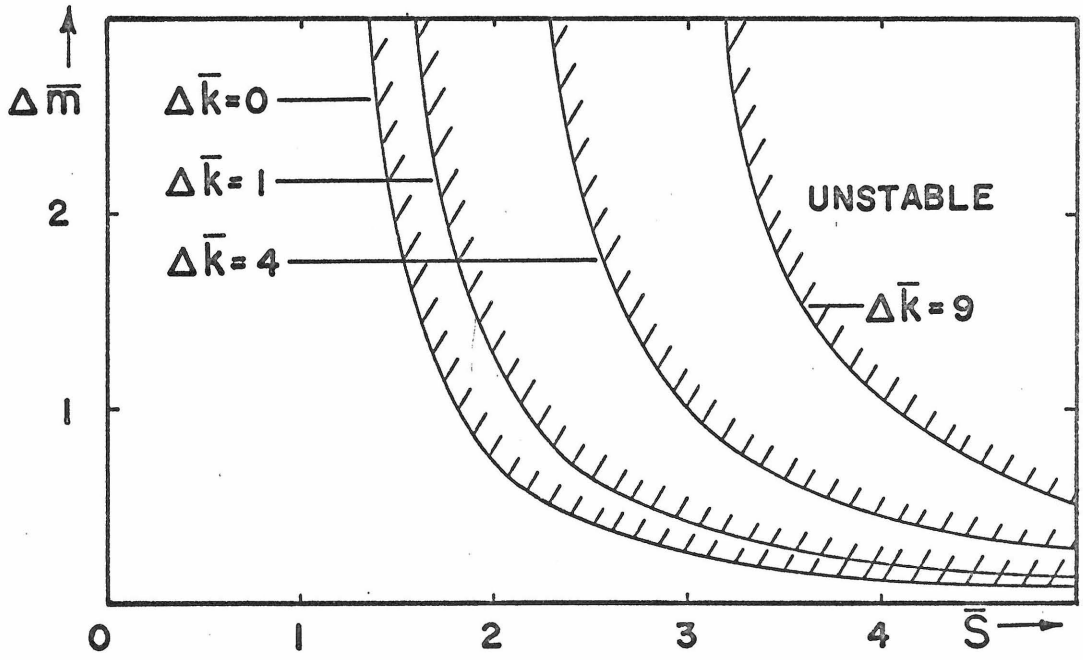

Fig. 8: Terminal speed $\bar{s}^*$ as a function of $\Delta\bar{m}$, for several values of $\Delta\bar{k}$.

terminal velocity decreases as $\Delta\bar{m}$ increases, and that there is no instability region immediately above $\bar{s} = 1$. In the spring-only cases, the width of the stiffness instability region increases with increasing $\Delta\bar{k}$, but there is no longer a region of instability at high speed ($\bar{s}^* = \infty$). The width of the stiffness instability region as a function of $\Delta\bar{k}$ is given by (2.64), and Figure 7 shows how this width varies with increasing $\Delta\bar{k}$. Figure 8 shows how the terminal velocity $\bar{s}^*$ varies with $\Delta\bar{m}$, for several fixed values of $\Delta\bar{k}$ ($\Delta\bar{k} = 0.0,\ 1.0,\ 4.0,\ 9.0$). Note that increasing $\Delta\bar{k}$ tends to increase the terminal velocity $\bar{s}^*$, at the expense of widening the stiffness instability region. As $\Delta\bar{k}$ increases, the stable region between the two instability zones narrows, and moves to a higher speed range.

The physical meaning of the frequencies shown in the frequency-speed plots may be obtained by recalling that the vertical deflection of the moving mass, $z(t)$, is related to the disk deflection $u(r, \theta, t)$ by Equation (2.8):

$$z(t) = \left[u(r, \theta, t) \right] \Big|_{\substack{r = r_L \\ \theta = \Omega t}}$$

Using the relations (2.1), (2.28), and (2.32), this becomes:

$$z(t) = \left[u(r, \theta, t) \right] \Big|_{\substack{r = r_L \\ \theta = \Omega t}} \qquad (2.72)$$

$$
\left.
\begin{aligned}
&= r_L \cdot \alpha(t) \cdot \sin\left[\Omega t - \beta(t)\right] \\
&= r_L \left[C(t)\sin\Omega t + D(t)\cos\Omega t\right] \\
&= r_L \cdot A(t)
\end{aligned}
\right\} \quad (2.72)\ \text{cont.}
$$

Therefore, the frequency components of A(t) will be the same as the frequency components of the motion of the moving mass, and in general the motion of the mass will be given by a linear combination of those frequencies shown in the frequency-speed plots.

2.5 Solutions to Initial Value Problems (Undamped)

It may be recalled that the deflection of the disk as seen from a reference frame rotating at constant angular velocity Ω is:

$$u'(r, \Phi, \tau) = r \cdot \left[A(\tau)\cos\Phi + B(\tau)\sin\Phi\right]$$

Hence the general solution for any initial conditions may be written:

$$
\begin{aligned}
u'(r,\Phi,\tau) = r \cdot e^{\lambda_1 \tau}&\left[A_1\cos\Phi + B_1\sin\Phi\right] \\
+re^{\lambda_2 \tau}&\left[A_2\cos\Phi + B_2\sin\Phi\right] \\
+re^{\lambda_3 \tau}&\left[A_3\cos\Phi + B_3\sin\Phi\right] \\
+re^{\lambda_4 \tau}&\left[A_4\cos\Phi + B_4\sin\Phi\right]
\end{aligned}
\quad (2.73)
$$

The ratios between the complex constants A_j and B_j ($j=1, 2, 3, 4$) are given by the eigenvector corresponding to the eigenvalue λ_j. Alternatively, this ratio may be found by substituting $A(\tau) = A_j e^{\lambda_j \tau}$ and $B(\tau) = B_j e^{\lambda_j \tau}$ into Equation (2.38) giving

$$B_j = \frac{-2\bar{s}\lambda_j}{(1-\bar{s}^2)+\lambda_j^2} A_j \tag{2.74}$$

It was demonstrated in the previous section that in two separate regions the eigenvalues of the problem were pure imaginary, while in two other regions the eigenvalues could have real parts. One of the later cases is the stiffness instability zone, which occurs when $1 < \bar{s}^2 < 1 + \Delta\bar{k}$. In this zone the stability of the solution depends on initial conditions.

2.5.1 Stiffness Instability Zone

To better understand how the stability of the system in the stiffness instability region depends on the initial conditions, consider the general solution for speeds $\bar{s}$ in this region. From Equation (2.65), the eigenvalues λ_i are of the form:

$$\lambda_1 = -\mu, \quad \lambda_2 = +\mu, \quad \lambda_3 = i\omega_u, \quad \lambda_4 = -i\omega_u \tag{2.75}$$

The general solution (2.73) may then be written:

$$u'(r,\Phi,\tau)= r\Big[A_1 e^{-\mu\tau}(\cos\Phi-\zeta\sin\Phi)+A_2 e^{\mu\tau}(\cos\Phi+\zeta\sin\Phi) + A_3 e^{i\omega_u\tau}(\cos\Phi+i\eta\sin\Phi)+A_4 e^{-i\omega_u\tau}(\cos\Phi-i\eta\sin\Phi)\Big] \tag{2.76}$$

where ζ and η are given from (2.74) as:

$$\zeta=\frac{-2\mu\bar{s}}{(1-\bar{s}^2)+\mu^2} \quad , \quad \eta=\frac{-2\omega_u\bar{s}}{(1-\bar{s}^2)-\omega_u^2}$$

Note that ζ and η are both real constants. It can be shown that if $u'(r,\Phi,\tau)$ (and hence $u(r,\theta,\tau)$) satisfies real initial conditions, then A_1 and A_2 are real and A_3 and A_4 are complex conjugates. Denoting

$$A_3=a_3+ia_4 \text{ and } A_4=a_3-ia_4, \tag{2.77}$$

the expression for $u'(r,\Phi,\tau)$ becomes:

$$u'(r,\Phi,\tau)= r\cdot\Big\{A_1 e^{-\mu\tau}(\cos\Phi-\zeta\sin\Phi)+A_2 e^{\mu\tau}(\cos\Phi+\zeta\sin\Phi) +2\Big[(a_3\cos\omega_u\tau-a_4\sin\omega_u\tau)\cos\Phi -(a_4\cos\omega_u\tau+a_3\sin\omega_u\tau)\eta\sin\Phi\Big]\Big\} \tag{2.78}$$

Note that all quantities in Equation (2.78) are real. The displacement of the load, $z(\tau)$, is simply $u'(r,\Phi,\tau)$ evaluated at $r=r_L$ and $\Phi=0$.

The deflection of the disk in the stationary reference frame is found by substituting $\Phi=\theta-\Omega t=\theta-\bar{s}\tau$. That is:

$$z(\tau)=r_L\cdot\left[A_1e^{-\mu\tau}+A_2e^{\mu\tau}+2(a_3\cos\omega_u\tau-a_4\sin\omega_u\tau)\right] \tag{2.79}$$

$$\begin{aligned}u(r,\theta,\tau)=r\cdot\Big\{&A_1e^{-\mu\tau}\left[\cos(\theta-\bar{s}\tau)-\zeta\sin(\theta-\bar{s}\tau)\right]\\&+A_2e^{\mu\tau}\left[\cos(\theta-\bar{s}\tau)+\zeta\sin(\theta-\bar{s}\tau)\right]\\&+2(a_3\cos\omega_u\tau-a_4\sin\omega_u\tau)\cos(\theta-\bar{s}\tau)\\&-2(a_4\cos\omega_u\tau+a_3\sin\omega_u\tau)\eta\sin(\theta-\bar{s}\tau)\Big\}\end{aligned} \tag{2.80}$$

The velocity of the disk in the stationary reference frame is given by $\frac{\partial u}{\partial t}=p\frac{\partial u}{\partial\tau}$. At time $\tau = 0$, the initial deflection and velocity are:

$$u(r,\theta,0)=r\cdot\left\{\left[A_1+A_2+2a_3\right]\cos\theta+\left[-\zeta A_1+\zeta A_2-2\eta a_4\right]\sin\theta\right\} \tag{2.81}$$

$$\begin{aligned}u_t(r,\theta,0)=r\cdot\Big\{&\left[(\zeta\bar{s}-\mu)A_1+(\mu-\zeta\bar{s})A_2+2(\bar{s}\eta-\omega_u)a_4\right]\cos\theta\\&+\left[(\zeta\mu+\bar{s})A_1+(\zeta\mu+\bar{s})A_2+2(\bar{s}-\omega_u\eta)a_3\right]\sin\theta\Big\}\end{aligned} \tag{2.82}$$

To make use of Equations (2.81) and (2.82), it is somewhat more convenient to specify the $C(\tau)$ and $D(\tau)$ coordinates at $\tau = 0$, rather than the Euler angles $\alpha(\tau)$ and $\beta(\tau)$ at $\tau = 0$. The relations between $C(\tau)$, $D(\tau)$ and $\alpha(\tau)$, $\beta(\tau)$ are given by (2.28) and (2.29). At $\tau = 0$, the initial displacement and velocity of the disk can then be written:

$$u(r,\theta,0)=r\cdot\left[C_1\cos\theta+D_1\sin\theta\right] \tag{2.83}$$

$$u_t(r,\theta,0)=r\cdot\left[C_2\cos\theta+D_2\sin\theta\right] \tag{2.84}$$

The constants C_1, C_2, D_1, and D_2 are known constants describing the initial conditions of the disk at $\tau = 0$. By comparing (2.81) and (2.82) with (2.83) and (2.84), the following four equations are obtained:

$$\begin{aligned} A_1 + A_2 + 2a_3 &= C_1 \\ -\zeta A_1 + \zeta A_2 - 2\eta a_4 &= D_1 \\ (\zeta\bar{s} - \mu) A_1 + (\mu - \zeta\bar{s}) A_2 + 2(\bar{s}\eta - \omega_u) a_4 &= C_2 \\ (\zeta\mu + \bar{s}) A_1 + (\zeta\mu + \bar{s}) A_2 + 2(\bar{s} - \omega_u \eta) a_3 &= D_2 \end{aligned} \tag{2.85}$$

A unique nontrivial solution for this system of equations exists if the determinant of the coefficients of A_1, A_2, a_3, and a_4 does not vanish. An evaluation of this determinant shows that in the stiffness instability region, $1 < \bar{s}^2 < 1 + \Delta\bar{k}$, the determinant is nonvanishing.

As an example of the dependence of the solution on initial conditions, consider the case:

$$\Delta\bar{k} = 1.0,\ \Delta\bar{m} = 1.0,\ \bar{c}_L = \bar{c} = 0.0,\ \bar{s} = 1.25 \tag{2.86}$$

$$\Rightarrow\ \mu = 0.2087\ ,\ \omega_u = 1.6807$$

As can be seen from Figure 4b, this value of $\bar{s}$ lies in the stiffness instability region. Four particular sets of initial conditions will be considered, and for simplicity, only the behavior of $\alpha(\tau)$ will be discussed.

Case 1: Exponential Growth (Unstable Response)

From Equations (2.79) and (2.80), it can be seen that if $A_1 = a_3 = a_4 = 0$, but $A_2 \neq 0$, then $u(r, \theta, \tau)$ and $z(\tau)$ will have positive exponential growth. This will be the case if (from (2.85)):

$$C_1 = A_2 \quad , \quad D_1 = \zeta A_2$$
$$C_2 = (\mu - \zeta\bar{s})A_2 \quad , \quad D_2 = (\zeta\mu + \bar{s})A_2 \tag{2.87}$$

The corresponding value of ζ, given by the equation following (2.76), is $\zeta = 1.0056$. Thus, Equations (2.87) give:

$$C_1 = A_2 \quad , \quad D_1 = 1.0056\, A_2$$
$$C_2 = -1.0484\, A_2 \quad , \quad D_2 = 1.4589\, A_2 \tag{2.89}$$

The Euler angle $\alpha(\tau)$, which is the angle the disk makes with the horizontal, can be found from Equation (2.80) using the transformations (2.28) and (2.29). Corresponding to the above initial conditions,

$$\alpha(\tau) = A_2\left[1 + \zeta^2\right]\frac{1}{2}\, e^{\mu\tau} \tag{2.90}$$

The initial conditions (2.89) were used along with a standard differential equation solving routine, to solve Equations (2.30) and (2.31) numerically for $C(\tau)$ and $D(\tau)$, from which $\alpha(\tau)$ was computed and compared with the analytical expression (2.90). A_2 was chosen so that $\alpha(0) = 1°$ (i.e., $A_2 = 0.0123$). The resulting solution agrees with the analytic expression (2.90) to four figures in $\alpha(\tau)$, and as Figure 9a shows,

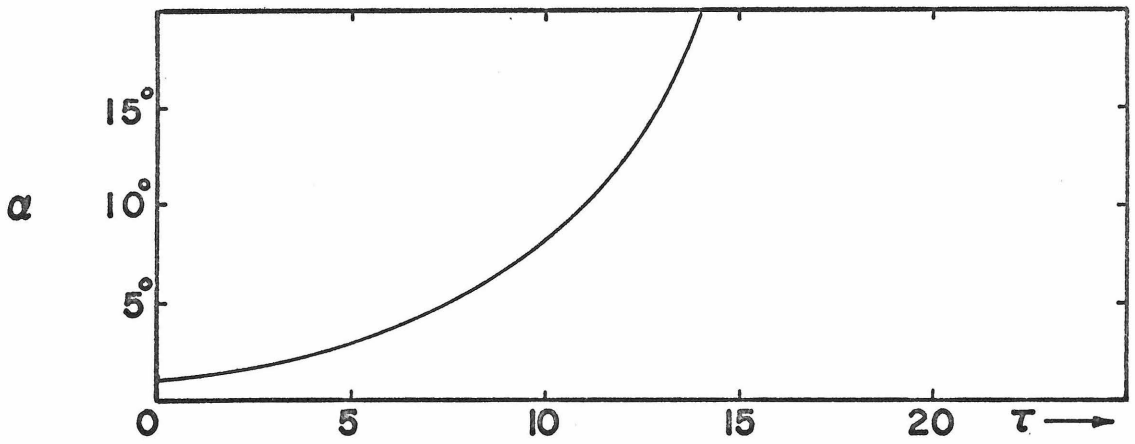

Fig. 9a: Unstable solution (Case 1)

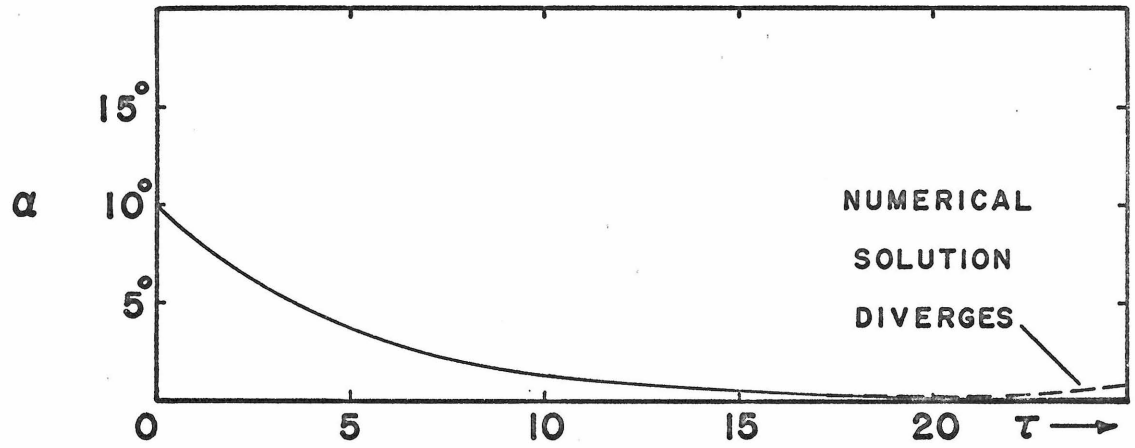

Fig. 9b: Stable solution (Case 2)

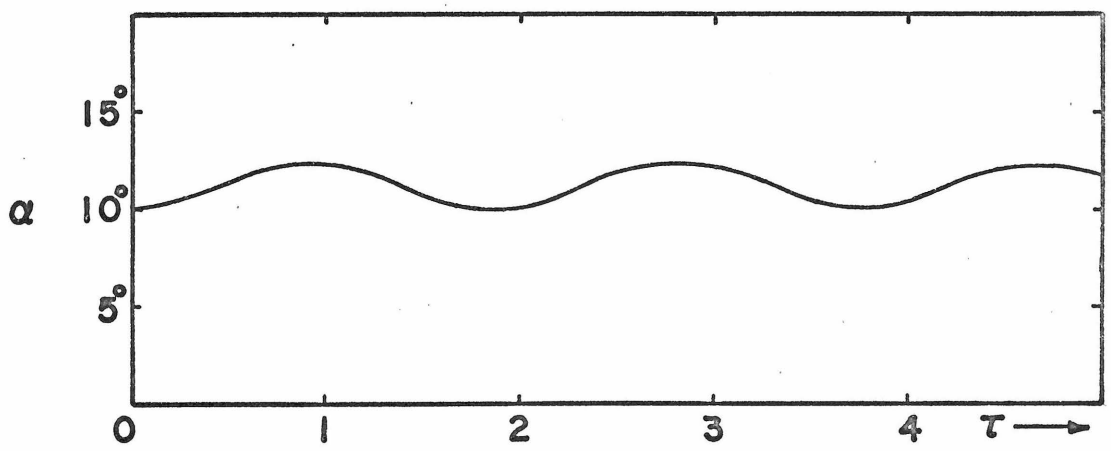

Fig. 9c: Oscillatory solution (Case 3)

there is no recognizable difference between the two results.

Case 2: Exponential Decay (Stable Response)

From Equations (2.79) and (2.80), it can be seen that if $A_2=a_3=a_4=0$, but $A_1 \neq 0$, then $u(r,\theta,\tau)$ and $z(\tau)$ will have negative exponential behavior. The analytical expression for $\alpha(\tau)$ becomes:

$$\alpha(\tau)= A_1\left[1+\zeta^2\right]\frac{1}{2}\, e^{-\mu\tau} \qquad (2.91)$$

The corresponding values of C_1, C_2, D_1, and D_2 were calculated from (2.85) and used as initial conditions in a numerical solution of Equations (2.30) and (2.31), from which $\alpha(\tau)$ was computed and compared to the analytic expression (2.91). The results of this comparison are shown in Figure 9b (the value of A_1 was chosen so that $\alpha(0) = 10°$). Note that the numerical solution began to diverge at $\tau \cong 17$, due to numerical round-off errors which bring in some of the positive exponential growth as in Case 1.

Case 3: Oscillatory Behavior (Stable Response)

If in Equations (2.79) and (2.80) the constants A_1 and A_2 are both zero, the disk response $u(r,\theta,\tau)$ and the load mass response will be oscillatory in nature. If $a_3 \neq 0$, but $A_1 = A_2 = a_4 = 0$, the expression for $\alpha(\tau)$ becomes:

$$\alpha(\tau) = 2a_3 \cdot \left[\cos^2 \omega_u \tau + \eta^2 \sin^2 \omega_u \tau\right]^{\frac{1}{2}}$$
$$= 2a_3 \cdot \left[\frac{1+\eta^2}{2} + \frac{1-\eta^2}{2} \cos 2\omega_u \tau\right]^{\frac{1}{2}} \qquad (2.92)$$

When the initial conditions evaluated from (2. 85) were used in the numerical solution of (2. 30) and (2. 31), the comparison with Equation (2. 92) was once again good, as shown in Figure 9c. In this particular example, the step size in τ was not small enough for good accuracy, as can be seen by the fact that the numerical solution dips below 10° at $\tau \cong 1.9$, whereas (2. 92) indicates that the value of $\alpha(0)$ is the minimum ($\eta^2 > 1$). Since $\omega_u = 1.6807$, the theoretical period for $\alpha(\tau)$ is $T = \frac{2\pi}{2\omega}$ $= \pi/1.6807 \cong 1.87$, agreeing well with the numerical result.

Case 4: Arbitrary Initial Conditions

When the initial conditions are such that more than one of the previous three types of motion are present, the disk response becomes much more complicated. Figure 9d illustrates such a case. Here, $\alpha(0)$ was chosen as 1°, and $\beta(0)$ as -90°. Figure 9d shows $\beta(\tau)$, which is the location of the nodal diameter in the fixed reference frame, and $z(\tau)$, which is the vertical displacement of the moving mass, as well as the angle of inclination, $\alpha(\tau)$. The figures are from the computer solution of Equations (2. 30) and (2. 31). Note that from the analytical expression for $z(\tau)$, Equation (2. 79), the frequency content of $z(\tau)$ should correlate with the eigenfrequency ω_u, which in this case is

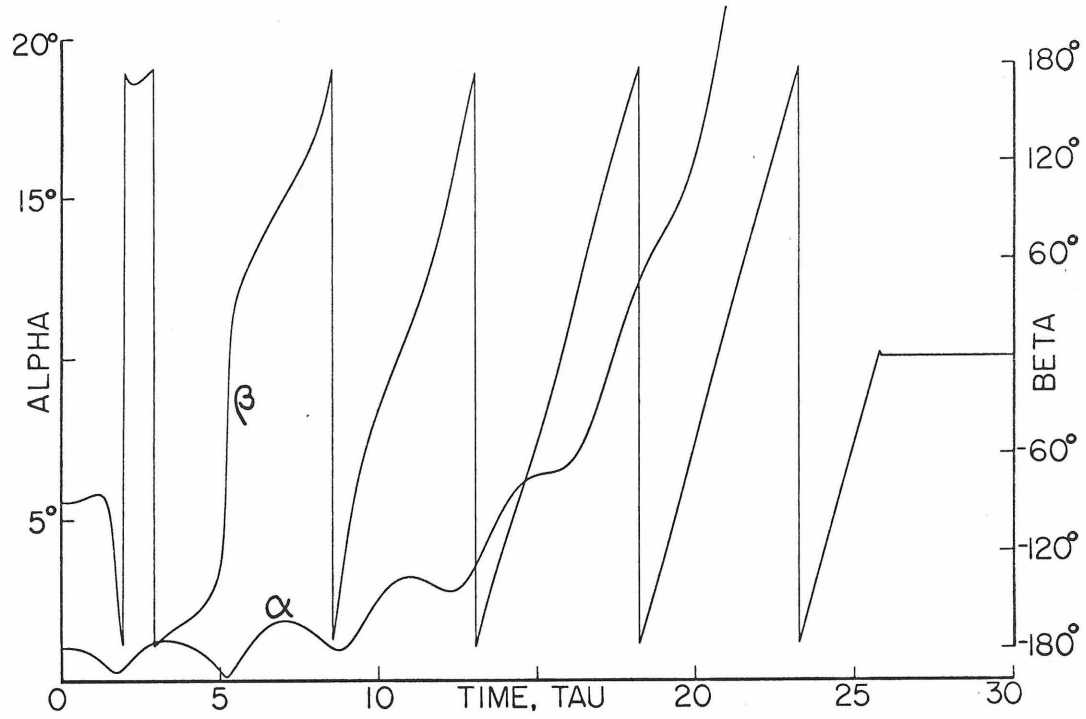

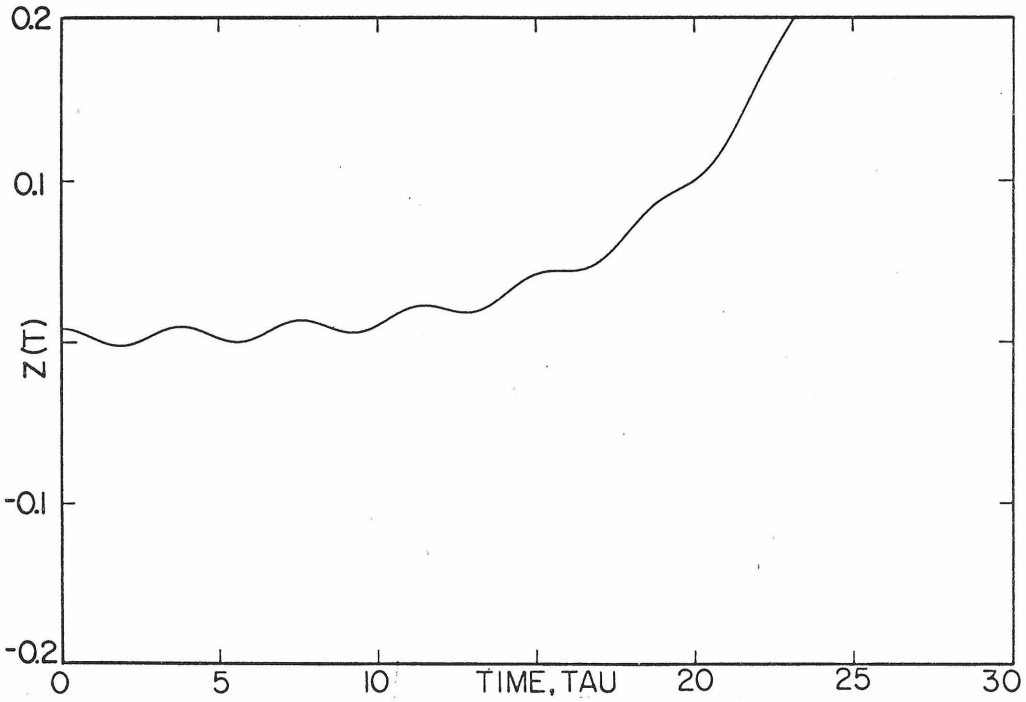

Fig. 9d: Undamped response in stiffness instability region.

($\Delta\bar{m}$=1.0, $\Delta\bar{k}$=1.0, $\bar{c}=\bar{c}_L$=0.0, $\bar{s}$=1.25).

1.6807. The period of the oscillations in $z(\tau)$ should then be $T = \frac{2\pi}{\omega_u} \cong 3.74$, which agrees well with the computer result.

Clearly, in the stiffness instability region the stability of the solution depends on the initial conditions at $\tau = 0$. Further, since the basic equations for $A(\tau)$ and $B(\tau)$ were written as an ordinary linear eigenvalue problem $P\frac{d\underline{x}}{d\tau} = Q\underline{x}$, if $\underline{x}(\tau) = \underline{y}(\tau) + \varepsilon\underline{w}(\tau)$, where $\underline{y}(\tau)$ is one of the "stable" solutions and $\underline{w}(\tau)$ represents an arbitrary perturbation, then the eigenvalue problem for $\underline{w}(\tau)$ is simply Case 4 discussed above. Thus, even the "stable" solutions in this region could be regarded as unstable because an arbitrary perturbation results in a solution that is unbounded in time. For these reasons, this region will be denoted as an unstable region of operation.

2.5.2 Terminal Instability Zone

In the region $\bar{s} > \bar{s}^*$, the eigenvalues are of the form (see Equation (2.68)):

$$\lambda_1 = i\omega + \mu, \quad \lambda_2 = -i\omega + \mu, \quad \lambda_3 = i\omega - \mu, \quad \lambda_4 = -i\omega - \mu \tag{2.93}$$

The general solution (2.73) then becomes:

$$\begin{aligned} u'(r,\Phi,\tau) = {} & A_1 e^{\mu\tau} e^{i\omega\tau} r\left[\cos\Phi - (G - iH)\sin\Phi\right] \\ & + A_2 e^{\mu\tau} e^{-i\omega\tau} r\left[\cos\Phi - (G + iH)\sin\Phi\right] \\ & + A_3 e^{-\mu\tau} e^{i\omega\tau} r\left[\cos\Phi + (G + iH)\sin\Phi\right] \\ & + A_4 e^{-\mu\tau} e^{-i\omega\tau} r\left[\cos\Phi + (G - iH)\sin\Phi\right] \end{aligned} \tag{2.94}$$

where G and H are the real constants:

$$G=\frac{2\mu\bar{s}\left[1-\bar{s}^2-\omega^2+\mu^2\right]+4\omega^2\mu\bar{s}}{\left[1-\bar{s}^2-\omega^2+\mu^2\right]^2-4\omega^2\mu^2}$$

$$H=\frac{4\omega\mu^2\bar{s}-2\mu\bar{s}\left[1-\bar{s}^2-\omega^2+\mu^2\right]}{\left[1-\bar{s}^2-\omega^2+\mu^2\right]^2-4\omega^2\mu^2} \qquad (2.95)$$

Equation (2.94) will be real if A_1 and A_2 are complex conjugates, and if A_3 and A_4 are also complex conjugates. Taking $A_1 = a_1 + ia_2$, $A_2 = a_1 - ia_2$, $A_3 = a_3 + ia_4$, $A_4 = a_3 - ia_4$, the expression for $u'(r, \Phi, \tau)$ becomes:

$$\begin{aligned} u'(r,\Phi,\tau) = 2e^{\mu\tau}\Big\{ & r\cos\Phi\left[a_3\cos\omega\tau - a_4\sin\omega\tau\right] \\ & + r\sin\Phi\left[(a_3G - a_4H)\cos\omega\tau - (a_3H + a_4G)\sin\omega\tau\right]\Big\} \\ & + 2e^{-\mu\tau}\Big\{r\cos\Phi\left[a_1\cos\omega\tau + a_2\sin\omega\tau\right] \\ & + r\sin\Phi\left[(-a_1G + a_2H)\cos\omega\tau - (a_1H + a_2G)\sin\omega\tau\right]\Big\} \end{aligned} \qquad (2.96)$$

The disk deflection in the fixed frame, $u(r, \theta, \tau)$, is found by substituting $\Phi = \theta - \bar{s}\tau$ in (2.96). The vertical deflection of the load mass, $z(\tau)$, is simply $u'(r_L, 0, \tau)$:

$$\begin{aligned} z(\tau) = 2e^{\mu\tau}\Big\{ & r_L\cdot\left[a_3\cos\omega\tau - a_4\sin\omega\tau\right]\Big\} \\ & + 2e^{-\mu\tau}\Big\{r_L\cdot\left[a_1\cos\omega\tau + a_2\sin\omega\tau\right]\Big\} \end{aligned} \qquad (2.97)$$

The real constants a_1, a_2, a_3, and a_4 are found by evaluating $u(r, \theta, 0)$ and $u_t(r, \theta, 0)$ in a fashion similar to the preceding section, although the algebra is more tedious. From (2.96) and (2.97), it is apparent that there will be a positive exponential term involved in the solution unless $a_3 = a_4 = 0$. Therefore, the region above $\bar{s} = \bar{s}^*$ is denoted as an unstable region. Figure 10 shows the result of a numerical solution of Equations (2.30) and (2.31) for the data $\Delta\bar{k} = 1.0$, $\Delta\bar{m} = 1.0$, $\bar{c}_L = \bar{c} = 0.0$, $\bar{s} = 3.0$ ($\bar{s}^* \cong 2.13$), with the initial conditions $\alpha(0) = 1°$, $\beta(0) = -90°$, and the initial velocity of a forward traveling wave.

2.5.3 Oscillatory Regions

In the regions $\bar{s} < 1$ and $[1+\Delta\bar{k}]^{\frac{1}{2}} < \bar{s} < \bar{s}^*$, the eigenvalues λ_i are of the form:

$$\lambda_1 = i\omega_L, \quad \lambda_2 = -i\omega_L, \quad \lambda_3 = i\omega_u, \quad \lambda_4 = -i\omega_u \tag{2.98}$$

The general solution may then be written:

$$\begin{aligned} u'(r, \Phi, \tau) = r\cdot\Big[A_1 e^{i\omega_L \tau}(\cos\Phi + i\eta_L \sin\Phi) + A_2 e^{-i\omega_L \tau}(\cos\Phi - i\eta_L \sin\Phi)\Big] \\ + r\cdot\Big[A_3 e^{i\omega_u \tau}(\cos\Phi + i\eta_u \sin\Phi) + A_4 e^{-i\omega_u \tau}(\cos\Phi - i\eta_u \sin\Phi)\Big] \end{aligned} \tag{2.99}$$

where η_L and η_u are given from (2.74) as:

$$\eta_L = \frac{-2\omega_L \bar{s}}{(1-\bar{s}^2) - \omega_L^2}, \qquad \eta_u = \frac{-2\omega_u \bar{s}}{(1-\bar{s}^2) - \omega_u^2}$$

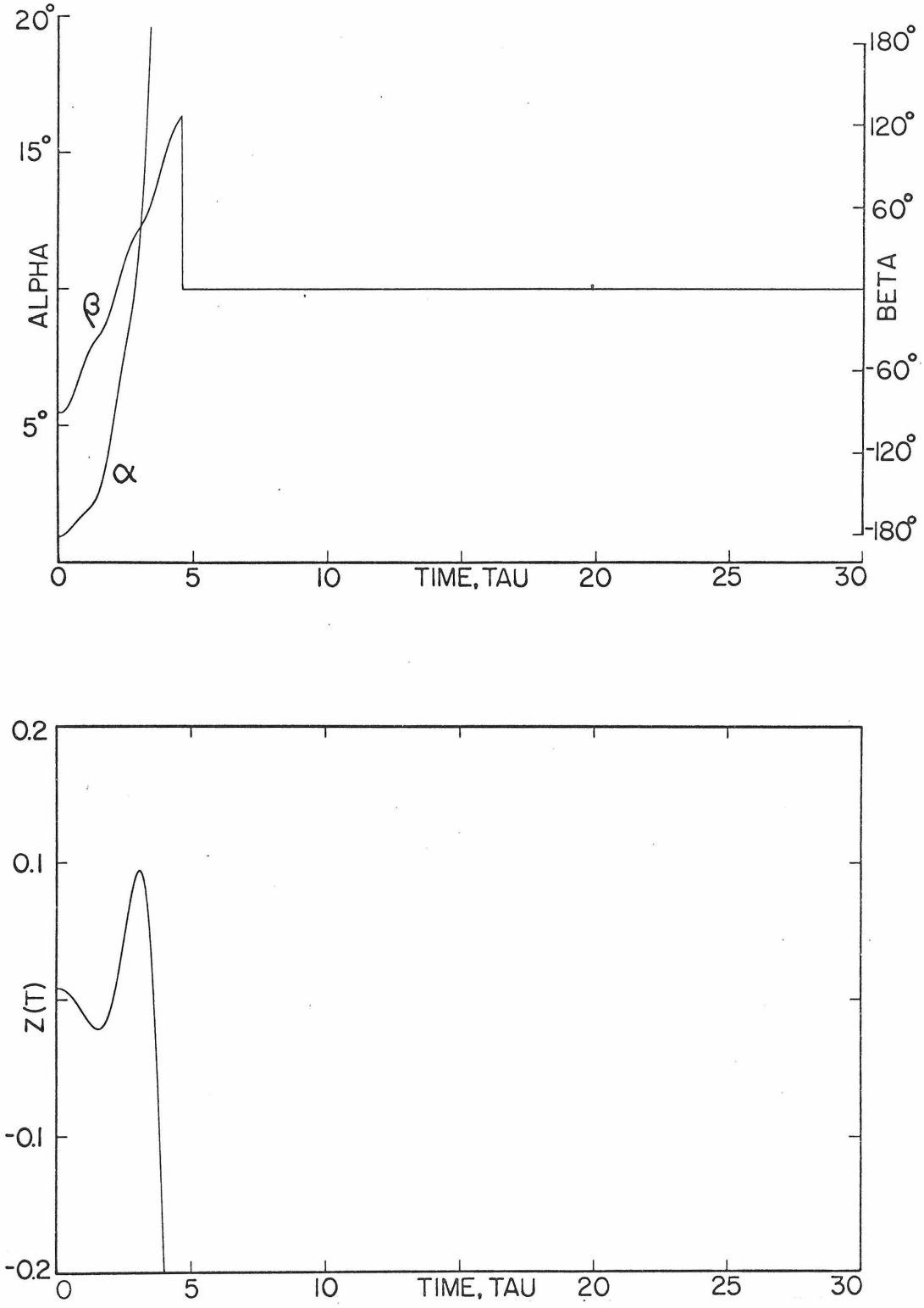

Fig. 10: Undamped response beyond terminal speed.

($\Delta\bar{m}$=1.0, $\Delta\bar{k}$=1.0, $\bar{c}=\bar{c}_L$=0.0, $\bar{s}$=3.0).

It can be shown that if $u'(r, \Phi, \tau)$ satisfies real initial conditions of the form (2.83) and (2.84), then A_1 and A_2 are complex conjugates, as are A_3 and A_4. Taking $A_1=a_1+ia_2$, $A_2=a_1-ia_2$, $A_3=a_3+ia_4$, and $A_4=a_3-ia_4$, the expression (2.99) becomes:

$$\begin{aligned} u'(r,\Phi,\tau)=r\cdot\Big[&2\cdot(a_1\cos\omega_L\tau-a_2\sin\omega_L\tau)\cos\Phi \\ &-2(a_2\cos\omega_L\tau+a_1\sin\omega_L\tau)\cdot\eta_L\sin\Phi \\ &+2(a_3\cos\omega_u\tau-a_4\sin\omega_u\tau)\cos\Phi \\ &-2(a_4\cos\omega_u\tau+a_3\sin\omega_u\tau)\cdot\eta_u\sin\Phi\Big] \end{aligned} \tag{2.100}$$

where all the constants are real. The deflection of the disk in the stationary reference frame, $u(r,\theta,\tau)$, is obtained by substituting $\Phi=\theta-\bar{s}\,\tau$ into Equation (2.100). The deflection of the moving mass is given by $z(\tau)=u'(r_L,0,\tau)$:

$$\begin{aligned} z(\tau)=r_L\cdot\Big[&2(a_1\cos\omega_L\tau-a_2\sin\omega_L\tau) \\ &+2(a_3\cos\omega_u\tau-a_4\sin\omega_u\tau)\Big] \end{aligned} \tag{2.101}$$

At $\tau=0$, the deflection $u(r,\theta,0)$ and velocity $u_t(r,\theta,0)$ in the stationary frame become:

$$u(r,\theta,0)=r\cdot\Big[(2a_1+2a_3)\cos\theta-(2\eta_L a_2+2\eta_u a_4)\sin\theta\Big] \tag{2.102}$$

$$\begin{aligned} u_t(r,\theta,0)=r\cdot\Big\{&\Big[2(\bar{s}\eta_L-\omega_L)a_2+2(\bar{s}\eta_u-\omega_u)a_4\Big]\cos\theta \\ &+\Big[2(\bar{s}-\omega_L\eta_L)a_1+2(\bar{s}-\omega_u\eta_u)a_3\Big]\sin\theta\Big\} \end{aligned} \tag{2.103}$$

Combining these equations with Equations (2.83) and (2.84) gives four equations for the four unknowns a_1, a_2, a_3, and a_4. From Equation (2.101) it is apparent that the frequency components of the displacement of the moving load will be relatively simple linear combinations of the two eigenfrequencies ω_L and ω_u. Similarly, the displacement of any point at fixed Φ in the rotating frame will have components of both frequencies superposed linearly. However, the motion as seen in the fixed reference frame will be very complicated, due to the nonlinear transformations (2.33) and (2.29). A relatively well-behaved example of oscillatory behavior is shown in Figure 11, for which $\Delta\bar{k}=1.0$, $\Delta\bar{m}=1.0$, $\bar{c}_L=\bar{c}=0.0$, and $\bar{s}=2.0$. The frequency components are $\omega_L=1.0000$ and $\omega_u=1.7320$. ($\omega_L=1.0000$ is due to the fact that $\sqrt{k/\bar{m}}=1.0$, exactly equal to ω_L for the disk with no attached spring and mass, thus having no effect on the lower natural frequency of the disk.) The initial conditions are $\alpha(0)=1°$, $\beta(0)=-90°$, and the initial disk velocity is selected so that only the $\omega_u=1.7320$ frequency component is present. This frequency is readily identifiable in the mass displacement record, since $T=\frac{2\pi}{\omega_u}\cong 3.62$ is very close to the period of $z(\tau)$. Further, since there is only one frequency component present, analogous to case 3 in 2.5.1, the behavior of $\alpha(\tau)$ is of the type (2.92). Thus, the frequency of $\alpha(\tau)$ is $2\omega_u$, and the period of $\alpha(\tau)$ is $T=\frac{2\pi}{2\omega_u}\cong 1.81$, which checks well with Figure 11. It should be emphasized again that this is

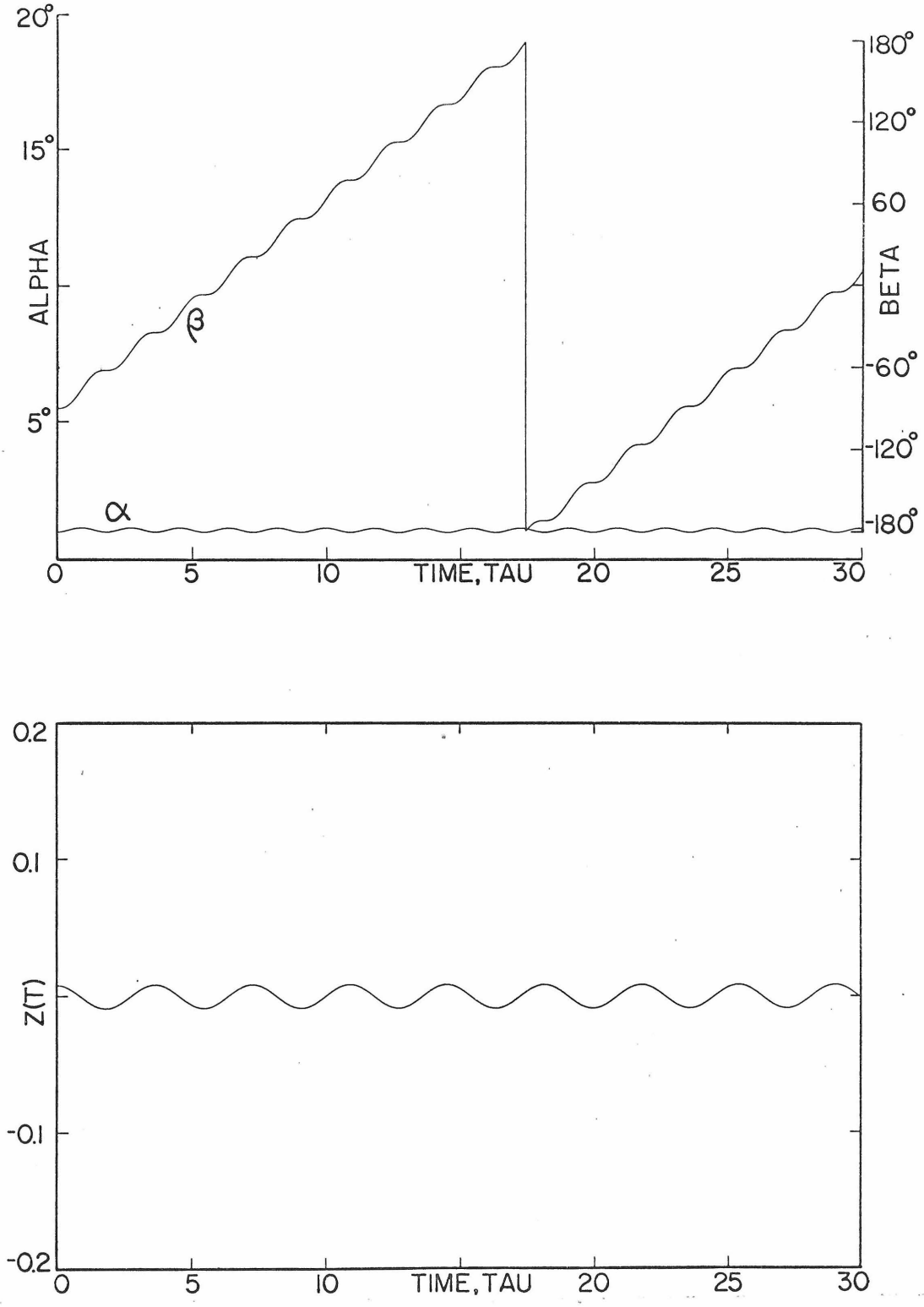

Fig. 11: Undamped response in supercritical stable region.

($\Delta\bar{m}=1.0$, $\Delta\bar{k}=1.0$, $\bar{c}=\bar{c}_L=0.0$, $\bar{s}=2.0$).

a special case where only one frequency component is present. In a following section, an example of a case in which both frequency components are present is studied with various values of foundation damping (refer to Figure 17). The response is of course much more complicated.

2.6 Properties of The Solution to The Damped Equations of Motion

When there is either load damping, $\bar{c}_L$, or foundation damping, $\bar{c}$, present in the problem, the polynomial for λ as given by Equation (2.45) is no longer a biquadratic, but a polynomial of degree four. Therefore, it is much more convenient to employ a root-finding routine on a computer rather than to attempt to find an analytic expression for λ. This was done using a standard double-precision root-finding routine. The results for several values of foundation damping for a moving mass only case, and a moving spring-mass case are shown in Figures 12 and 13 respectively. Note that only the positive values of $\mathrm{Im}\{\lambda\}$ are plotted; in fact, there is a negative value corresponding with each positive value $\mathrm{Im}\{\lambda\}$, so that each branch of the $\mathrm{Re}\{\lambda\}$ plot has associated with it one positive and one negative value of $\mathrm{Im}\{\lambda\}$. That is, the values of λ are generally complex conjugates. The only exception to this occurs when $\mathrm{Im}\{\lambda\}$ vanishes, in which case the corresponding values of $\mathrm{Re}\{\lambda\}$ are not equal.

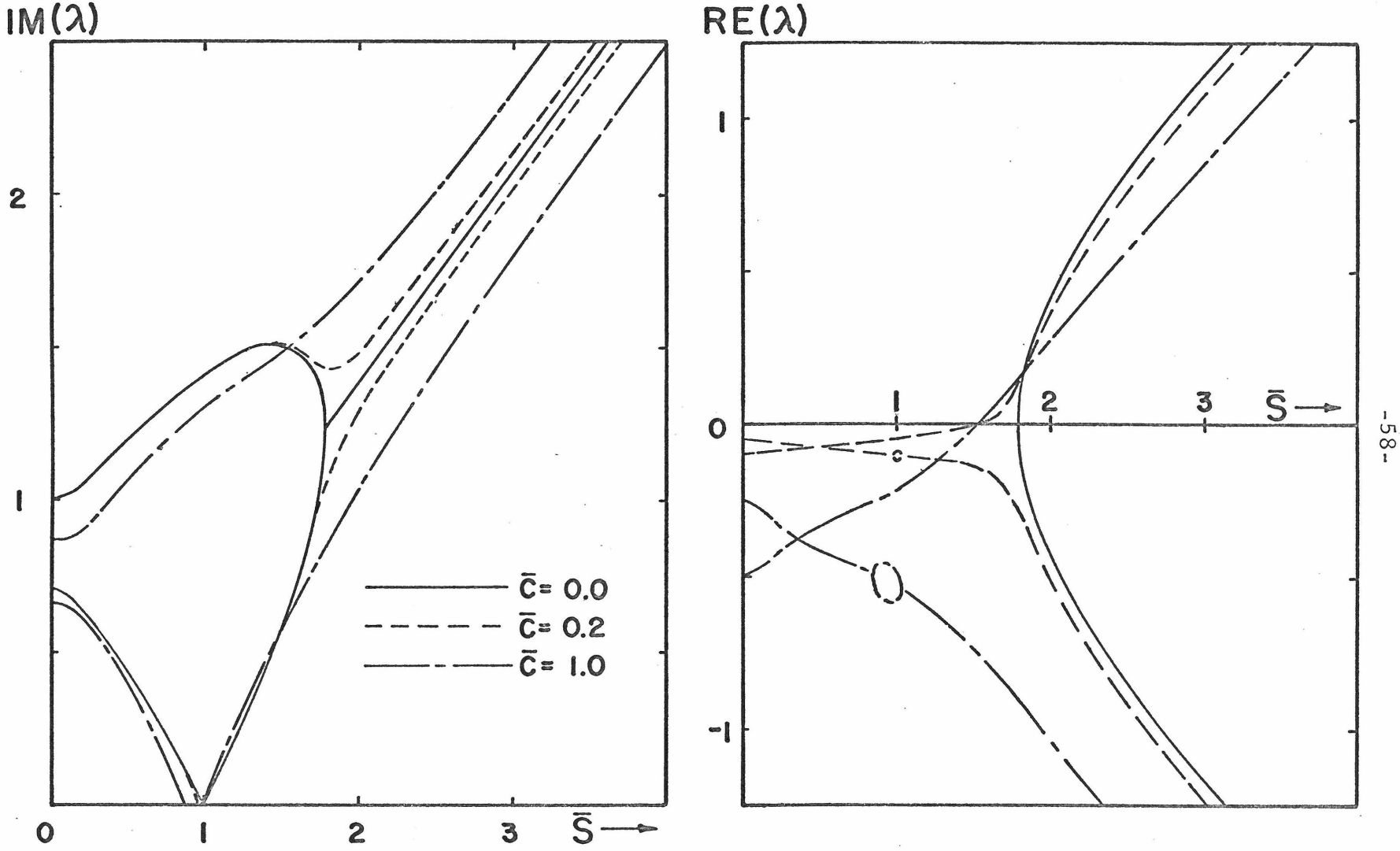

Fig. 12: Frequency-speed diagram, mass only ($\Delta\bar{m} = 1.0$), with foundation damping.

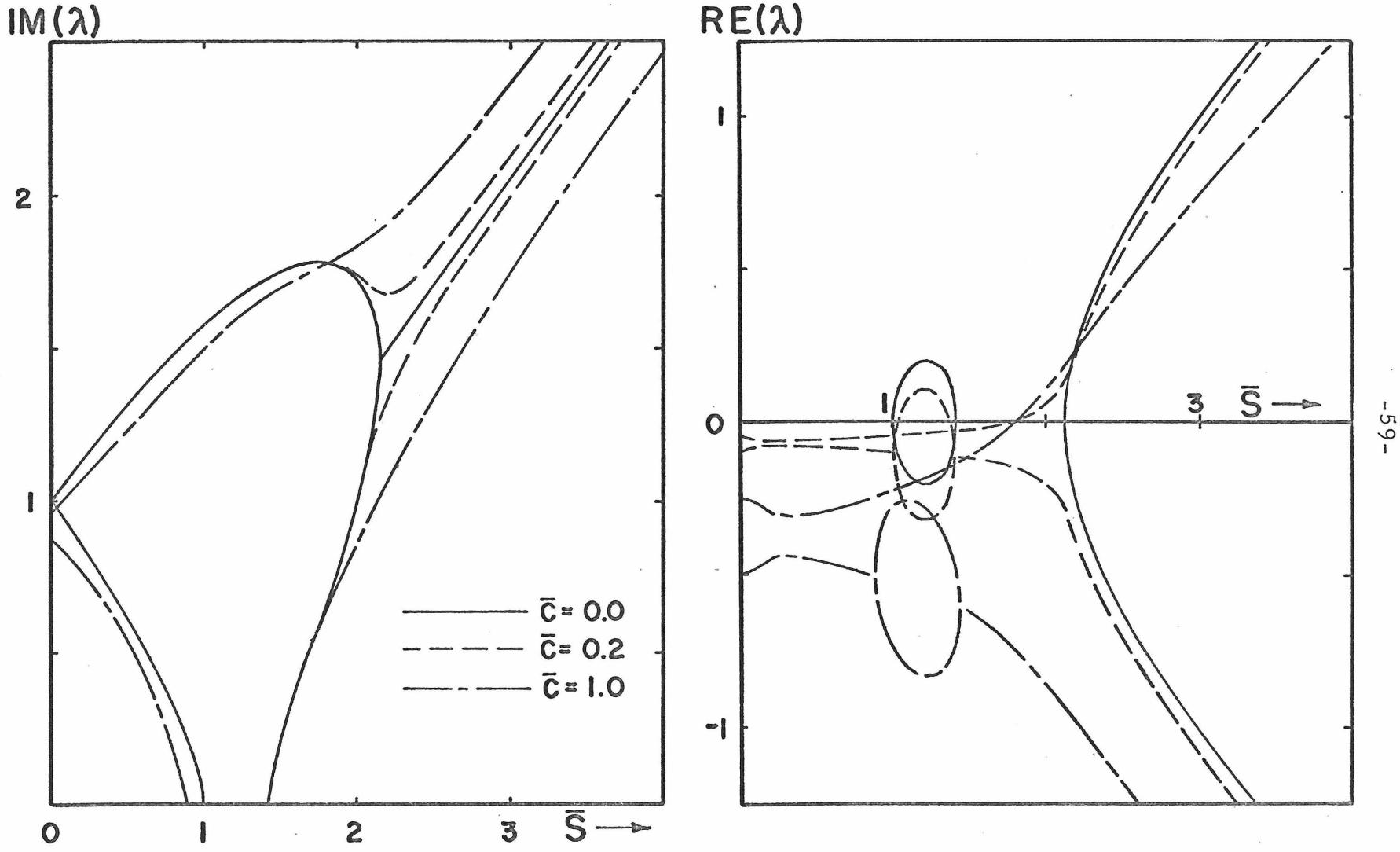

Fig. 13: Frequency-speed diagram with foundation damping ($\Delta\bar{m}=1.0$, $\Delta\bar{k}=1.0$)

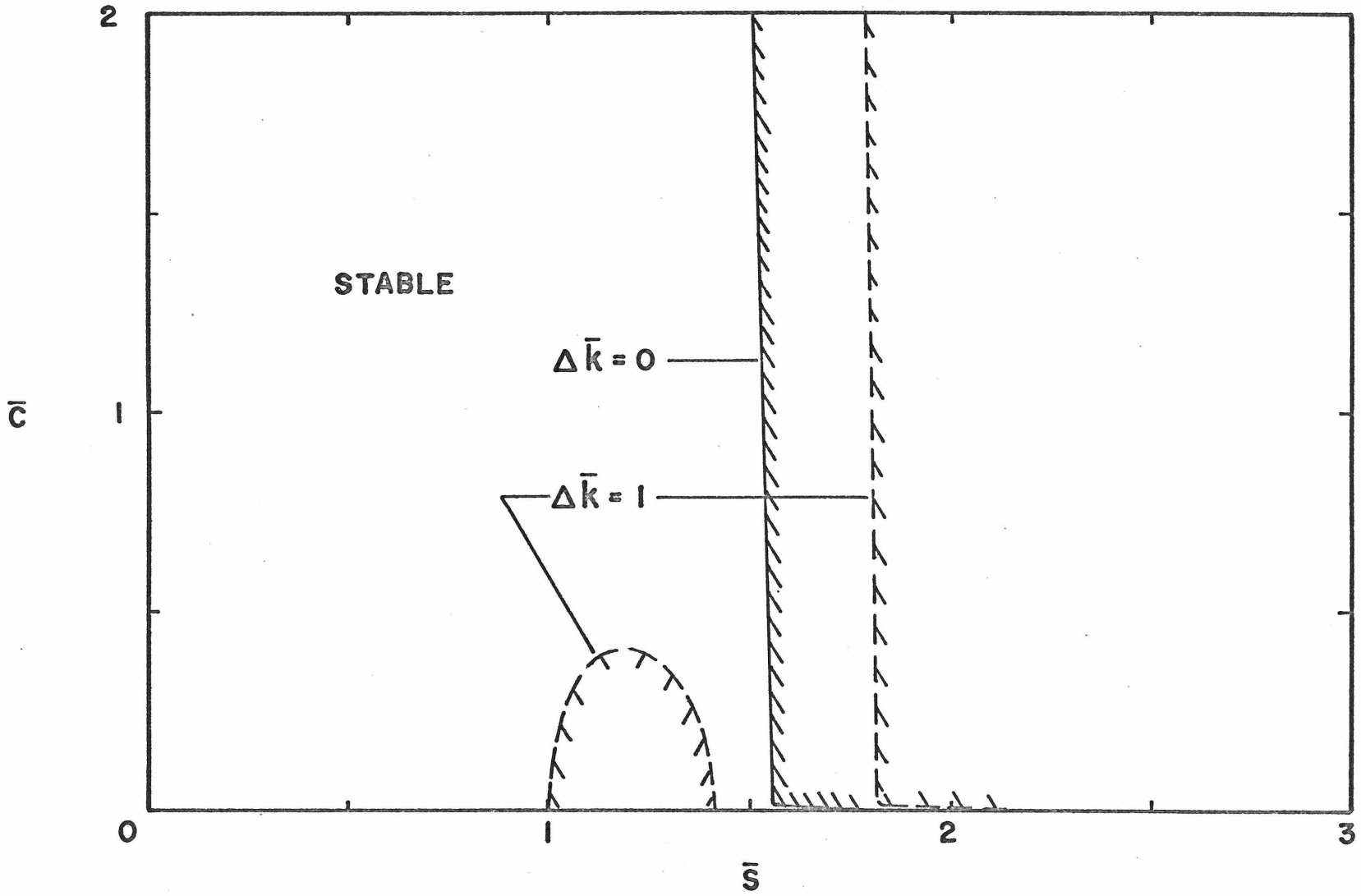

Fig. 14: Stability boundaries as a function of foundation damping for Figures 12 and 13.

As the foundation damping is increased, the general tendency of the Re$\{\lambda\}$ curves is to shift downward. Below the critical speed ($\bar{s}=1$), the amplitude of the motion will decay due to the negative Re$\{\lambda\}$ contribution. In the moving spring-mass case, Figure 13, the stiffness instability zone narrows with increasing foundation damping, and eventually disappears completely. The terminal instability zone is still present, but in general the magnitude of Re$\{\lambda\}$ is less than the value in the undamped case, so that the amplitude grows at a lesser rate. Note, however, that the terminal stable velocity, $\bar{s}^*$, shifts toward a lower value in both cases, so that in neglecting foundation damping one would predict too high a terminal velocity $\bar{s}^*$. This will be discussed further as an initial value problem in the next section.

Figure 14 shows in detail the behavior of the terminal stability boundaries of Figures 12 and 13, and the behavior of the stiffness instability region of Figure 13, as the foundation damping coefficient $\bar{c}$ varies.

Figures 15 and 16 correspond to data of Figures 12 and 13, except that the load damping $\bar{c}_L$ is being varied and the foundation damping $\bar{c}$ is taken as zero. Below $\bar{s}=1$, the behavior is as expected, with Re$\{\lambda\}$ less than zero, so that the amplitude decays exponentially. For $\bar{s}>1$, however, a positive Re$\{\lambda\}$ appears, indicating unstable behavior beyond that point. The behavior of the system in this region

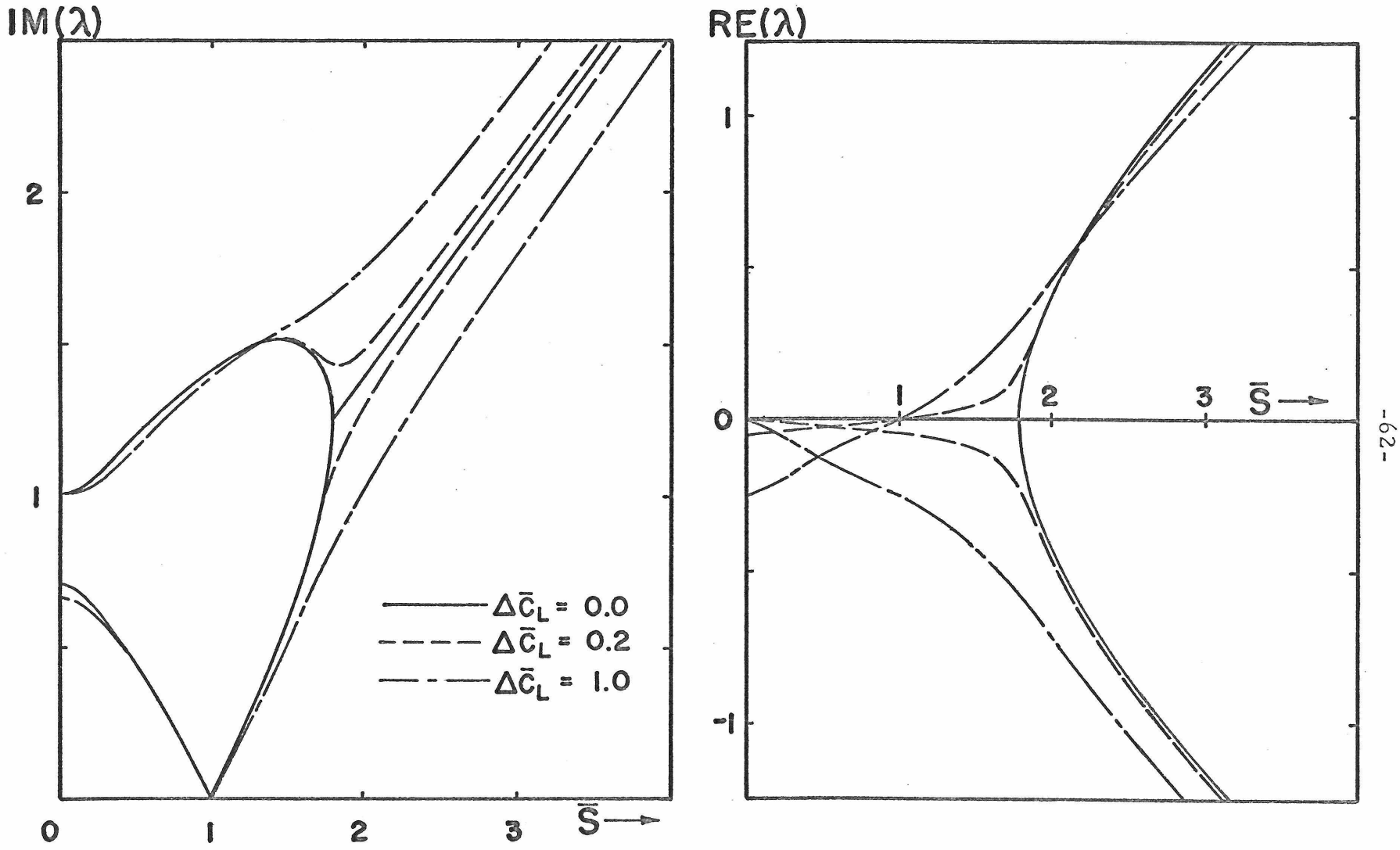

Fig. 15: Frequency-speed diagram, mass only ($\Delta\bar{m}$=1.0), with load damping.

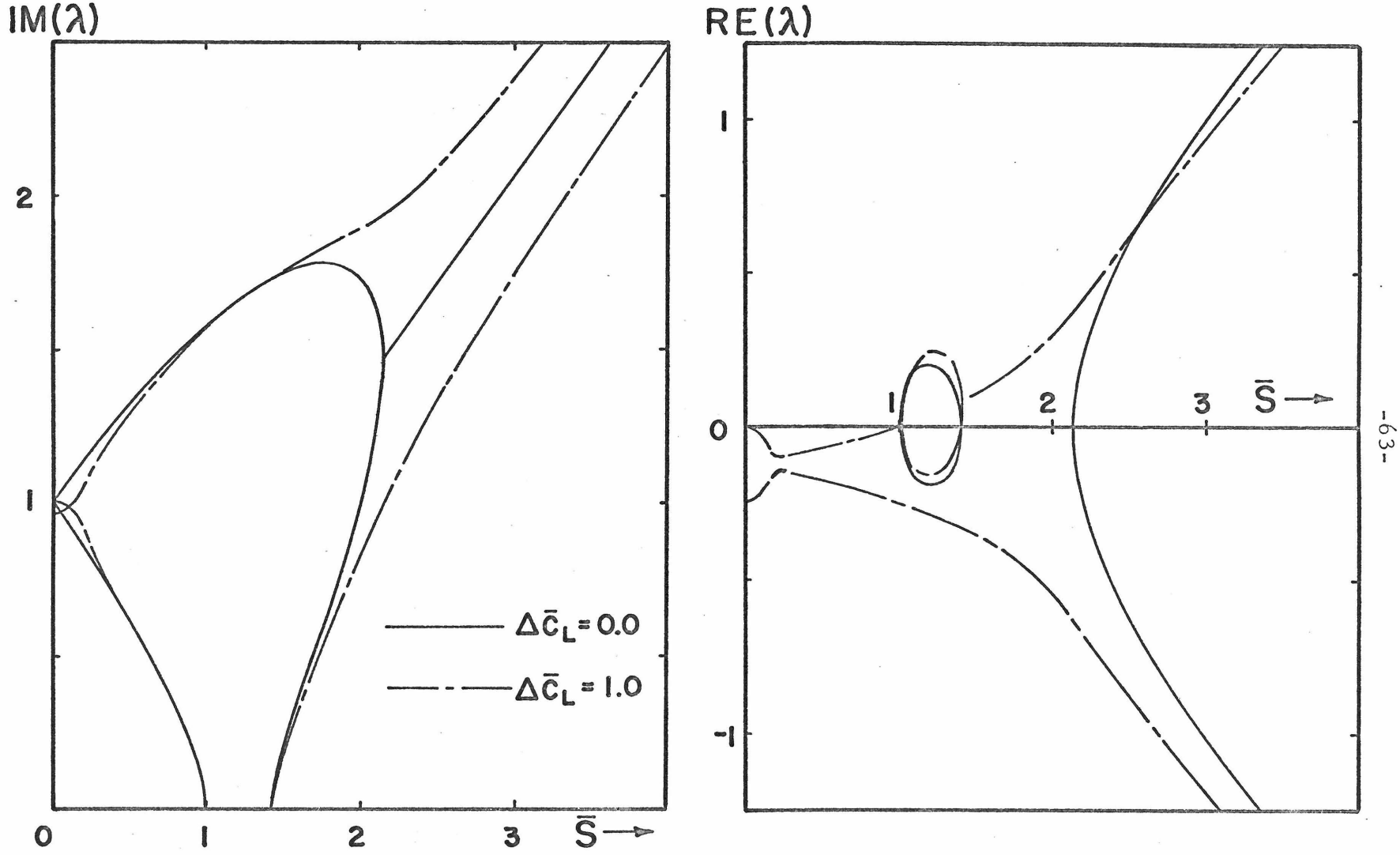

Fig. 16: Frequency-speed diagram with load damping ($\Delta\bar{m}$=1. 0, $\Delta\bar{k}$ = 1. 0).

when load damping and foundation damping are simultaneously present appears to be worthy of further study.

2.7 Solutions to Initial Value Problems (Damped)

To further understand the qualitative behavior of the damped system, the damped forms of Equations (2.30) and (2.31) were solved numerically using a standard differential equation solving routine. Figure 17 shows the transient response of $\alpha(\tau)$ and $\beta(\tau)$ for the undamped case and with two values of foundation damping. Note that even in the undamped case, the behavior of $\alpha(\tau)$ and $\beta(\tau)$ is highly nonlinear, as was discussed following Equation (2.103). The initial conditions in this case were chosen arbitrarily.

Figures 18a and 18b have the same parameters as Figure 9d, with added foundation damping of $\bar{c}=0.2$ and $\bar{c}=1.0$ respectively. The load speed $\bar{s}=1.25$ is in the stiffness instability region for the undamped case. Figure 13, which is the Frequency-Speed plot for these cases, shows that as damping is increased, the positive value of $\mathrm{Re}\{\lambda\}$ decreases in magnitude, and finally becomes negative. Figures 18a and 18b support this conclusion.

One of the more important conclusions in section 2.2.3 was that when foundation damping is added, the terminal velocity $\bar{s}^*$ decreases. From Figure 13, it is apparent that at $\bar{s}=2.0$ (which in the undamped case gave an oscillatory response) the response with sufficient

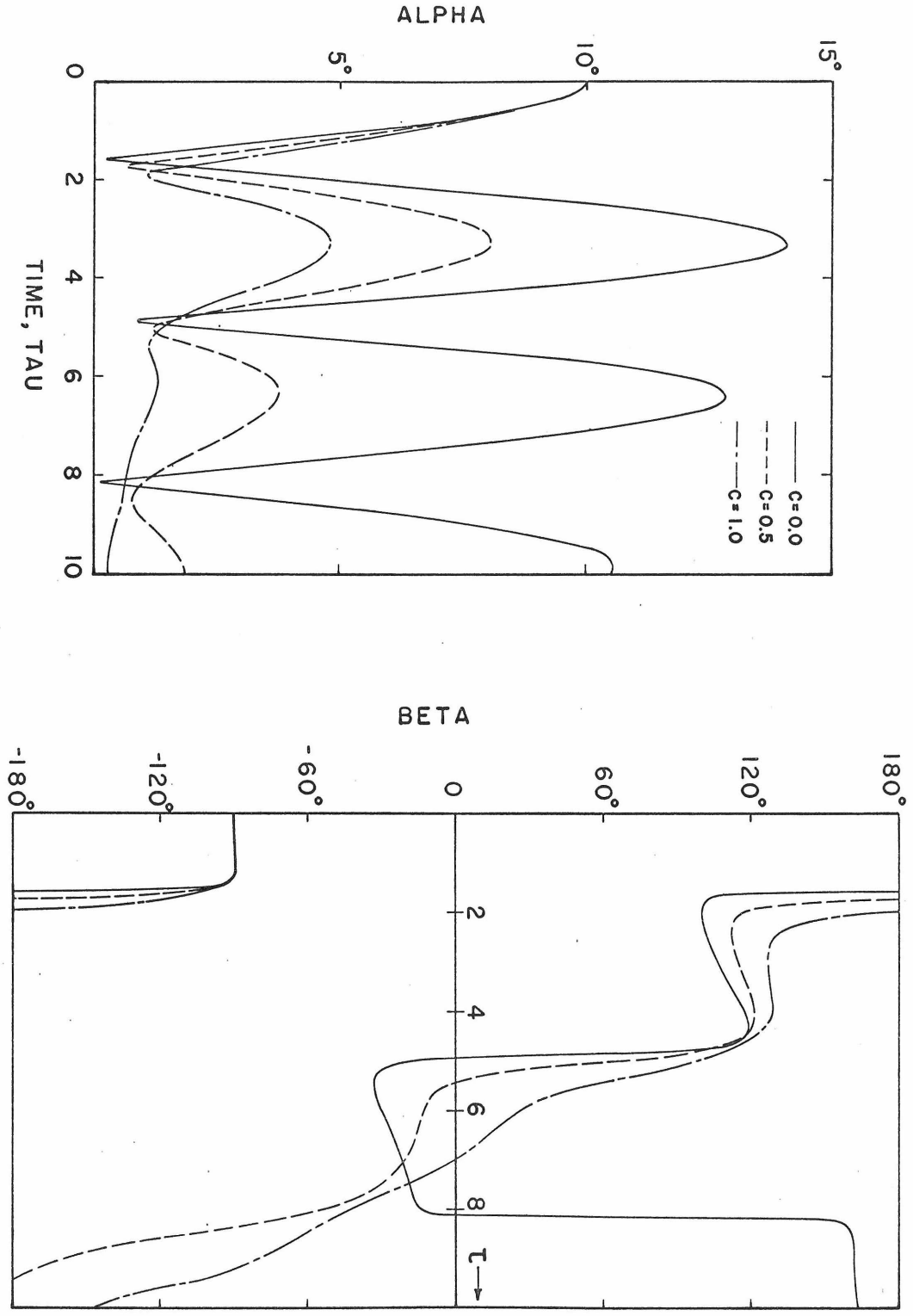

Fig. 17: Influence of foundation damping below critical speed.

($\bar{s}$=0.5, $\Delta\bar{m}$=1.0, $\Delta\bar{k}$=1.0, $\bar{c}_L$= 0.0, $\bar{c}$=0.0, 0.5, 1.0).

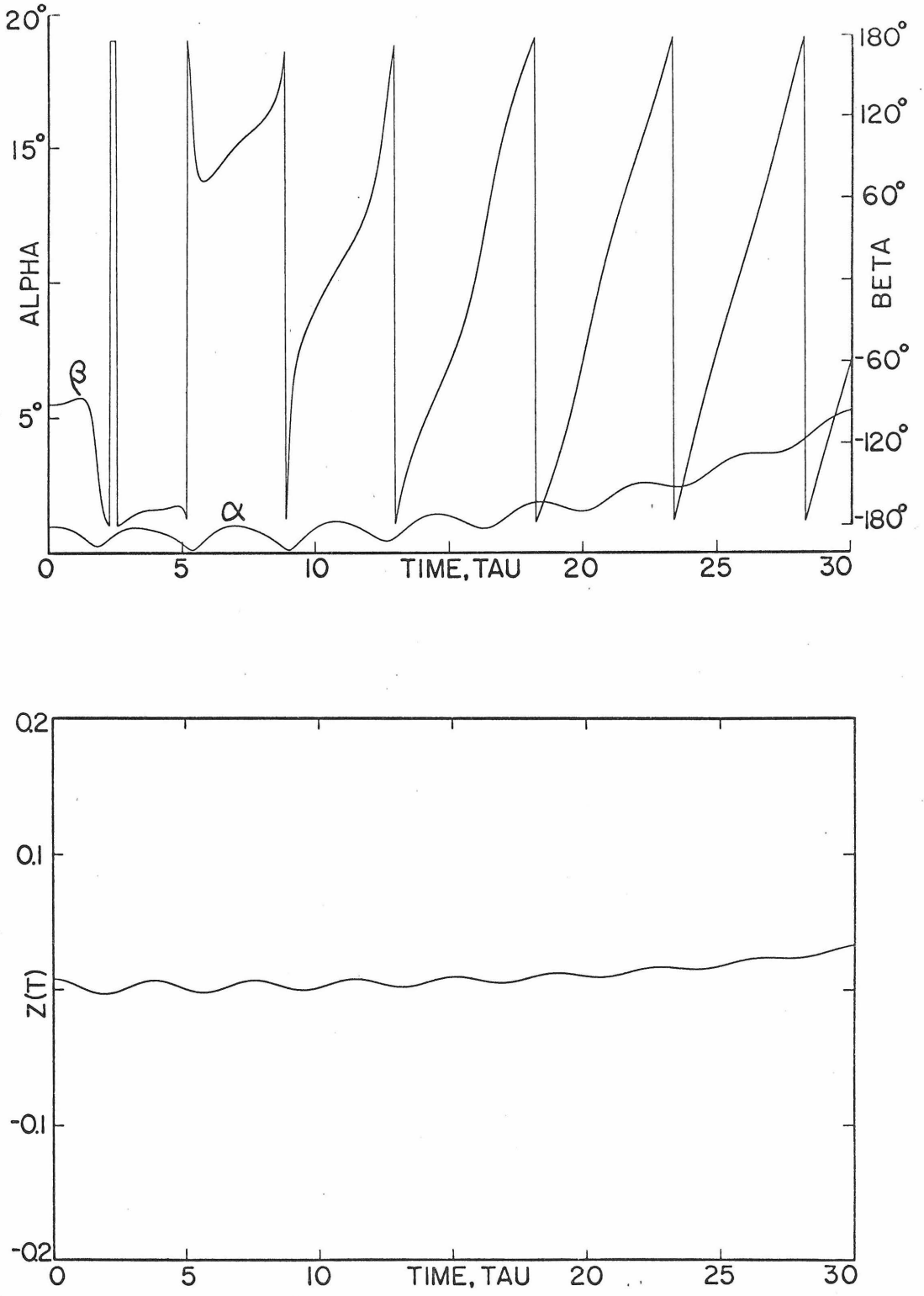

Fig. 18a: Lightly damped response in stiffness instability region. ($\Delta\bar{m}=1.0$, $\Delta\bar{k}=1.0$, $\bar{c}=0.2$, $\bar{c}_L=0.0$, $\bar{s}=1.25$).

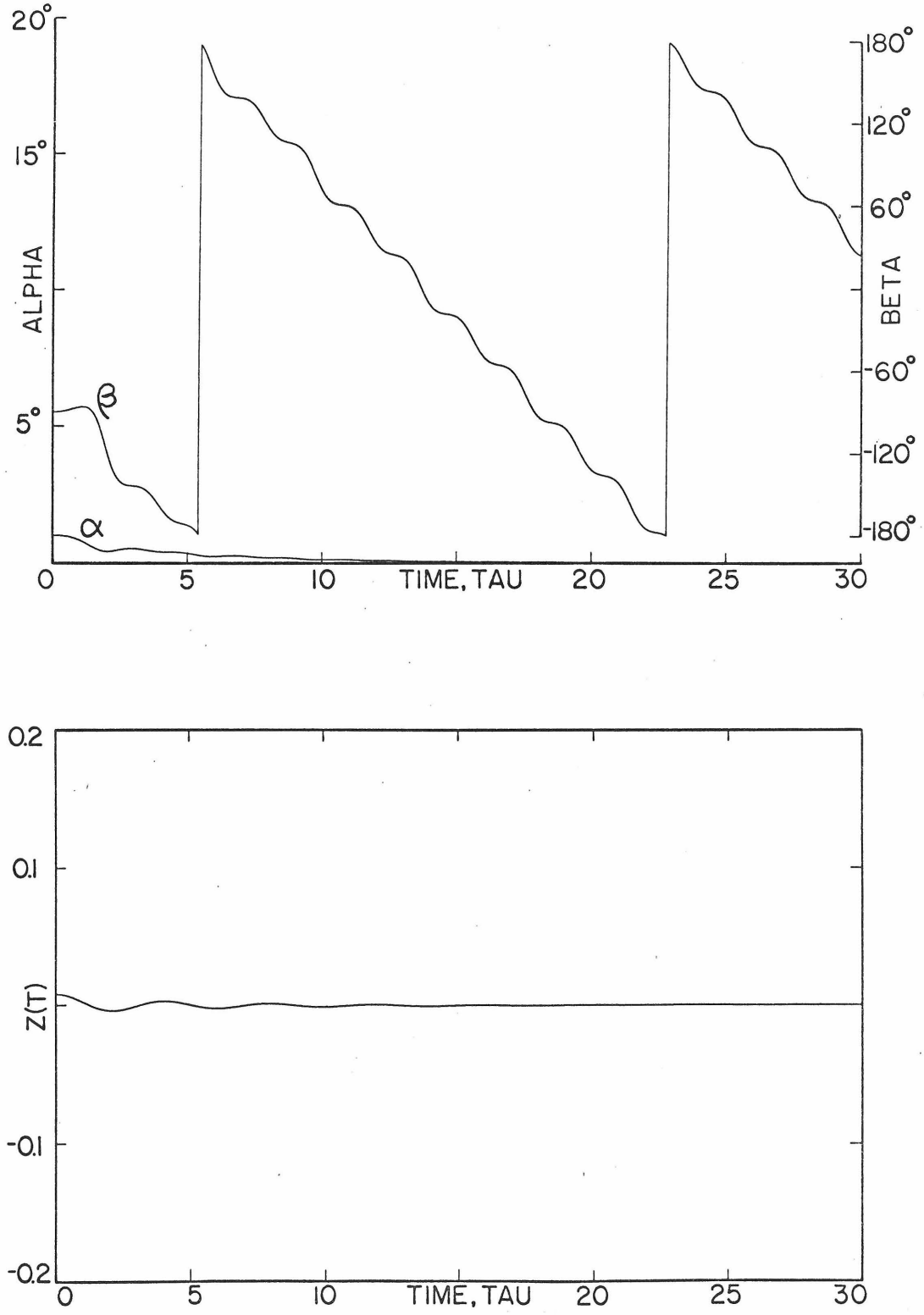

Fig. 18b: Moderately damped response in stiffness instability region.

($\Delta\bar{m}$=1.0, $\Delta\bar{k}$=1.0, $\bar{c}$=1.0, $\bar{c}_L$=0.0, $\bar{s}$=1.25).

foundation damping should become unstable. Figure 19 has the same parameters as Figure 11 (the undamped oscillatory case), with the exception of added foundation damping $\bar{c} = 1.0$. In this example, the initial conditions were such that the higher of the two frequency components, $\omega_u \cong 1.83$, is the only one present. The period of the oscillatory part of $z(\tau)$ is then $\frac{2\pi}{1.83} = 3.43$, agreeing well with the numerical solution. After a few cycles, the negative exponential component has decayed appreciably, and the positive exponential component may be estimated from the response of $z(\tau)$. If z_1 and z_2 are peaks of the response, with corresponding times τ_1 and τ_2, the exponential component, μ, is given approximately by:

$$\mu \cong \frac{1}{\tau_2 - \tau_1} \cdot \mathrm{Ln}\left(\frac{z_2}{z_1}\right)$$

Using the peaks at $\tau_1 \cong 17.1$ and $\tau_2 \cong 27.2$, with corresponding values $z_1 \cong .46$ and $z_2 \cong 1.37$, the calculated value of μ is 0.108. The positive value of $\mathrm{Re}\{\lambda\}$ as calculated from the fourth order polynomial (2.45) for this case is 0.1070, agreeing quite well with the numerical solution.

2.8 Discussion

The techniques and results of this chapter are fundamental to understanding the dynamic behavior of the three degree of freedom rigid disk and elastic disk problems presented in the following chapters. In each case, the transformation (2.28) is used to reduce

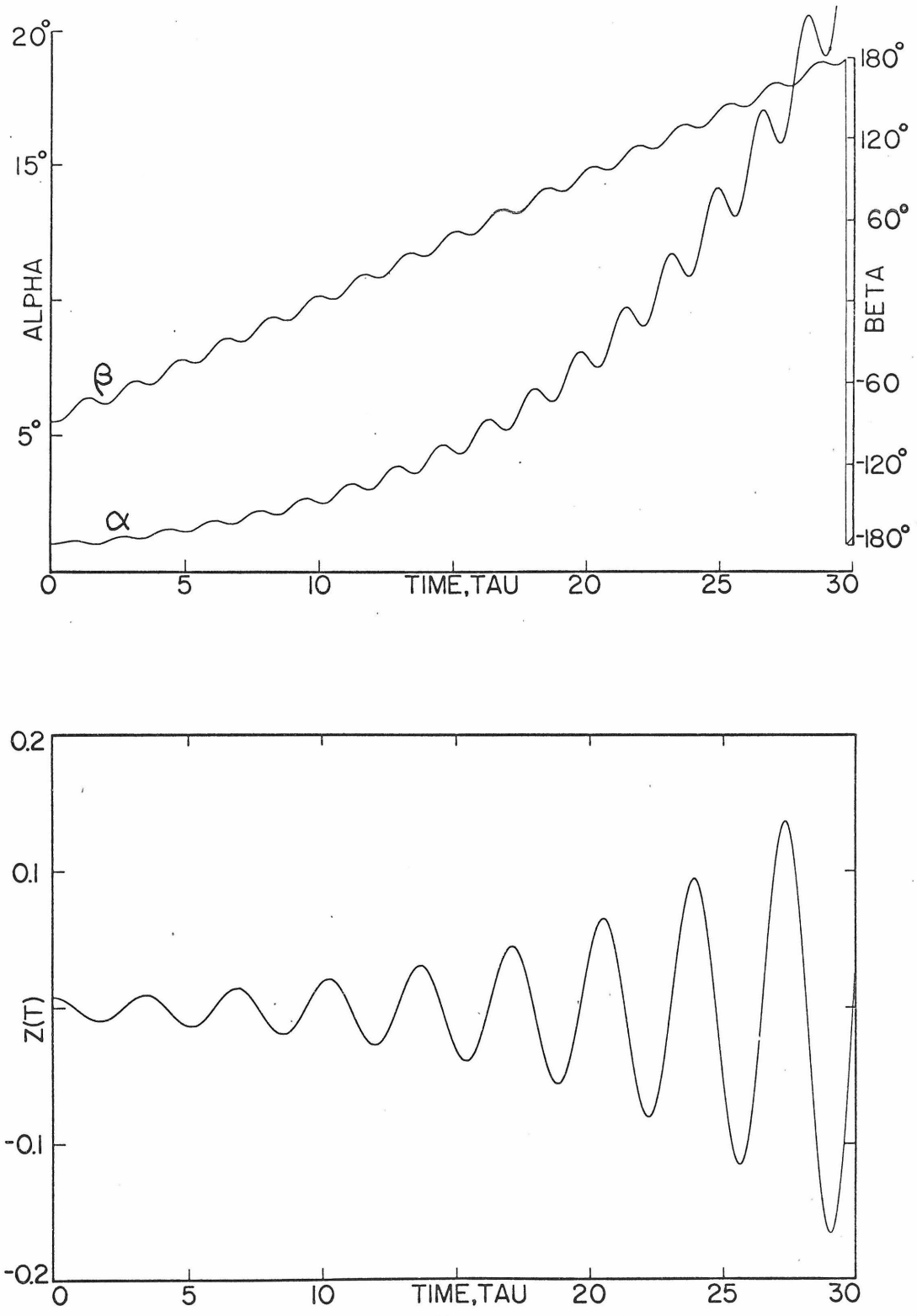

Fig. 19: Damped response in supercritical region.

($\Delta\bar{m}$=1.0, $\Delta\bar{k}$=1.0, $\bar{c}$=1.0, $\bar{c}_L$=0.0, $\bar{s}$=2.0).

a nonlinear set of differential equations to a set of coupled linear differential equations with periodic coefficients. The second transformation (2. 32) yields a linear set of coupled differential equations with constant coefficients, so that the equations may be arranged as an ordinary eigenvalue problem. The eigenvalues are plotted as a function of load speed, and the resulting Frequency-Speed diagrams provide one of the major sources of information about the dynamic response of the disk-spring-mass system. When the eigenvalues are all pure imaginary, the motion of moving mass is given by a simple linear combination of the corresponding frequencies. Further, the motion of the disk as seen from a reference frame rotating with the mass will appear as a linear combination of these frequencies.

The two types of instabilities, and instability regions, discussed in this chapter will appear in the other problems as well. In general, the speed ranges corresponding to the instability regions will be immediately apparent from the Frequency-Speed diagram. Hence, the Frequency-Speed diagram actually contains information about transient response and stability as well as steady-state response.

III. THREE DEGREE OF FREEDOM RIGID DISK

3.1 Introduction

The three degree of freedom rigid disk problem discussed in this chapter is in many ways similar to the two degree of freedom problem of the previous chapter. However, the addition of another degree of freedom introduces a third type of dynamic instability which arises from modal coupling. The three basic types of instability are fundamental to understanding the complex behavior of elastic disks.

The solution procedure is identical to that in the previous chapter. The nonlinear equations describing the dynamic response of the disk-spring-mass system are transformed into a linear set of coupled differential equations with constant coefficients. The equations may then be written as a matrix eigenvalue problem, so that an exact solution may be obtained.

3.2 Formulation of Equations of Motion

If the rigid disk of Chapter 2 (refer to Figure 1) is given an additional degree of freedom by allowing the disk to translate vertically, then deflection of the disk $u(r, \theta, t)$ for small angles $\alpha(t)$ is:

$$u(r, \theta, t) = r \cdot \alpha(t) \cdot \sin\left[\theta - \beta(t)\right] + v(t) \qquad (3.1)$$

Thus, the vertical displacement of the center of the disk is given by $v(t)$, and the Euler angles $\alpha(t)$ and $\beta(t)$ are defined as before. The disk is assumed to be supported by a Winkler foundation of modulus k as in chapter 2.

In this case, the kinetic energy, potential energy, and dissipation function as defined in (2.2), (2.4), and (2.6) respectively, become:

$$T_D = \pi\rho h\left[\frac{1}{4}a^4(\dot{\alpha}^2 + \alpha^2\dot{\beta}^2) + a^2(\dot{v}^2)\right] \tag{3.2}$$

$$V_D = \frac{1}{2}\pi k\left[\frac{1}{4}a^4(\alpha^2) + a^2(v^2)\right] \tag{3.3}$$

$$F_D = \frac{1}{2}\pi c\left\{\frac{1}{4}a^4(\dot{\alpha}^2 + \alpha^2\dot{\beta}^2) + a^2(\dot{v}^2)\right\} \tag{3.4}$$

As in Chapter 2, the deflection, velocity, and acceleration of the attached moving mass are given by (2.8), (2.10), and (2.12). The kinetic energy, potential energy, and dissipation function of the moving load then become:

$$T_L = \frac{1}{2}m_L\left\{r_L\left[\dot{\alpha}\sin(\Omega t-\beta) + \alpha(\Omega-\dot{\beta})\cos(\Omega t-\beta)\right] + \dot{v}\right\}^2 \tag{3.5}$$

$$V_L = \frac{1}{2}k_L\left[r_L\alpha\sin(\Omega t-\beta) + v\right]^2 \tag{3.6}$$

$$F_L = \frac{1}{2}c_L\left\{r_L\left[\dot{\alpha}\sin(\Omega t-\beta) + \alpha(\Omega-\dot{\beta})\cos(\Omega t-\beta)\right] + \dot{v}\right\}^2 \tag{3.7}$$

The Lagrangian and dissipation functions for the system consisting of the three degree of freedom disk with the moving spring, mass, and dashpot are then:

$$L = T - V = (T_D + T_L) - (V_D + V_L) \tag{3.8}$$

$$F = F_D + F_L \tag{3.9}$$

Using Lagrange's Equations (2.24), a set of three coupled nonlinear differential equations with periodic coefficients can be obtained. These are:

$$\begin{aligned}
&\ddot{\alpha} - \alpha\dot{\beta} + p^2\alpha + \frac{c}{2\rho h}\dot{\alpha} \\
&+\Delta\frac{m_L}{M}\left\{\left[\ddot{\alpha} - \alpha(\Omega-\dot{\beta})^2\right]\sin^2(\Omega t-\beta) + \frac{1}{r_L}\ddot{v}\sin(\Omega t-\beta)\right. \\
&\left.+\left[2\dot{\alpha}(\Omega-\dot{\beta}) - \alpha\ddot{\beta}\right]\sin(\Omega t-\beta)\cos(\Omega t-\beta)\right\} \\
&+\Delta\frac{k_L}{M}\left\{\alpha\sin^2(\Omega t-\beta) + \frac{1}{r_L}v\sin(\Omega t-\beta)\right\} \\
&+\Delta\frac{c_L}{M}\left\{\dot{\alpha}\sin^2(\Omega t-\beta) + \alpha(\Omega-\dot{\beta})\sin(\Omega t-\beta)\cos(\Omega t-\beta) + \frac{1}{r_L}\dot{v}\sin(\Omega t-\beta)\right\} = 0
\end{aligned} \tag{3.10}$$

$$\begin{aligned}
&\alpha^2\ddot{\beta} + 2\alpha\dot{\alpha}\dot{\beta} + \frac{c}{2\rho h}\alpha^2\dot{\beta} \\
&+\Delta\frac{m_L}{M}\left\{\left[\alpha^2\ddot{\beta} - 2\alpha\dot{\alpha}(\Omega-\dot{\beta})\right]\cos^2(\Omega t-\beta) - \alpha\cdot\frac{1}{r_L}\ddot{v}\cos(\Omega t-\beta)\right. \\
&\left.+\left[\alpha^2(\Omega-\dot{\beta})^2 - \alpha\ddot{\alpha}\right]\sin(\Omega t-\beta)\cos(\Omega t-\beta)\right\} \\
&-\Delta\frac{k_L}{M}\left\{\alpha^2\sin(\Omega t-\beta)\cos(\Omega t-\beta) + \alpha\frac{1}{r_L}v\cos(\Omega t-\beta)\right\} \\
&-\Delta\frac{c_L}{M}\left\{\alpha^2(\Omega-\dot{\beta})\cos^2(\Omega t-\beta) + \alpha\dot{\alpha}\sin(\Omega t-\beta)\cos(\Omega t-\beta) + \alpha\frac{1}{r_L}\dot{v}\cos(\Omega t-\beta)\right\} = 0
\end{aligned} \tag{3.11}$$

$$
\begin{aligned}
&\ddot{v}+\frac{c}{2\rho h}\dot{v}+p^2 v \\
&+\frac{m_L}{M}\left\{r_L\left[\ddot{\alpha}-\alpha(\Omega-\dot{\beta})^2\right]\sin(\Omega t-\beta)+r_L\left[2\dot{\alpha}(\Omega-\dot{\beta})-\alpha\ddot{\beta}\right]\cos(\Omega t-\beta)+\ddot{v}\right\} \\
&+\frac{k_L}{M}\left\{r_L\,\alpha\sin(\Omega t-\beta)+v\right\} \\
&+\frac{c_L}{M}\left\{r_L\left[\dot{\alpha}\sin(\Omega t-\beta)+\alpha(\Omega-\dot{\beta})\cos(\Omega t-\beta)\right]+\dot{v}\right\}=0
\end{aligned}
\tag{3.12}
$$

where, as before:

$$
\Delta=\left(\frac{2r_L}{a}\right)^2,\quad M=2\rho h\pi a^2,\quad p^2=\frac{k}{2\rho h} \tag{3.13}
$$

Using the same transformations as in Chapter 2,

$$
\begin{aligned}
C(t) &= -\alpha(t)\sin\beta(t) \\
D(t) &= \alpha(t)\cos\beta(t)
\end{aligned}
\tag{3.14}
$$

The Equations of motion (3.10), (3.11), and (3.12) become:

$$
\begin{aligned}
&\left[\left(1+\Delta\frac{m_L}{2M}\right)+\Delta\frac{m_L}{2M}\cos 2\Omega t\right]\ddot{C}+\left[\Delta\frac{m_L}{2M}\sin 2\Omega t\right]\ddot{D}+\left[\Delta\frac{m_L}{M}\cos\Omega t\right]\ddot{\bar{v}} \\
&+\left[\left(\frac{c}{2\rho h}+\Delta\frac{c_L}{2M}\right)+\Delta\frac{c_L}{2M}\cos 2\Omega t-2\Omega\Delta\frac{m_L}{2M}\sin 2\Omega t\right]\dot{C} \\
&+\left[\left(2\Omega\Delta\frac{m_L}{2M}\right)+2\Omega\Delta\frac{m_L}{2M}\cos 2\Omega t+\Delta\frac{c_L}{2M}\sin 2\Omega t\right]\dot{D}+\left[\Delta\frac{c_L}{M}\cos\Omega t\right]\dot{\bar{v}} \\
&+\left[\left(p^2+\Delta\frac{k_L}{2M}-\Omega^2\Delta\frac{m_L}{2M}\right)+\left(\Delta\frac{k_L}{2M}-\Omega^2\Delta\frac{k_L}{2M}\right)\cos 2\Omega t-\Omega\Delta\frac{c_L}{2M}\sin 2\Omega t\right]C \\
&+\left[\left(\Omega\Delta\frac{c_L}{2M}\right)+\Omega\Delta\frac{c_L}{2M}\cos 2\Omega t+\left(\Delta\frac{k_L}{2M}-\Omega^2\Delta\frac{m_L}{2M}\right)\sin 2\Omega t\right]D+\left[\Delta\frac{k_L}{M}\cos\Omega t\right]\bar{v} \\
&=0
\end{aligned}
\tag{3.15}
$$

$$\left[\Delta\frac{m_L}{2M}\sin 2\Omega t\right]\ddot{C}+\left[\left(1+\Delta\frac{m_L}{2M}\right)-\Delta\frac{m_L}{2M}\cos 2\Omega t\right]\ddot{D}+\left[\Delta\frac{m_L}{M}\sin\Omega t\right]\ddot{\bar{v}}$$
$$+\left[\left(-2\Omega\Delta\frac{m_L}{2M}\right)+2\Omega\Delta\frac{m_L}{2M}\cos 2\Omega t+\Delta\frac{c_L}{2M}\sin 2\Omega t\right]\dot{C}$$
$$+\left[\left(\frac{c}{2\rho h}+\Delta\frac{c_L}{2M}\right)-\Delta\frac{c_L}{2M}\cos 2\Omega t+2\Omega\Delta\frac{m_L}{2M}\sin 2\Omega t\right]\dot{D}+\left[\Delta\frac{c_L}{M}\sin\Omega t\right]\dot{\bar{v}}$$
$$+\left[\left(-\Omega\Delta\frac{c_L}{2M}\right)+\Omega\Delta\frac{c_L}{2M}\cos 2\Omega t+\left(\Delta\frac{k_L}{2M}-\Omega^2\Delta\frac{m_L}{2M}\right)\sin 2\Omega t\right]C \qquad (3.16)$$
$$+\left[\left(p^2+\Delta\frac{k_L}{2M}-\Omega^2\Delta\frac{m_L}{2M}\right)-\left(\Delta\frac{k_L}{2M}-\Omega^2\Delta\frac{m_0}{2M}\right)\cos 2\Omega t+\Omega\Delta\frac{c_L}{2M}\sin 2\Omega t\right]D+\left[\Delta\frac{k_L}{M}\sin\Omega t\right]\bar{v}$$
$$= 0$$

$$\left[1+\frac{m_L}{M}\right]\ddot{\bar{v}}+\left[\frac{m_L}{M}\cos\Omega t\right]\ddot{C}+\left[\frac{m_L}{M}\sin\Omega t\right]\ddot{D}$$
$$+\left[\frac{c}{2\rho h}+\frac{c_L}{M}\right]\dot{\bar{v}}+\left[-2\Omega\frac{m_L}{M}\sin\Omega t+\frac{c_L}{M}\cos\Omega t\right]\dot{C} \qquad (3.17)$$
$$+\left[2\Omega\frac{m_L}{M}\cos\Omega t+\frac{c_L}{M}\sin\Omega t\right]\dot{D}+\left[p^2+\frac{k_L}{M}\right]\bar{v}$$
$$+\left[\left(\frac{k_L}{M}-\Omega^2\frac{m_L}{M}\right)\cos\Omega t-\Omega\frac{c_L}{M}\sin\Omega t\right]C+\left[\left(\frac{k_L}{M}-\Omega^2\frac{m_L}{M}\right)\sin\Omega t+\Omega\frac{c_L}{M}\cos\Omega t\right]D=0$$

where $\bar{v}=\frac{1}{r_L}v$. The vertical displacement v(t) has been normalized in this way so that the load radius r_L appears only in $\Delta=\left(\frac{2r_L}{a}\right)^2$ in the equations above.

As in the two degree of freedom problem, the equations describing the system may be transformed to an equivalent set of differential equations by using the transformation (2.32). That is, let A(t) and B(t) be related to C(t) and D(t) by:

$$A(t)=C(t)\cos\Omega t+D(t)\sin\Omega t$$
$$B(t)=-C(t)\sin\Omega t+D(t)\cos\Omega t \qquad (3.18)$$

The vertical displacement $\bar{v}(t)$ remains the same. Again, this transformation corresponds to a change from the fixed reference frame to a frame rotating with angular velocity Ω, in which the disk displacement is $u'(r,\bar{\Phi},t)=r\left[A(t)\cos\bar{\Phi}+B(t)\sin\bar{\Phi}\right]+v(t)$. The result of the transformation (3.18) is a set of three coupled linear differential equations with constant coefficients. These equations involve coupling in the second derivative terms as well as the lower order terms, but it is relatively easy to rearrange the equations so that the second derivatives uncouple. The equations, in normalized form, are:

$$(1+\bar{m}+\Delta\bar{m})\frac{d^2A}{d\tau^2}+(\bar{c}+\bar{m}\,\bar{c}+\Delta\bar{c}_L)\frac{dA}{d\tau}-2(1+\bar{m})\bar{s}\frac{dB}{d\tau}$$
$$+(\Delta\bar{c}_L-\Delta\bar{m}\,\bar{c})\frac{d\bar{v}}{d\tau}+\left[(1+\bar{m})(1-\bar{s}^2)+\Delta\bar{k}\right]A \qquad (3.19)$$
$$-\bar{s}\,\bar{c}(1+\bar{m})B+(\Delta\bar{k}-\Delta\bar{m})\bar{v}=0$$

$$\frac{d^2B}{d\tau^2}+2\bar{s}\frac{dA}{d\tau}+\bar{c}\frac{dB}{d\tau}+\bar{s}\,\bar{c}A+(1-\bar{s}^2)B=0 \qquad (3.20)$$

$$(1+\bar{m}+\Delta\bar{m})\frac{d^2\bar{v}}{d\tau^2}+(\bar{c}_L-\bar{m}\,\bar{c})\frac{dA}{d\tau}+2\bar{m}\,\bar{s}\frac{dB}{d\tau}$$
$$+(\bar{c}+\bar{c}\Delta\bar{m}+\bar{c}_L)\frac{d\bar{v}}{d\tau}+(\bar{k}-\bar{m}+\bar{m}\,\bar{s}^2)A \qquad (3.21)$$
$$+\bar{s}\,\bar{c}\,\bar{m}\,B+(1+\Delta\bar{m}+\bar{k})\bar{v}=0$$

As in Chapter 2, the quantities appearing in (3.19), (3.20), and (3.21) are:

$$\tau = pt \ , \quad \bar{m} = \frac{m_L}{M} \ , \quad \bar{k} = \frac{1}{p^2} \cdot \frac{k_L}{M}$$
$$\bar{c}_L = \frac{1}{p} \frac{c_L}{M}, \quad \bar{c} = \frac{1}{p} \cdot \frac{c}{2\rho h} \ , \quad \bar{s} = \frac{\Omega}{p} \tag{3.22}$$

3.3 Solution of Equations of Motion

Equations (3.20), (3.21), and (3.22) may be rewritten as a matrix differential equation:

$$P \frac{d\underline{x}}{d\tau} = Q\underline{x} \ , \ \underline{x}(0) = \underline{f} \tag{3.23}$$

where $\underline{x}$ is a six element column vector and P and Q are six by six matrices with constant coefficients:

$$\underline{x} = \begin{Bmatrix} \bar{v} \\ A \\ B \\ \frac{d\bar{v}}{d\tau} \\ \frac{dA}{d\tau} \\ \frac{dB}{d\tau} \end{Bmatrix} , \quad P = \begin{bmatrix} 1 & 0 & 0 & 0 & 0 & 0 \\ 0 & 1 & 0 & 0 & 0 & 0 \\ 0 & 0 & 1 & 0 & 0 & 0 \\ 0 & 0 & 0 & 1+\bar{m}+\Delta\bar{m} & 0 & 0 \\ 0 & 0 & 0 & 0 & 1+\bar{m}+\Delta\bar{m} & 0 \\ 0 & 0 & 0 & 0 & 0 & 1 \end{bmatrix} \tag{3.24}$$

$$Q = \begin{bmatrix} 0 & 0 & 0 & 1 & 0 & 0 \\ 0 & 0 & 0 & 0 & 1 & 0 \\ 0 & 0 & 0 & 0 & 0 & 1 \\ -(1+\Delta\bar{m}+\bar{k}) & -(\bar{k}-\bar{m}+\bar{m}\bar{s}^2) & -\bar{s}\bar{c}\bar{m} & -(\bar{c}+\bar{c}\Delta\bar{m}+\bar{c}_L) & -(\bar{c}_L-\bar{m}\bar{c}) & -2\bar{m}\bar{s} \\ -(\Delta\bar{k}-\Delta\bar{m}) & -[(1+\bar{m})(1-\bar{s}^2)+\Delta\bar{k}] & \bar{s}\bar{c}(1+\bar{m}) & -(\Delta\bar{c}_L-\Delta\bar{m}\bar{c}) & -(\bar{c}+\bar{m}\bar{c}+\Delta\bar{c}_L) & 2(1+\bar{m})\bar{s} \\ 0 & -\bar{s}\bar{c} & -(1-\bar{s}^2) & 0 & -2\bar{s} & -\bar{c} \end{bmatrix}$$

Premultiplying by P^{-1}, Equation (3.23) becomes:

$$\frac{d\underline{x}}{d\tau} = P^{-1}Q\underline{x} \tag{3.25}$$

Assuming a solution of the form

$$\underline{x} = e^{\lambda\tau}\underline{\Phi} \tag{3.26}$$

where $\underline{\Phi}$ is a constant vector, (3.25) becomes:

$$(P^{-1}Q - \lambda I)\underline{x} = 0 \tag{3.27}$$

For a nontrivial solution, the determinant of $(P^{-1}Q - \lambda I)$ must vanish:

$$|P^{-1}Q - \lambda I| = 0 \tag{3.28}$$

Expanding this determinant, a sixth order polynomial for λ is obtained:

$$a_0 + a_1\lambda + a_2\lambda^2 + a_3\lambda^3 + a_4\lambda^4 + a_5\lambda^5 + a_6\lambda^6 = 0 \tag{3.29}$$

Although the analytic expressions for $a_0, \ldots a_6$ have been obtained by straightforward computation of Equation (3.28), it is generally more convenient to evaluate the eigenvalues and eigenvectors of (3.28) by using one of the standard numerical eigenvalue routines on a digital computer. This technique is used throughout the remainder of this chapter, unless otherwise indicated.

When there is no damping in the system ($\overline{c}_L = \overline{c} = 0$), the sixth order equation for λ reduces to a cubic equation in λ^2. Thus, if only the eigenfrequencies of the system are desired, it may be more convenient

to solve the cubic equation rather than solve the matrix eigenvalue problem. The cubic equation for λ^2 is:

$$b_0 + b_2\lambda^2 + b_4\lambda^4 + b_6\lambda^6 = 0 \tag{3.30}$$

where

$$b_0 = \left[1+(1+\Delta)\bar{k}\right] - 2\left[1+(1+\Delta)\bar{k}\right]\bar{s}^2 + (1+\bar{k})\bar{s}^4$$

$$b_2 = \left[3+\bar{m}+\Delta\bar{m}+(2+2\Delta)\bar{k}\right] + \left[(2-\Delta)\bar{k} - (2\bar{m}-\Delta\bar{m})\right]\bar{s}^2 + (1+\bar{m})\bar{s}^4$$

$$b_4 = \left[3+2\bar{m}+2\Delta\bar{m}+(1+\Delta)\bar{k}\right] + \left[2+2\bar{m}-\Delta\bar{m}\right]\bar{s}^2$$

$$b_6 = 1+\bar{m}+\Delta\bar{m}$$

When the eigenvectors are also desired, it is easier to return to the form (3.28).

3.4 Properties of the Solutions to the Equations of Motion

Case 1: $\bar{m} = \bar{k} = \bar{c}_L = \bar{c} = 0$.

This corresponds to the free vibration of the disk alone, with no moving mass or spring. The matrix differential Equation (3.25) becomes:

$$\frac{d}{d\tau}\begin{Bmatrix} \bar{v} \\ A \\ B \\ \frac{d\bar{v}}{d\tau} \\ \frac{dA}{d\tau} \\ \frac{dB}{d\tau} \end{Bmatrix} = \begin{bmatrix} 0 & 0 & 0 & 1 & 0 & 0 \\ 0 & 0 & 0 & 0 & 1 & 0 \\ 0 & 0 & 0 & 0 & 0 & 1 \\ -1 & 0 & 0 & 0 & 0 & 0 \\ 0 & \bar{s}^2-1 & 0 & 0 & 0 & 2\bar{s} \\ 0 & 0 & \bar{s}^2-1 & 0 & -2\bar{s} & 0 \end{bmatrix} \begin{Bmatrix} \bar{v} \\ A \\ B \\ \frac{d\bar{v}}{d\tau} \\ \frac{dA}{d\tau} \\ \frac{dB}{d\tau} \end{Bmatrix} \tag{3.31}$$

The characteristic Equation (3.28) is therefore

$$(\lambda^2+1)\left[\lambda^2+(1+\bar{s})^2\right]\cdot\left[\lambda^2+(1-\bar{s})^2\right]=0 \tag{3.32}$$

$$\Rightarrow \lambda_{1,2}=\pm i(1+\bar{s}),\ \lambda_{3,4}=\pm i(1-\bar{s}),\ \lambda_{5,6}=\pm i \tag{3.33}$$

Corresponding to these six eigenvalues are the six complex eigenvectors:

$$\underline{x}_1=\begin{Bmatrix} 0 \\ -1 \\ -i \\ 0 \\ -i(1+\bar{s}) \\ 1+\bar{s} \end{Bmatrix},\quad \underline{x}_2=\begin{Bmatrix} 0 \\ -1 \\ i \\ 0 \\ i(1+\bar{s}) \\ 1+\bar{s} \end{Bmatrix},\quad \underline{x}_3=\begin{Bmatrix} 0 \\ 1 \\ -i \\ 0 \\ i(1-\bar{s}) \\ 1-\bar{s} \end{Bmatrix},\quad \underline{x}_4=\begin{Bmatrix} 0 \\ 1 \\ i \\ 0 \\ -i(1-\bar{s}) \\ 1-\bar{s} \end{Bmatrix} \tag{3.34}$$

$$\underline{x}_5 = \begin{Bmatrix} 1 \\ 0 \\ 0 \\ i \\ 0 \\ 0 \end{Bmatrix} \quad , \quad \underline{x}_6 = \begin{Bmatrix} 1 \\ 0 \\ 0 \\ -i \\ 0 \\ 0 \end{Bmatrix}$$

The general solution is thus of the form:

$$\begin{aligned} \underline{x}(\tau) = {} & c_1 e^{i(1+\bar{s})\tau} \underline{x}_1 + c_2 e^{-i(1+\bar{s})\tau} \underline{x}_2 \\ & + c_3 e^{i(1-\bar{s})\tau} \underline{x}_3 + c_4 e^{-i(1-\bar{s})\tau} \underline{x}_4 \\ & + c_5 e^{i\tau} \underline{x}_5 + c_6 e^{-i\tau} \underline{x}_6 \end{aligned} \tag{3.35}$$

As in Chapter 2, $\underline{x}(\tau)$ will be real if $c_2 = \tilde{c}_1$, $c_4 = \tilde{c}_3$, and $c_6 = \tilde{c}_5$. The constants c_i may be written:

$$\begin{aligned} c_1 &= d_1 + id_2 , \quad c_3 = d_3 + id_4 , \quad c_5 = d_5 + id_6 \\ c_2 &= d_1 - id_2 , \quad c_4 = d_3 - id_4 , \quad c_6 = d_5 - id_6 \end{aligned} \tag{3.36}$$

The expression for $\underline{x}(\tau)$ may then be written in real form as:

$$\begin{aligned} \underline{x}(\tau) = {} & 2d_1 \underline{r}_1(\tau) + 2d_2 \underline{r}_2(\tau) + 2d_3 \underline{r}_3(\tau) + 2d_4 \underline{r}_4(\tau) \\ & + 2d_5 \underline{r}_5(\tau) + 2d_6 \underline{r}_6(\tau) \end{aligned} \tag{3.37}$$

The vectors $\underline{r}_1(\tau)$, $\underline{r}_2(\tau)$, $\underline{r}_3(\tau)$, and $\underline{r}_4(\tau)$ correspond directly to the vectors in Equations (2.54) of Chapter 2, as would be expected by comparing (3.34) with (2.50). The terms in the six-dimensional vectors $\underline{r}_1(\tau)\ldots\underline{r}_4(\tau)$ corresponding to $\overline{v}(\tau)$ and $\frac{d\overline{v}}{d\tau}$ are zero. Hence, the physical meaning of the vectors $\underline{r}_1(\tau)\ldots\underline{r}_4(\tau)$ is exactly the same as in Chapter 2, and the discussion following Equation (2.54) applies to these motions also. The new vectors $\underline{r}_5(\tau)$ and $\underline{r}_6(\tau)$ are:

$$\underline{r}_5(\tau)=\begin{Bmatrix}\cos\tau\\0\\0\\-\sin\tau\\0\\0\end{Bmatrix}\quad,\qquad \underline{r}_6(\tau)\begin{Bmatrix}-\sin\tau\\0\\0\\-\cos\tau\\0\\0\end{Bmatrix} \tag{3.38}$$

Clearly, the vectors $\underline{r}_5(\tau)$ and $\underline{r}_6(\tau)$ correspond to vertical translational vibrations of the disk. The frequency of vibration is equal to 1 in the τ domain (p in the t domain) and is independent of the speed of the rotating reference frame because there are no wave motions associated with this mode. The Frequency-Speed plot shown in Figure 20 indicates the behavior of the eigenfrequencies for this case.

It is interesting to note that in the stationary reference frame ($\overline{s}=0$) the frequency of the vertical translational motion is equal to the frequency of the disk vibrating about a nodal diameter (refer to Equation (2.58)). This additional degeneracy, which is due to the

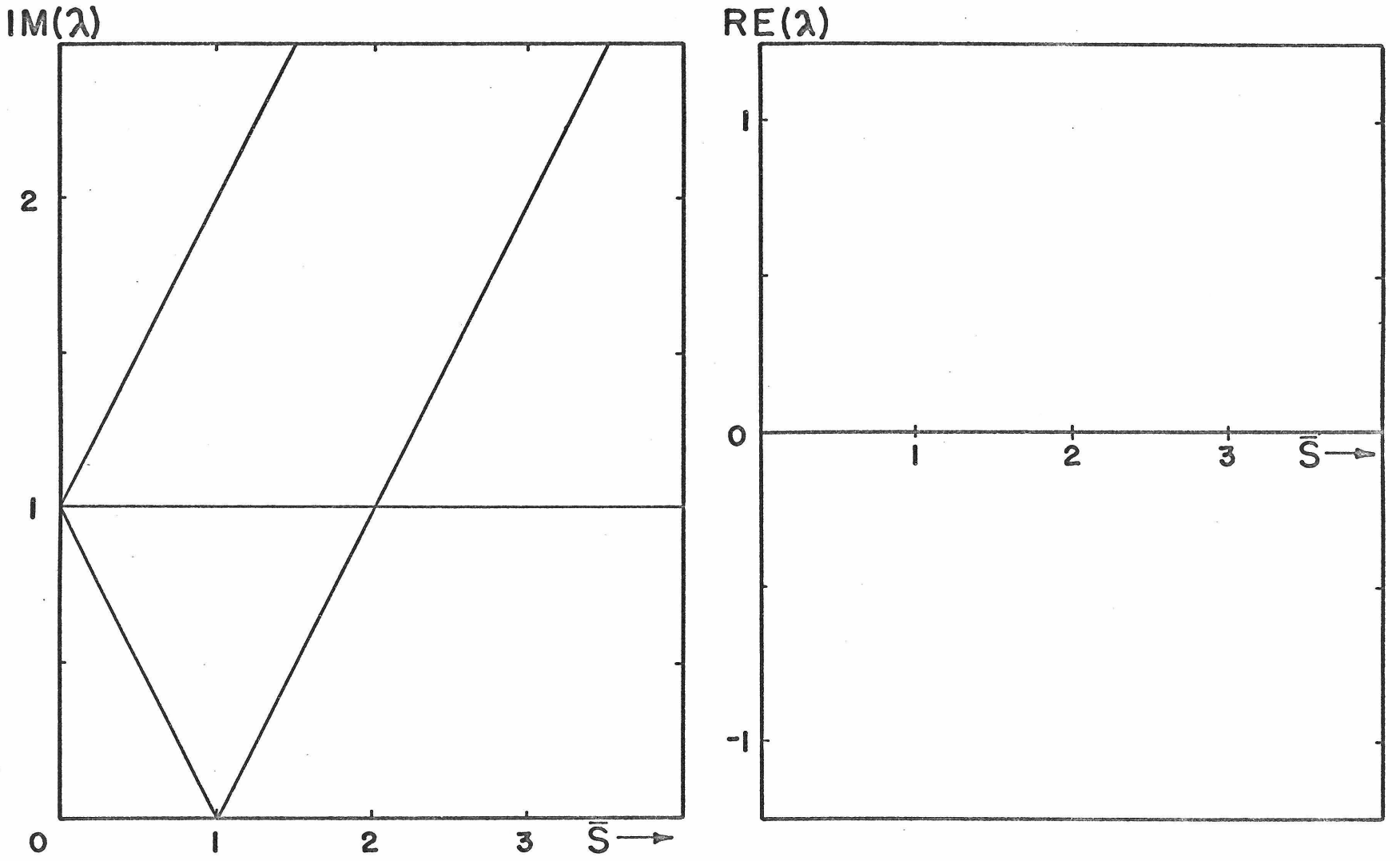

Fig. 20: Frequency-speed diagram for the 3-degree-of-freedom rigid disk.

properties of the Winkler foundation, could be removed by attaching a point mass or spring at the disk center, r=0. The frequency of the vertical translational motion would then be changed, but the frequencies of the wave (wobbling) motions would not be changed, since the disk center always lies on the line of nodes. Thus, the frequency of the vertical motion shown as a horizontal line in Figure 20 could be increased or decreased by including a spring or mass at r=0.

Case 2: $\bar{m} \neq 0$, $\bar{k} \neq 0$, $\bar{c}_L \neq 0$, $\bar{c} \neq 0$.

The behavior of the system with an attached moving spring-mass is most easily discussed by referring first to specific examples. Figure 21 shows the Frequency-Speed plot for a disk with a moving mass only, for both the undamped case and with one value of foundation damping ($\bar{c} = 0.0$ and 0.5). The other parameters are $\bar{k} = 0.0$, $\bar{m} = 1.0$, $\bar{c}_L = 0.0$, and $\Delta = 1.0$. Note that Δ must be specified individually in these cases, because $\bar{k}$ and $\bar{m}$ appear alone in (3.24) and not as products with Δ as was always the case in Chapter 2. Figure 21 is much like Figure 12, which is the two degree of freedom disk with the same parameters ($\Delta = 1.0$, $\bar{k} = 0.0$, $\bar{m} = 1.0$), but with one major difference. A new region of instability appears in the region $1.45 \leq \bar{s} \leq 1.95$, characterized by the loop which appears in the $\mathrm{Re}\{\lambda\}$

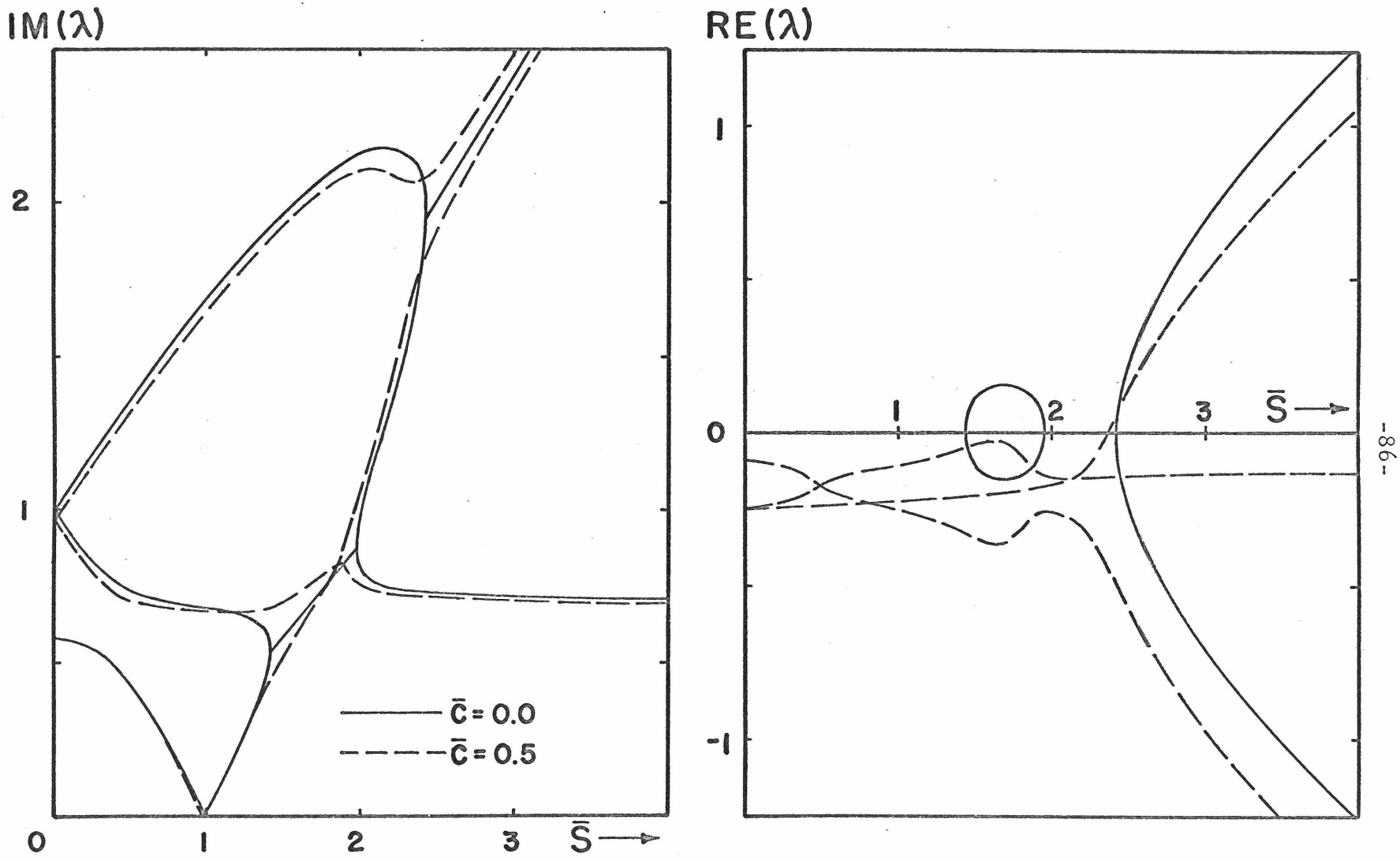

Fig. 21: Typical frequency-speed diagram, mass only; damped and undamped

(Δ=1.0, $\bar{m}$ = 1.0, $\bar{k}$ = 0.0, $\bar{c}_L$ = 0.0, $\bar{c}$ = 0.0, 0.5)

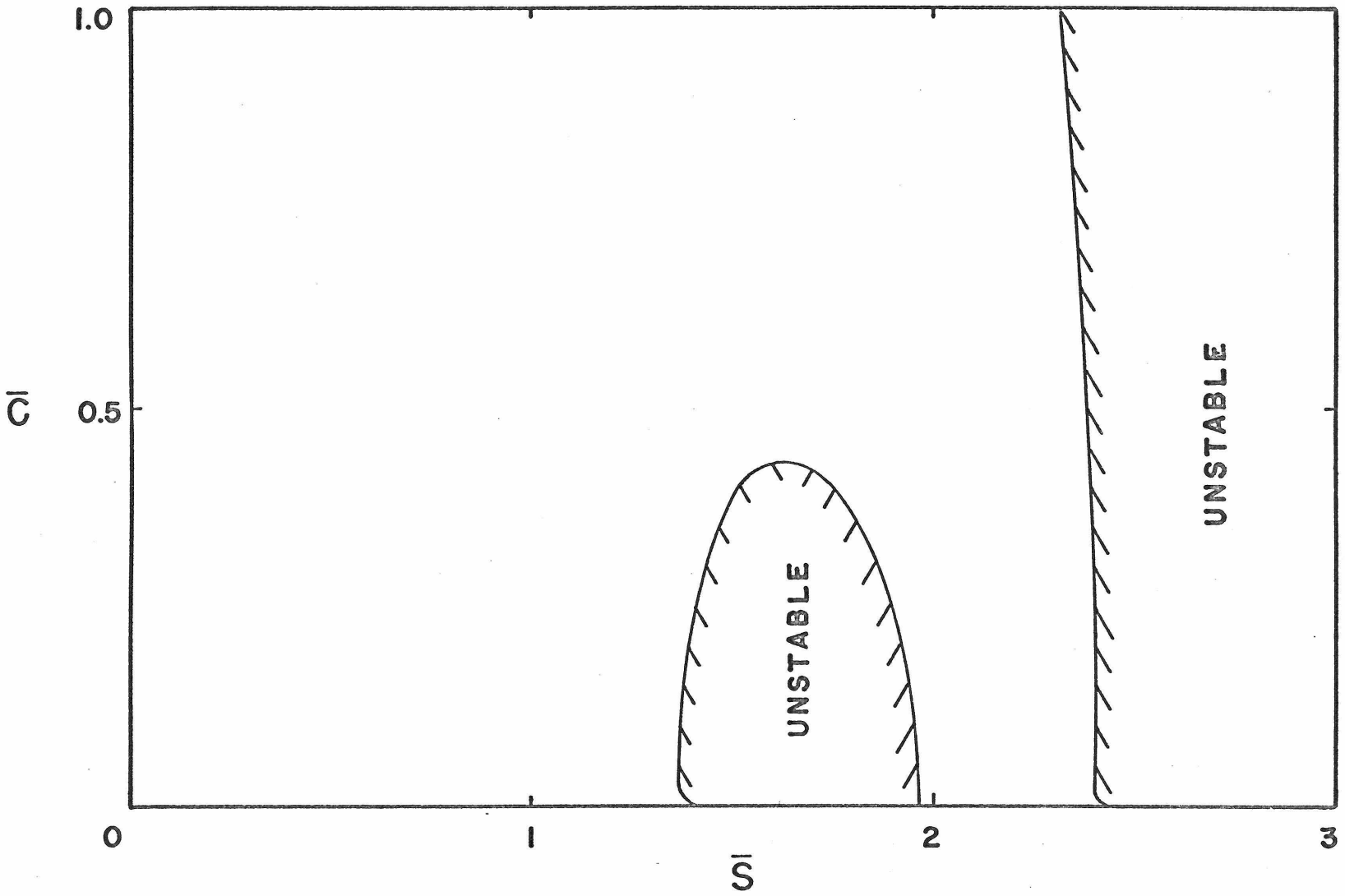

Fig. 22: Stability boundaries as a function of foundation damping for Fig. 21.

plane. Since this region arises because of modal coupling, it will be referred to as the "modal coupling instability region".

The eigenvalues in this new instability region for the undamped case have the form:

$$\lambda_1 = i\omega_L + \mu\,,\quad \lambda_2 = i\omega_L - \mu\,,\quad \lambda_3 = -i\omega_L + \mu,\quad \lambda_4 = -i\omega_L - \mu$$
$$\lambda_5 = i\omega_u\,,\quad \lambda_6 = -i\omega_u \tag{3.34}$$

As foundation damping $\bar{c}$ is added to the system, the $\mathrm{Re}\{\lambda\}$ branches move downward, tending to stabilize the system. Furthermore, as $\bar{c}$ increases, the modal coupling instability region narrows and eventually disappears completely, as indicated in Figure 22. The terminal stability velocity $\bar{s}^*$ decreases slightly as $\bar{c}$ is increased, although not as markedly as in the two degree of freedom case.

Figure 23 has the same parameters as Figure 21, with the exception of an added spring, $\bar{k} = 2.0$. Here, as in the two degree of freedom case, there is a stiffness instability region immediately above $\bar{s} = 1$. The boundaries of this region in the undamped case can be found analytically from Equation (3.30) with λ set equal to zero. The resulting quadratic equation for $\bar{s}^2$ can then be solved to give the values of $\bar{s}^2$ at the boundaries of the instability region. The stiffness instability region is thus given by:

$$1 < \bar{s}^2 < 1 + \frac{\Delta\bar{k}}{1+\bar{k}} \tag{3.40}$$

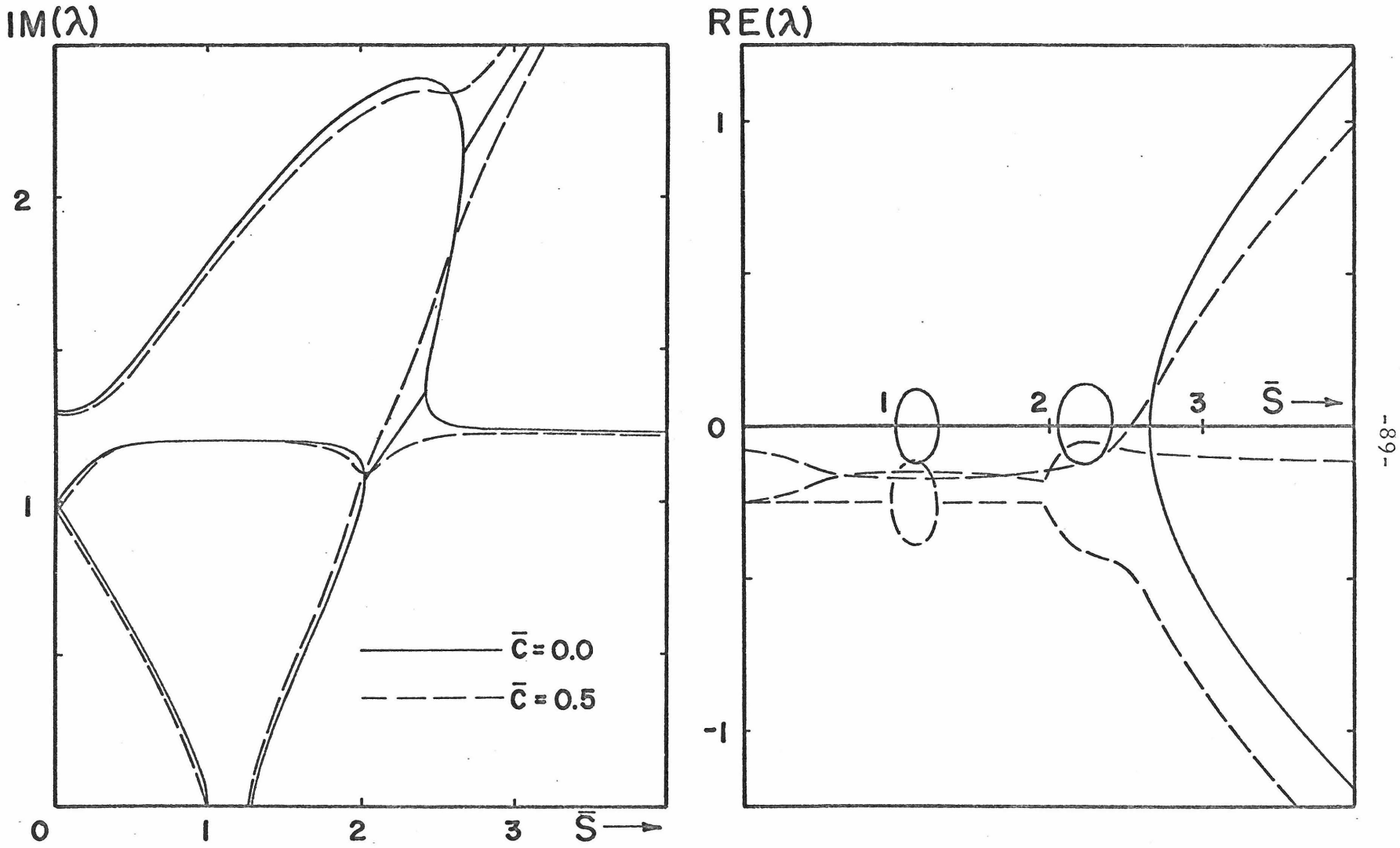

Fig. 23: Typical frequency-speed diagram, damped and undamped.

(Δ=1.0, $\bar{m}$=1.0, $\bar{k}$=2.0, $\bar{c}_L$=0.0, $\bar{c}$=0.0, 0.5)

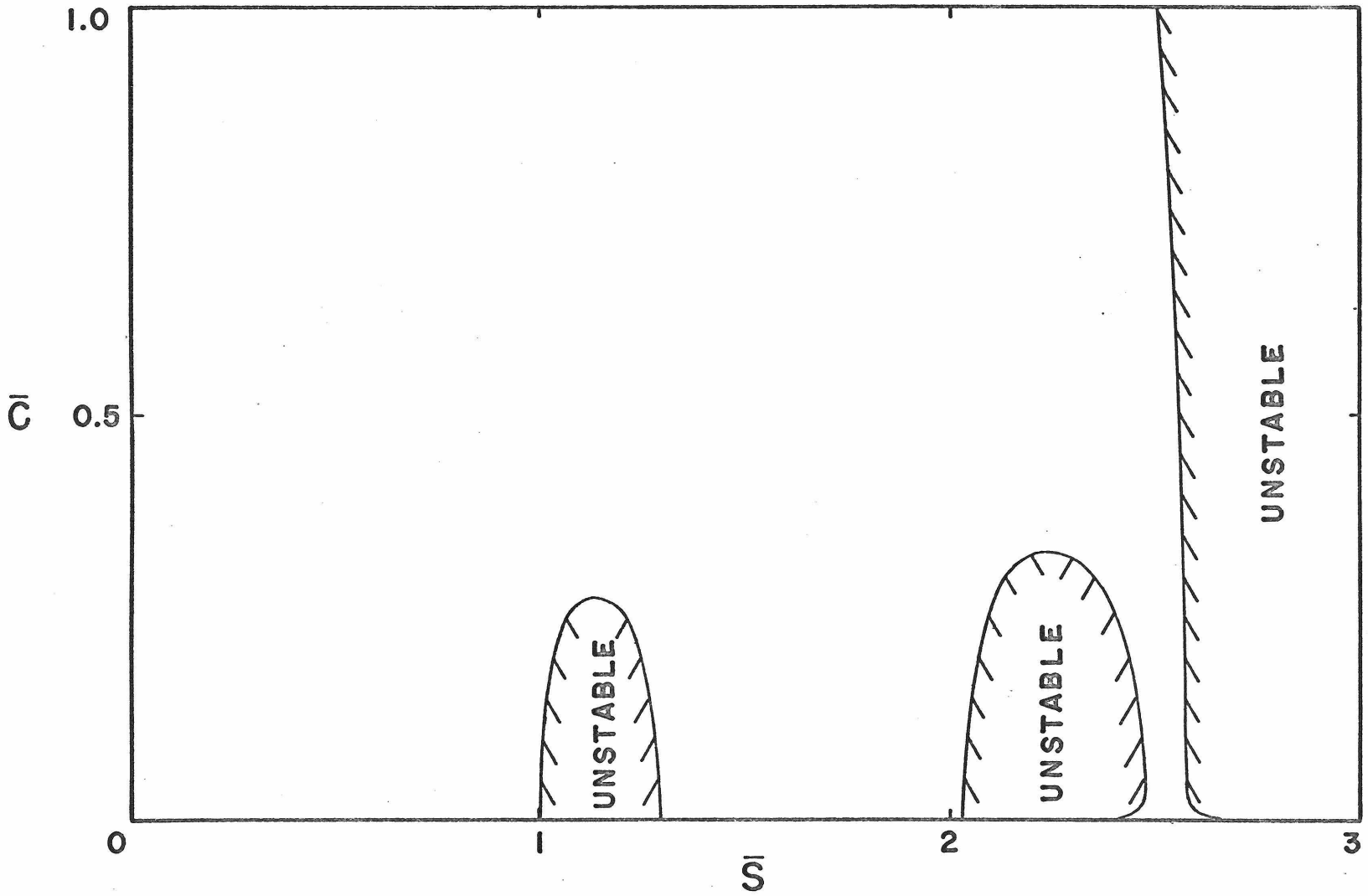

Fig. 24: Stability boundaries as a function of foundation damping for Fig. 23.

When compared with the two degree of freedom result (2.64), it is evident that this instability region is always narrower in the three degree of freedom case than in the former case.

As in the mass only case of Figure 21, there is a new instability region caused by modal coupling. This region lies between the stiffness instability region and the terminal velocity. As foundation damping $\bar{c}$ is added, the $\mathrm{Re}\{\lambda\}$ branches shift downward, stabilizing the system. Both the modal coupling instability region and the stiffness instability region narrow and then disappear entirely, as Figure 24 indicates. The stiffness instability region stabilizes first, when $\bar{c} \cong 0.28$, and when $\bar{c}$ exceeds 0.33 the modal coupling instability zone stabilizes. The terminal velocity $\bar{s}^*$ decreases slightly as in the previous cases.

Note that in Figure 20, the intersection of the branch corresponding to vertical translational motion with the branch corresponding to the forward wave motion occurs at $\bar{s} = 2$ with a frequency equal to 1. If the natural frequency of the attached spring and mass alone is less than p, (that is, if $1 > \frac{1}{p^2}\frac{k_L}{m_L} = \frac{\bar{k}}{\bar{m}}$), then the mode coupling instability region will be entirely below $\bar{s} = 2$. However, if the natural frequency of the attached spring and mass alone is greater than p, (that is, if $1 < \frac{1}{p^2}\frac{k_L}{m_L} = \frac{\bar{k}}{\bar{m}}$), then the modal coupling instability region will lie

entirely above $\bar{s} = 2$. Figure 21 is an example of the former case and Figure 23 is an example of the latter.

If $\frac{\bar{k}}{\bar{m}} = \frac{1}{p^2} \frac{k_L}{m_L} = 1$, then the mode coupling instability region disappears completely, even without damping. This is because the attached spring and mass have precisely the same frequency as the vertical translational mode of the disk, and hence do not affect the vibration of that mode at all, eliminating modal coupling. Such a case is shown in Figure 25, which has a stiffness instability region, but no modal coupling instability region. As foundation damping $\bar{c}$ is added, the stiffness instability region narrows and then disappears completely, as shown in Figure 26.

Figure 27 shows how the stiffness instability region and the modal coupling instability region change in width as the spring stiffness $\bar{k}$ is varied continuously. The parameters Δ and $\bar{m}$ are held fixed at $\Delta = 1.0$ and $\bar{m} = 1.0$ as in Figures 21, 23, and 25. Thus, Figure 25 is the special case when $\bar{k} = 1$, corresponding to the point at which the modal coupling instability region disappears, and Figure 21 and 23 have the values $\bar{k} = 0.0$ and $\bar{k} = 2.0$ respectively.

Figure 28 shows the behavior of the terminal velocity as $\bar{m}$ is varied continuously, for $\Delta = 1.0$ and for $\bar{k} = 0.0$, 1.0, and 2.0. Thus, the terminal velocities of Figures 21, 23, and 25 are given by $\bar{m} = 1.0$, with the corresponding values of $\bar{k}$. The curves plotted in Figures 27 and 28 are for zero foundation damping, $\bar{c} = 0.0$.

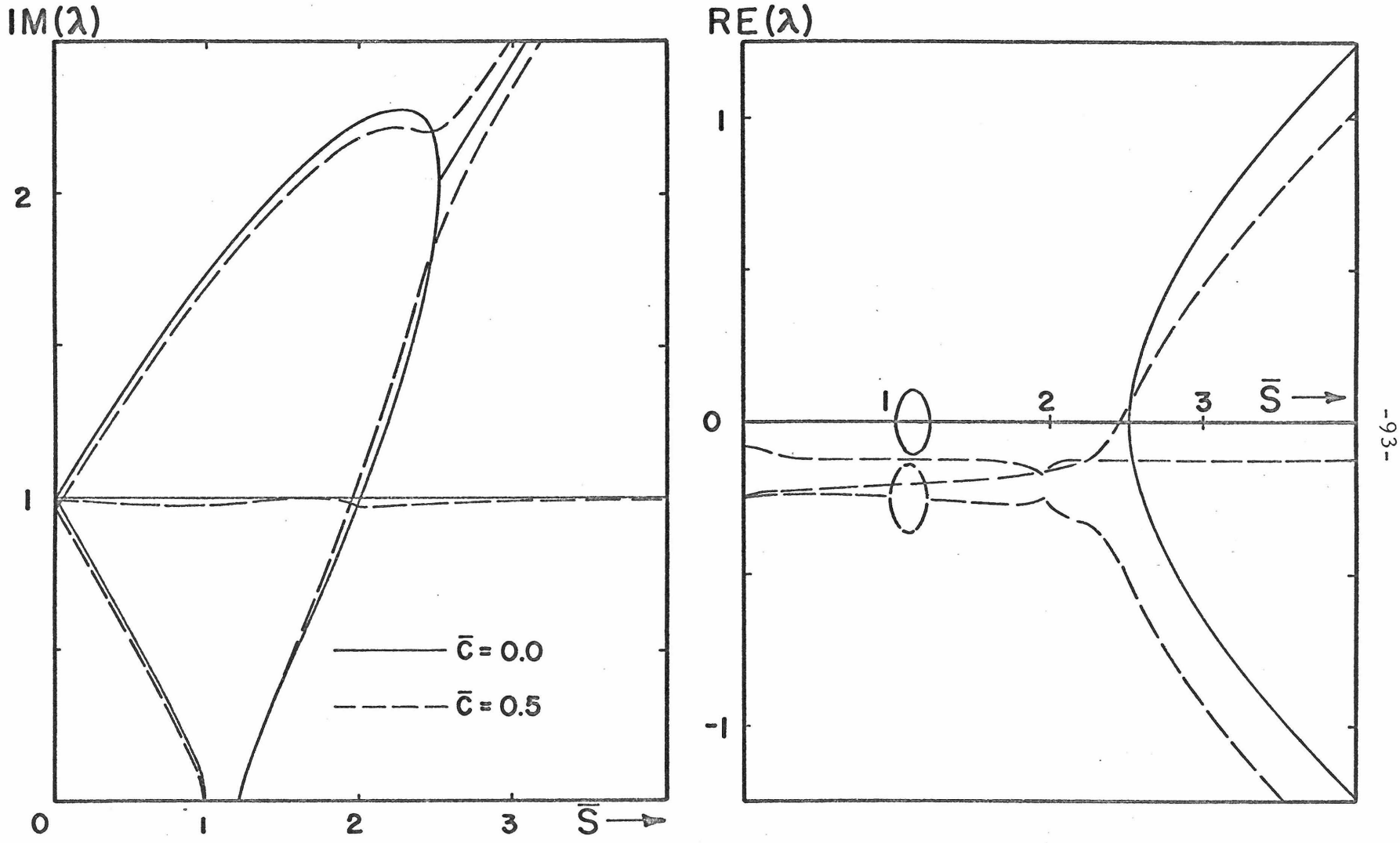

Fig. 25: Frequency-speed diagram for tuned mass-spring.

($\Delta = 1.0$, $\bar{m} = 1.0$, $\bar{k} = 1.0$, $\bar{c}_L = 0.0$, $\bar{c} = 0.0,\ 0.5$)

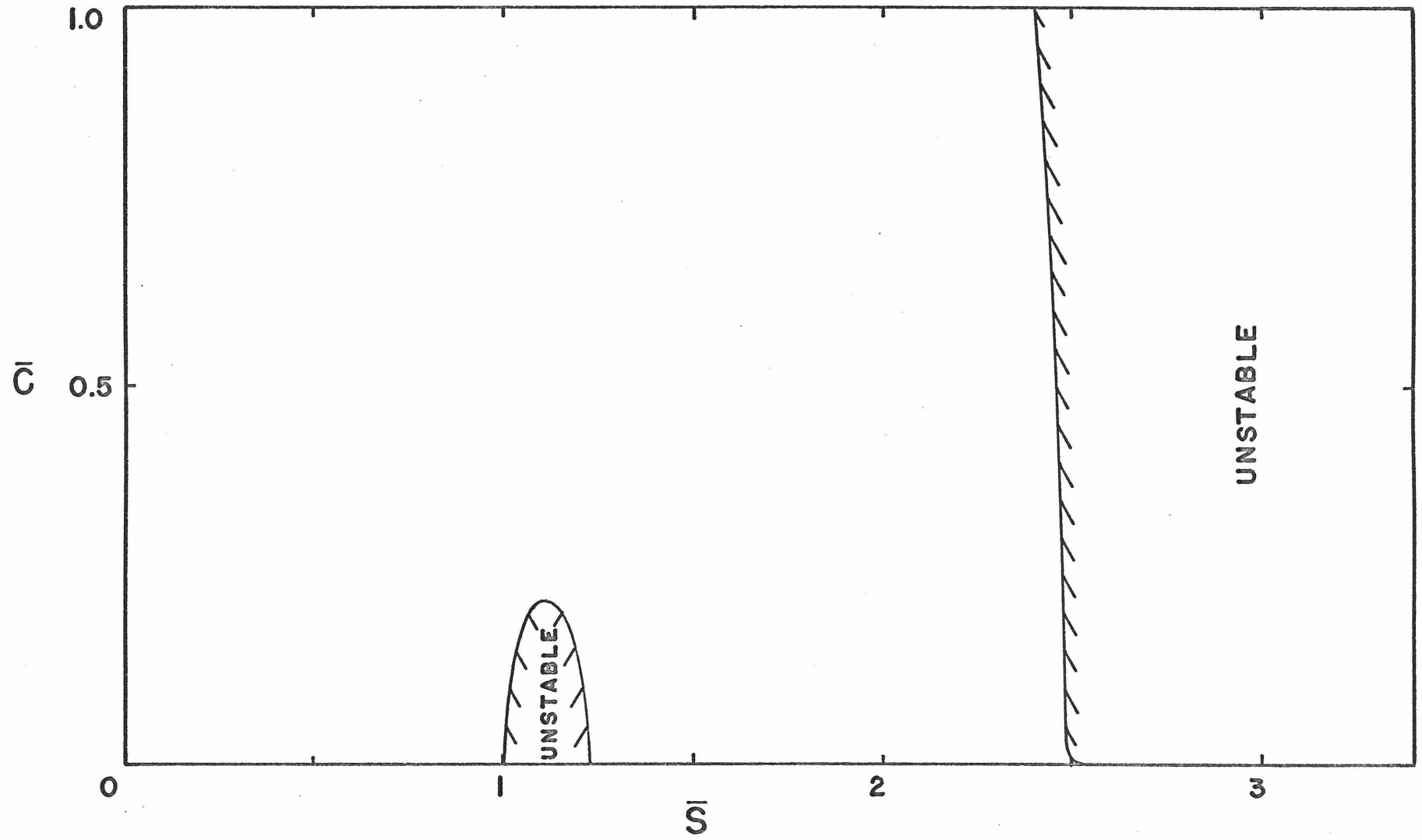

Fig. 26: Stability boundaries as a function of foundation damping for Fig. 25.

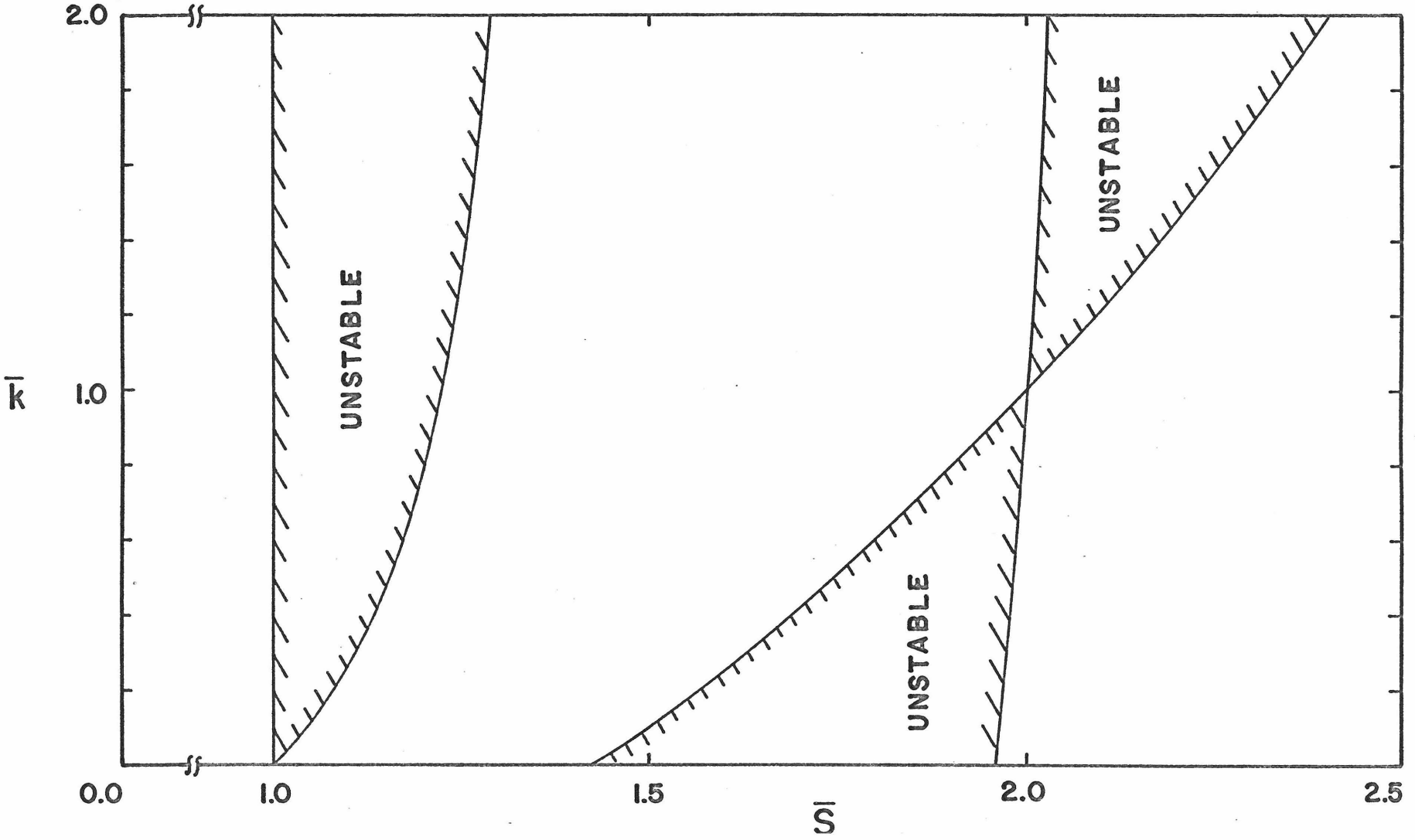

Fig. 27: Lower instability boundaries as a function of $\bar{k}$.

(Δ=1.0, $\bar{m}$= 1.0, $\bar{c}_L = \bar{c}$ = 0.0)

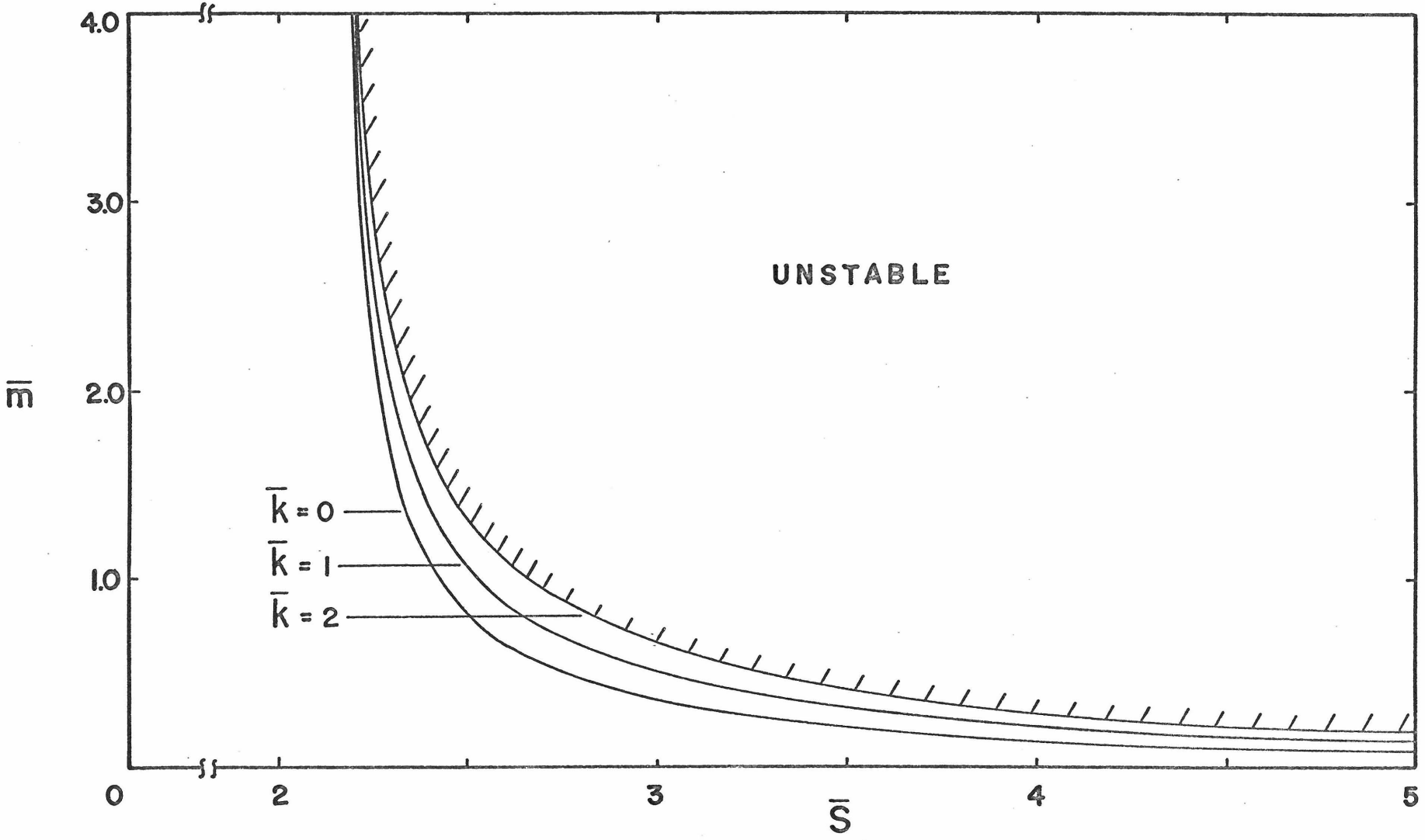

Fig. 28: Terminal speed $\bar{s}^*$ as a function of $\Delta\bar{m}$, for several values of $\bar{k}$.

The physical meaning of the frequencies shown in the Frequency-Speed plots is the same as in Chapter 2. The vertical deflection of the moving mass, $z(t)$, is related to the disk deflection $u(r, \theta, t)$ by Equations (2.8) and (3.1):

$$\begin{aligned} z(t) &= \left[u(r,\theta,t)\right]\Big|_{\substack{r=r_L \\ \theta=\Omega t}} \\ &= r_L \cdot \alpha(t)\sin\left[\Omega t - \beta(t)\right] + v(t) \\ &= r_L \cdot \left[C(t)\sin\Omega t + D(t)\cos\Omega t\right] + v(t) \\ &= r_L \cdot A(t) + v(t) \end{aligned} \tag{3.41}$$

Therefore, the frequency components of $A(t)$ and $v(t)$, which are given by the Frequency-Speed plot, will be the same as the frequency components of the moving mass. Further, the mass motion will be a simple linear combination of these frequencies.

3.5 Modal Participation

Corresponding to each of the six eigenvalues λ_i is a complex eigenvector $\underline{y}_i$. In order to describe the motion of the system in a relatively simple fashion, the eigenvectors of the disk-spring-mass system $\underline{y}_i$ may be expressed as a linear combination of the eigenvectors describing the motion of the disk alone, $\underline{x}_i$. The vectors $\underline{x}_i$ given by (3.34) are linearly independent and thus form a basis in which any

other vector can be decomposed. That is:

$$\underline{y}_i = \delta_{1i}\underline{x}_1 + \delta_{2i}\underline{x}_2 + \delta_{3i}\underline{x}_3 + \delta_{4i}\underline{x}_4 + \delta_{5i}\underline{x}_5 + \delta_{6i}\underline{x}_6 \qquad (3.42)$$

If the vectors $\underline{x}_j$ and $\underline{y}_i$ are unit vectors, then the δ_{ij} will be measures of the participation of the modes of the disk alone in the more complicated motions of the disk-spring-mass system. The vectors may be normalized so that $(\underline{x}_i, \underline{\tilde{x}}_i)=1$. Equations (3.34) then give the eigenvectors $\underline{x}_i$ in normalized form as:

$$\underline{x}_1 = \begin{Bmatrix} 0 \\ -\frac{1}{n_1} \\ -\frac{i}{n_1} \\ 0 \\ -\frac{i(1+\bar{s})}{n_1} \\ \frac{1+\bar{s}}{n_1} \end{Bmatrix}, \quad \underline{x}_2 = \begin{Bmatrix} 0 \\ -\frac{1}{n_1} \\ \frac{i}{n_1} \\ 0 \\ \frac{i(1+\bar{s})}{n_1} \\ \frac{1+\bar{s}}{n_1} \end{Bmatrix}, \quad \underline{x}_3 = \begin{Bmatrix} 0 \\ \frac{1}{n_2} \\ -\frac{i}{n_2} \\ 0 \\ \frac{i(1-\bar{s})}{n_2} \\ \frac{1-\bar{s}}{n_2} \end{Bmatrix} \qquad (3.43)$$

$$\underline{x}_4 = \begin{Bmatrix} 0 \\ \frac{1}{n_2} \\ \frac{i}{n_2} \\ 0 \\ -\frac{i(1-\bar{s})}{n_2} \\ \frac{1-\bar{s}}{n_2} \end{Bmatrix}, \quad \underline{x}_5 = \begin{Bmatrix} \frac{1}{\sqrt{2}} \\ 0 \\ 0 \\ \frac{i}{\sqrt{2}} \\ 0 \\ 0 \end{Bmatrix}, \quad \underline{x}_6 = \begin{Bmatrix} \frac{1}{\sqrt{2}} \\ 0 \\ 0 \\ -\frac{i}{\sqrt{2}} \\ 0 \\ 0 \end{Bmatrix} \qquad (3.43) \text{ cont.}$$

where

$$n_1 = \left\{2\left[1+(1+\bar{s})^2\right]\right\}^{\frac{1}{2}} \quad , \quad n_2 = \left\{2\left[1+(1-\bar{s})^2\right]\right\}^{\frac{1}{2}}$$

The constants δ_{ij} in (3.42) are in general complex, although if all the eigenvalues λ_i are pure imaginary as in a stable region then the δ_{ij} are all real. Because the $\underline{y}_i$ and $\underline{x}_j$ are all unit vectors, and since the $\underline{x}_j$ are orthogonal, in a stable region:

$$\sum_{j=1}^{6} \delta_{ji}^2 = 1 \quad \text{(i fixed)} \qquad (3.44)$$

If any of the δ_{ij} are complex, as in an unstable region, δ_{ij}^2 must be replaced by $\delta_{ij}\tilde{\delta}_{ij}$ in (3.44).

In matrix form, (3.42) becomes:

$$\{\underline{y}_1\underline{y}_2\cdots\underline{y}_6\}=\{\underline{x}_1\underline{x}_2\cdots\underline{x}_6\}\begin{bmatrix}\delta_{11} & \delta_{12}\cdots & \delta_{16}\\ \delta_{21} & \delta_{22}\cdots & \delta_{26}\\ \vdots & & \vdots\\ \delta_{61} & \delta_{62}\cdots & \delta_{66}\end{bmatrix} \tag{3.45}$$

Hence, the δ matrix is obtained by premultiplying (3.45) by the matrix $\{\underline{x}_1\underline{x}_2\cdots\underline{x}_6\}^{-1}$.

The vectors $\underline{x}_1$ and $\underline{x}_2$ correspond to backward traveling waves, $\underline{x}_3$ and $\underline{x}_4$ correspond to forward traveling waves, and $\underline{x}_5$ and $\underline{x}_6$ correspond to vertical motions. Hence the backward, forward, and vertical modal participation factors for a given vector $\underline{y}_i$ can be defined as:

$$\begin{aligned}\delta_b^2 &= \delta_{1i}^2 + \delta_{2i}^2\\ \delta_f^2 &= \delta_{3i}^2 + \delta_{4i}^2\\ \delta_v^2 &= \delta_{5i}^2 + \delta_{6i}^2\end{aligned} \tag{3.46}$$

The modal participation factors δ_b, δ_f, and δ_v are therefore measures of the relative amplitudes of forward and backward waves and vertical motion in the composition of an eigenvector $\underline{y}_i$ of the disk-spring-mass system. From (3.45), it follows that $\delta_b^2+\delta_f^2+\delta_v^2=1$. If the δ_{ij} are not all real, then the squares of the moduli must be used in (3.46).

Figures 29a, b, and c show the modal participation factors as a function of speed for each of the three undamped branches of Figure 23. The three branches are denoted as vertical, backward, and forward

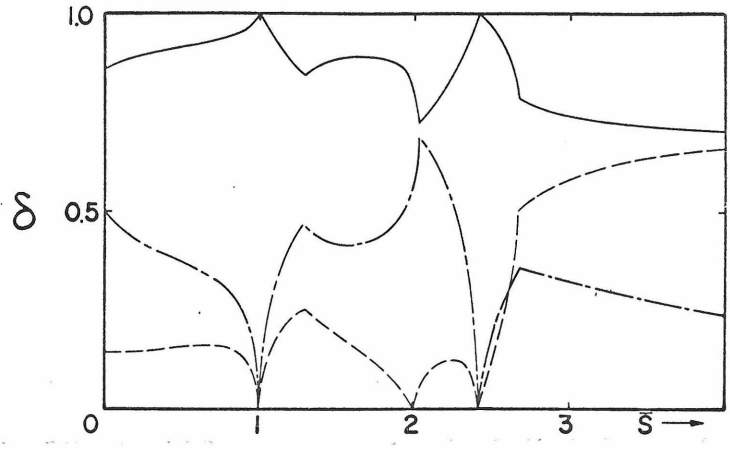

Fig. 29a: Undamped forward branch.

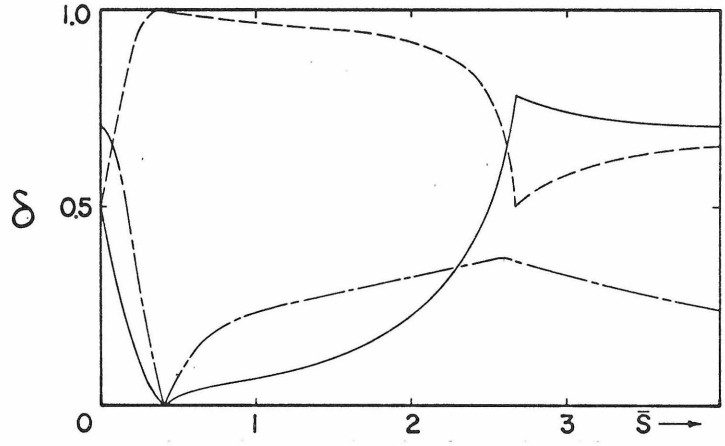

Fig. 29b: Undamped backward branch.

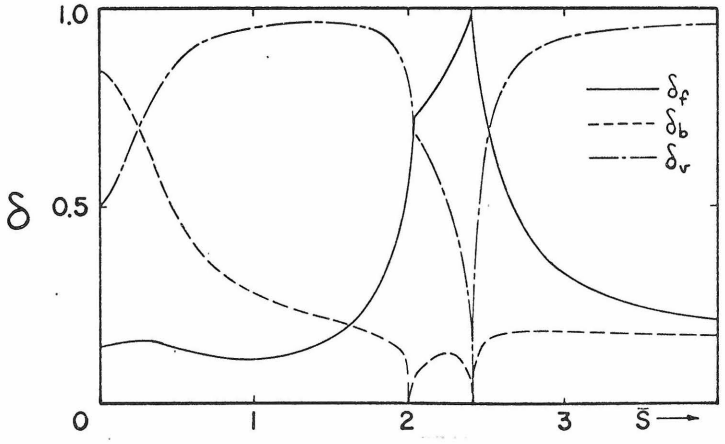

Fig. 29c: Undamped vertical branch

Figs. 29a, b, c: Modal Participation Factors.

depending on their proximity to the corresponding branches in the disk-only case of Figure 20.

The backward branch of Figure 23 is the branch which begins at $\mathrm{Im}\{\lambda\} \cong 1.29$. Figure 29b shows the modal participation factors for the motion along this backward branch. Note that at $\bar{s}=0$, which occurs when the attached spring and mass are stationary, the motion is composed of equal parts of forward and backward wave components, as well as some vertical motion. This motion may be pictured as follows: If no vertical motion were allowed, then the equal forward and backward waves would superpose to form a nodal diameter at right angles to a radial line through the attached spring and mass. However, there is a vertical motion with the same frequency superposed, so the disk will go up and down as well as rocking back and forth. The nodal line will remain perpendicular to a radial line through the attached spring and mass, but will no longer be a diameter of the disk. Instead the nodal line will be a chord lying between the disk center and the point of attachment of the spring and mass. The frequency of this mode is increased over that of the disk alone ($\omega_{\text{disk}}=p$) because the frequency of the attached spring and mass taken alone is greater than p. (The normalized frequency of the disk alone is 1, and that of the spring-mass is $\sqrt{2}$; hence it is not surprising that the frequency of the system lies somewhere in between, at $\mathrm{Im}\{\lambda\} \cong 1.29$).

As the load speed increases, the motion of the backward wave predominates, until at $\bar{s} \cong 0.414$ the motion is entirely a backward moving wave. This is because at $\bar{s} = \sqrt{2}-1$, the frequency of the backward branch of the disk alone is exactly equal to $\sqrt{2}$ (see Figure 20). The spring and mass have the same frequency, and hence the mode shape of the disk alone remains unaffected. As the speed increases further, the backward wave motion predominates until terminal velocity $\bar{s}^*$ is reached, where there is a greater contribution from the forward wave.

The modal participation components of the vertical and forward branches behave similarly to the backward branch discussed above, but are somewhat more complicated because the character of the solution changes more often as $\bar{s}$ increases. The forward branch has six distinguishable regions of behavior, for example: stable oscillations below $\bar{s} = 1$, the stiffness instability region, a second oscillatory region, the modal coupling instability region, a third oscillatory region, and finally the terminal instability zone.

Figures 30a, b, and c show the behavior of the modal participation factors along the damped branches of Figure 23. These figures generally resemble the plots for the undamped case, except that they appear to be smoothed somewhat so that the various regions of behavior are no longer as distinct. The forward branch plot, Figure 30a,

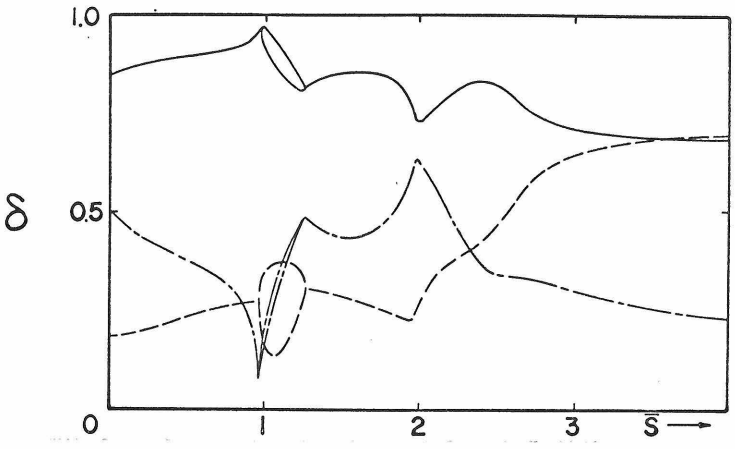

Fig. 30a: Damped forward branch.

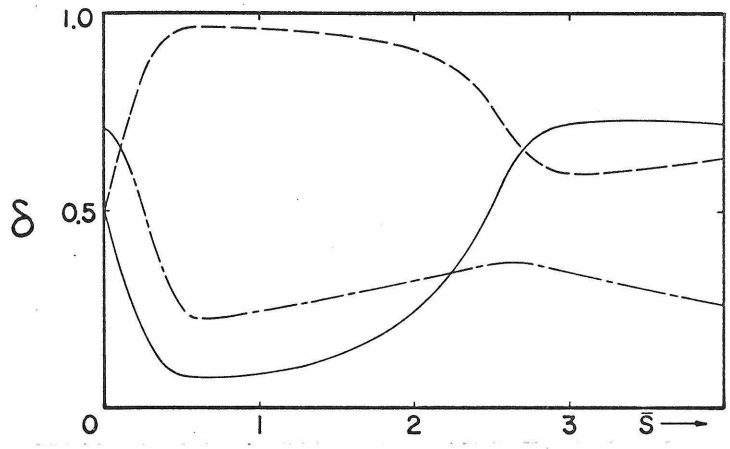

Fig. 30b: Damped backward branch.

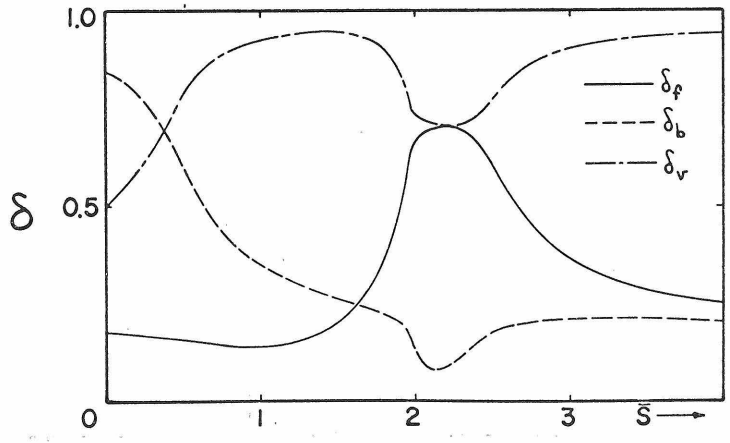

Fig. 30c: Damped vertical branch.

Figs. 30a, b, c: Modal Participation Factors.

now has double branches in the region $0.95 \leq \bar{s} \leq 1.25$, indicating that the two solutions possible on this branch in this region have somewhat different motions. (At $\bar{s} = 1.1$, for example, the two values of λ corresponding to the forward branch are $\lambda \cong -0.1$ and $\lambda \cong -0.4$. This is the only region in which the eigenvalues are not complex conjugates.) In general, the modal participation factor which predominates in each plot is the one which would describe the motion of the disk alone along each branch, even for this case of relatively large load parameters.

3.6 Discussion

The introduction of a third degree of freedom has of course resulted in a more complicated set of differential equations. However, the transformation techniques developed in Chapter 2 reduce the nonlinear equations to a set of coupled linear differential equations with constant coefficients, so that an ordinary eigenvalue problem may be solved. The stiffness instability region and the terminal instability zone which were important characteristics of the two degree of freedom problem remain as significant features of this more complicated case. In addition, a new region of instability has appeared due to modal coupling. These same three types of instability will be present in the following chapters involving the dynamic response of elastic disks.

IV. ELASTIC DISK

4.1 Introduction

In the previous chapters, the dynamic behavior of rigid disks with moving massive loads was studied. Other problems of physical importance include the response of elastic disks subjected to similar loading systems. If the disk deflections are small, and the disk is thin, the motion of a flexible disk can be described by the following partial differential equation:[19]

$$\rho\frac{\partial^2 u}{\partial t^2}+\frac{Eh^2}{3(1-\sigma^2)}\left[\frac{\partial^2}{\partial r^2}+\frac{1}{r}\frac{\partial}{\partial r}+\frac{1}{r^2}\frac{\partial^2}{\partial\theta^2}\right]^2 u=\frac{1}{2h}q(r,\theta,t) \qquad (4.1)$$

When the transverse force $q(r,\theta,t)$ is a known function of space and time, Equation (4.1) may be solved by well-known methods. However, in the case of a moving massive load, the applied force depends on the disk displacement, velocity, and acceleration, and hence $q(r,\theta,t)$ is not known explicitly. The fact that the applied force is a function of the unknown quantity complicates the problem considerably.

The technique used in this chapter is the eigenfunction expansion method most often used when $q(r,\theta,t)$ is a known function of space and time. Since $q(r,\theta,t)$ depends on the deflection $u(r,\theta,t)$ in this case, substitution of the eigenfunction series and the use of orthogonality relationships will yield a set of coupled differential equations for the

eigenfunction coefficients. These equations strongly resemble (3.10)-(3.12), or (3.15)-(3.17), depending on how the eigenfunction series is written, but there will be an infinite set of equations rather than only three. If the series is truncated so that an approximate solution is sought, then there will be a finite system of equations but the complications of coupling and periodic coefficients will remain. This finite system of equations can be transformed into an ordinary eigenvalue problem by the methods developed in Chapters 2 and 3. The Frequency-Speed plots obtained in this way indicate areas of instability directly analogous to those discussed in the previous chapters.

4.2 Free Vibration of an Elastic Disk

The partial differential equation describing the small amplitude vibrations of an elastic disk with no loads applied is:

$$\rho\frac{\partial^2 u}{\partial t^2}+\frac{Eh^2}{3(1-\sigma^2)}\left[\frac{\partial^2}{\partial r^2}+\frac{1}{r}\frac{\partial}{\partial r}+\frac{1}{r^2}\frac{\partial^2}{\partial\theta^2}\right]^2 u=0 \qquad (4.2)$$

where $b\le r\le a$, $0\le\theta\le 2\pi$.

Using the separation of variables technique, let:

$$u(r,\theta,t)=T(t)\Psi(r,\theta) \qquad (4.3)$$

The resulting equations for $T(t)$ and $\Psi(r,\theta)$ are:

$$\frac{d^2T}{dt^2}+p^2T=0 \qquad (4.4)$$

$$\left[\frac{\partial^2}{\partial r^2}+\frac{1}{r}\frac{\partial}{\partial r}+\frac{1}{r^2}\frac{\partial^2}{\partial \theta^2}\right]^2 \Psi - \kappa^4 \Psi = 0 \tag{4.5}$$

where

$$\kappa^4 = \frac{3\rho(1-\sigma^2)p^2}{Eh^2} \tag{4.6}$$

Equation (4.5) may be satisfied by:

$$\left[\frac{\partial^2}{\partial r^2}+\frac{1}{r}\frac{\partial}{\partial r}+\frac{1}{r^2}\frac{\partial^2}{\partial \theta^2}\right] \Psi \pm \kappa^2 \Psi = 0 \tag{4.7}$$

Separating variables once again, let:

$$\Psi(r,\theta) = W(r)\Theta(\theta) \tag{4.8}$$

Substituting (4.8) into (4.7), the following equations are obtained for $W(r)$ and $\Theta(\theta)$:

$$\frac{d^2\Theta}{d\theta^2}+j^2\Theta = 0 \tag{4.9}$$

$$r^2\frac{d^2W}{dr^2}+r\frac{dW}{dr}+(\pm\kappa^2 r^2 - j^2)W = 0 \tag{4.10}$$

Continuity in θ requires that j be an integer (j=0, 1, 2...). The value of j corresponds to the number of nodal diameters of the motion. With j an integer, the solution to (4.10) has the form:

$$W(r) = \alpha J_j(\kappa r)+\beta Y_j(\kappa r)+\gamma I_j(\kappa r)+\delta K_j(\kappa r) \tag{4.11}$$

where $J_j(\kappa r)$ and $Y_j(\kappa r)$ are Bessel functions of order j, and $I_j(\kappa r)$ and $K_j(\kappa r)$ are modified Bessel functions of order j.

Associated with the fourth order partial differential Equation (4. 2) are four boundary conditions on the disk displacement $u(r, \theta, t)$ and its derivatives. For example, if the inner boundary (r=b) is clamped, and the outer boundary is free, the boundary conditions are:

$$\begin{aligned} &\left[u\right]\Big|_{r=b} = 0 \\ &\left[\frac{\partial u}{\partial r}\right]\Big|_{r=b} = 0 \\ &\left[M_r\right]\Big|_{r=a} = 0 \\ &\left[Q_r - \frac{1}{r}\frac{\partial M_{r\theta}}{\partial \theta}\right]\Big|_{r=a} = 0 \end{aligned} \tag{4.12}$$

The bending moments M_r, $M_{r\theta}$ and the shearing force Q_r are related to the deflection $u(r, \theta, t)$ by:

$$\begin{aligned} M_r &= -\frac{Eh^2}{3(1-\sigma^2)}\left[\frac{\partial^2 u}{\partial r^2} + \sigma\left(\frac{1}{r}\frac{\partial u}{\partial r} + \frac{1}{r^2}\frac{\partial^2 u}{\partial \theta^2}\right)\right] \\ M_{r\theta} &= (1-\sigma)\frac{Eh^2}{3(1-\sigma^2)}\left[\frac{1}{r}\frac{\partial^2 u}{\partial r \partial \theta} - \frac{1}{r^2}\frac{\partial u}{\partial \theta}\right] \\ Q_r &= -\frac{Eh^2}{3(1-\sigma^2)}\frac{\partial}{\partial r}\left[\frac{\partial^2 u}{\partial r^2} + \frac{1}{r}\frac{\partial u}{\partial r} + \frac{1}{r^2}\frac{\partial^2 u}{\partial \theta^2}\right] \end{aligned} \tag{4.13}$$

When the expression (4. 11) for W(r) is substituted into the four boundary conditions (4. 12), a system of four linear algebraic equations is obtained for the constants α, β, γ, and δ. Because these equations are homogeneous, the determinant of the coefficients must vanish for

a nontrivial solution. The values of κ for which this determinant vanishes are the eigenvalues of the problem. For fixed j, there are an infinite number of eigenvalues κ_{jn} (n=0, 1, 2, . . .) and as j corresponds to the number of nodal diameters of the mode of vibration, so n corresponds to the number of nodal circles. The ratios of the constants α, β, γ, and δ are given by (4.12) with κ replaced by κ_{jn}, and the frequency of vibration of the mode is given by a rearrangement of (4.6):

$$p_{jn}^2 = \frac{Eh^2 \kappa_{jn}^4}{3\rho(1-\sigma^2)} \tag{4.14}$$

The general solution to the problem for arbitrary initial conditions may be written as a linear combination of all these modes. That is, the deflection $u(r, \theta, t)$ may be expressed as:

$$u(r, \theta, t) = \sum_{j=0}^{\infty} \sum_{n=0}^{\infty} T_{jn}(t) \Psi_{jn}(r, \theta) \tag{4.15}$$

$$= \sum_{j=0}^{\infty} \sum_{n=0}^{\infty} T_{jn}(t) \sin(j\theta - \epsilon_{jn}) W_{jn}(r) \tag{4.16}$$

The time dependent part of (4.15) may be written in either real or complex form as:

$$T_{jn}(t) = F_{jn}\sin(pt - t_{jn}), \quad \left[F_{jn}, t_{jn}\ \text{real}\right]$$
$$= E_{jn}e^{ip_{jn}t} + \tilde{E}_{jn}e^{-ip_{jn}t} \tag{4.17}$$

where $\tilde{E}_{jn}$ is the complex conjugate of E_{jn}.

The spatial eigenfunctions $\Psi_{jn}(r,\theta)$ are orthogonal and may be normalized so that they satisfy the orthogonality condition:

$$\int_0^{2\pi}\int_b^a \Psi_{jn}(r,\theta)\Psi_{k\ell}(r,\theta)\,r\,dr\,d\theta = \delta_{jk}\delta_{n\ell} \tag{4.18}$$

The δ_{jn} and $\delta_{k\ell}$ are Kronecker delta functions, and should not be confused with the delta appearing in Equation (4.11).

A typical mode of vibration thus has j nodal diameters and n nodal circles, and vibrates with frequency p_{jn}. If $j \geq 1$, the mode can be thought of as a superposition of a forward traveling wave and a backward traveling wave, since

$$\sin p_{jn}t \sin j\theta = \frac{1}{2}\cos j\left(\theta - \frac{p_{jn}}{j}t\right) - \frac{1}{2}\cos j\left(\theta + \frac{p_{jn}}{j}t\right) \tag{4.19}$$

The first term on the right hand side of (4.19) corresponds to a forward traveling wave with velocity p_{jn}/j, while the second term is a backward traveling wave with velocity $-p_{jn}/j$. The relation

between this decomposition and the discussion following Equation (2.60) in Chapter 2 should be quite clear. The forward and backward wave components of the flexible disk are analogous to the forward and backward "wobbling" motions of the rigid disk.

If the mode has j = 0 (i.e., no nodal diameters), the decomposition into forward and backward waves does not apply. These modes are analogous to the vertical translational motion v(t) discussed in Chapter 3.

If a normal mode having one or more nodal diameters is viewed from a reference frame rotating at constant angular velocity Ω, the backward traveling wave will appear speeded up, and the forward traveling wave will appear slowed down. The wave velocities will be $-(\frac{1}{j}p_{jn}+\Omega)$ and $(\frac{1}{j}p_{jn}-\Omega)$ for the backward and forward wave components respectively. When $\Omega=\frac{1}{j}p_{jn}$ the forward traveling wave will appear stationary. The value of Ω corresponding to this condition is known as the critical speed of the mode with j nodal diameters and n nodal circles. A typical Frequency-Speed plot for a centrally clamped disk is shown in Figure 31.

4.3 Equations of Motion for Elastic Disk with Moving Spring and Mass

When the disk has a transverse load applied, the equation of motion has the form:

$$\rho\frac{\partial^2 u}{\partial t^2}+\frac{Eh^2}{3(1-\sigma^2)}\left[\frac{\partial^2}{\partial r^2}+\frac{1}{r}\frac{\partial}{\partial r}+\frac{1}{r^2}\frac{\partial^2}{\partial\theta^2}\right]^2 u=\frac{1}{2h}q(r,\theta,t) \qquad (4.20)$$

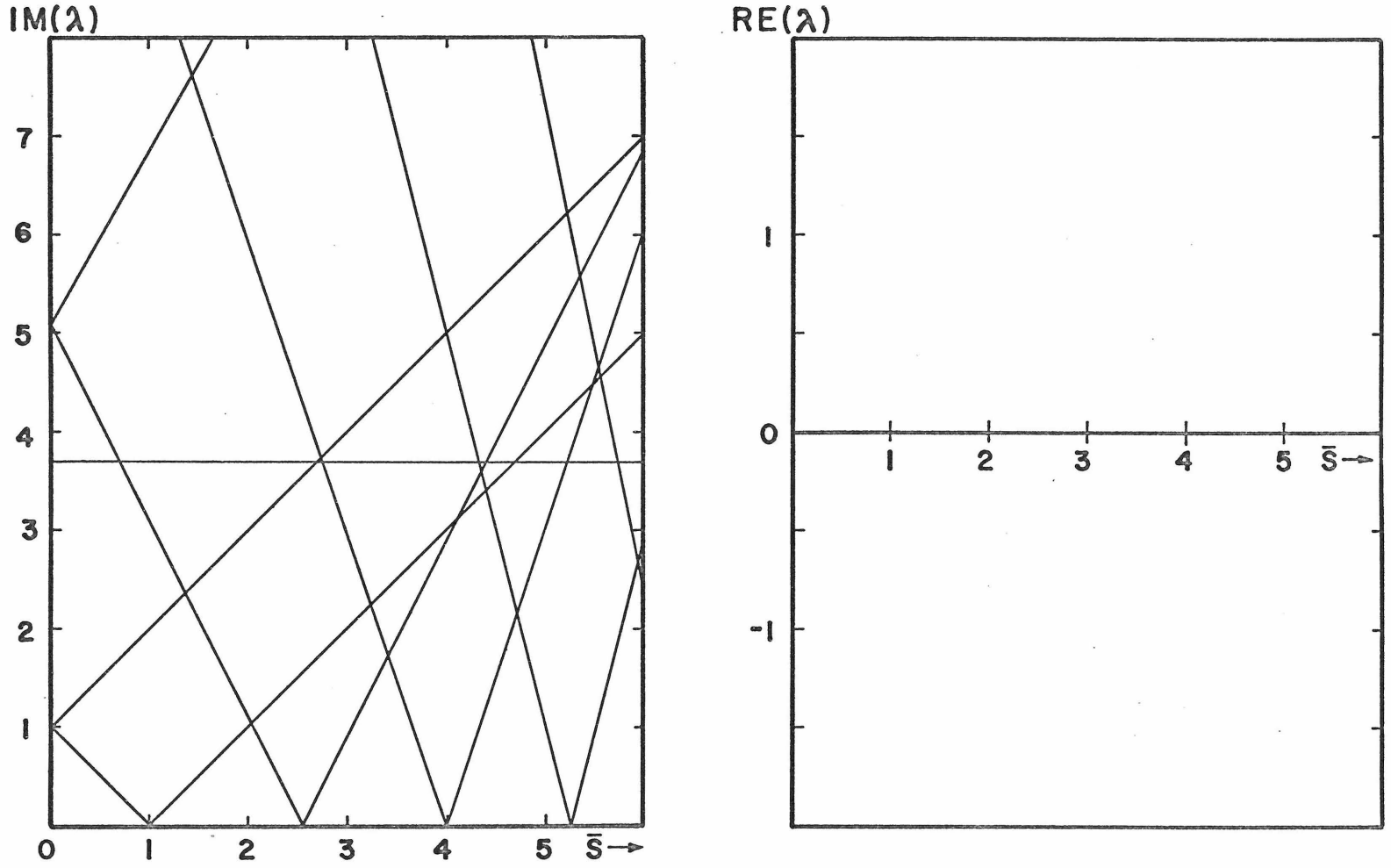

Fig. 31: Frequency-speed diagram for elastic disk. ($\bar{m}=\bar{k}=\bar{c}_L=0.0$)

The transverse load $q(r,\theta,t)$ has units of force per unit area. The force applied to the disk is just that due to the moving spring, mass, and dashpot. Using delta functions to denote that the position of the load is given by $\theta=\Omega t$, $r=r_L$, the transverse load $q(r,\theta,t)$ becomes:

$$q(r,\theta,t)=\delta(\theta-\Omega t)\frac{\delta(r-r_L)}{r_L}\left[-f(t)\right] \tag{4.21}$$

where f(t) is the force on the attached moving mass. If the mass deflection is z(t), then:

$$f(t)=m_L\frac{d^2z}{dt^2}+c_L\frac{dz}{dt}+k_Lz \tag{4.22}$$

As in the previous chapters, the displacement z(t) of the attached mass is assumed to be equal to that of the disk at the point $r=r_L$, $\theta=\Omega t$. That is:

$$z(t)=\left[u(r,\theta,t)\right]\Big|_{\substack{r=r_L\\ \theta=\Omega t}} \tag{4.23}$$

Similarly, the velocity and acceleration of the mass are equal to the first and second <u>total</u> derivatives of (4.23)

$$\left.\begin{aligned}\frac{dz}{dt}&=\frac{d}{dt}\left\{\left[u(r,\theta,t)\right]\Big|_{\substack{r=r_L\\ \theta=\Omega t}}\right\}\\ &\\ &\end{aligned}\right\} \tag{4.24}$$

$$= \left[\frac{\partial u}{\partial t} + \Omega \frac{\partial u}{\partial \theta}\right]\Bigg|_{\substack{r=r_L \\ \theta=\Omega t}} \Bigg\} \quad \text{(4.24) cont.}$$

$$\frac{d^2 z}{dt^2} = \frac{d^2}{dt^2}\left\{\left[u(r,\theta,t)\right]\Big|_{\substack{r=r_L \\ \theta=\Omega t}}\right\} \quad \text{(4.25)}$$

$$= \left[\frac{\partial^2 u}{\partial t^2} + 2\Omega \frac{\partial^2 u}{\partial t \partial \theta} + \Omega^2 \frac{\partial^2 u}{\partial \theta^2}\right]\Bigg|_{\substack{r=r_L \\ \theta=\Omega t}}$$

Hence, the partial differential equation for the disk-spring-mass-dashpot system becomes:

$$\rho \frac{\partial^2 u}{\partial t^2} + \frac{Eh^2}{3(1-\sigma^2)}\left[\frac{\partial^2}{\partial r^2} + \frac{1}{r}\frac{\partial}{\partial r} + \frac{1}{r^2}\frac{\partial^2}{\partial \theta^2}\right]^2 u$$

$$= -\frac{1}{2h}\,\delta(\theta-\Omega t)\,\frac{\delta(r-r_L)}{r_L}\left\{m_L\left[\frac{\partial^2 u}{\partial t^2} + 2\Omega \frac{\partial^2 u}{\partial t \partial \theta} + \Omega^2 \frac{\partial^2 u}{\partial \theta^2}\right]\right. \quad \text{(4.26)}$$

$$\left. + c_L\left[\frac{\partial u}{\partial t} + \Omega \frac{\partial u}{\partial \theta}\right] + k_L u\right\}$$

Since the eigenfunctions of the homogeneous problem form a complete set and span the space of the problem the disk deflection $u(r, \theta, t)$ may be written as an infinite series of those functions. That is:

$$u(r,\theta,t)=\sum_{n=0}^{\infty} T_{0n}(t)W_{0n}(r) + \sum_{j=1}^{\infty}\sum_{n=0}^{\infty} T_{jn}(t)\sin\left[j\theta - \epsilon_{jn}(t)\right]W_{jn}(r) \qquad (4.27)$$

Those modes having zero nodal diameters have been separated from the double sum for clarity. Comparing (4.27) with Equation (3.1) of Chapter 3, it is apparent that the $T_{0n}(t)$ are analogous to the vertical motion v(t) of that chapter, whereas $T_{jn}(t)$ and $\epsilon_{jn}(t)$ are comparable to $\alpha(t)$ and $\beta(t)$ in (3.1).

It is apparent that substituting the eigenfunction series (4.27) into the partial differential Equation (4.26), and utilizing the orthogonality condition given by (4.18), will yield a set of nonlinear coupled ordinary differential equations for the eigenfunction coefficients. These equations will be analogous to Equations (3.10), (3.11), and (3.12) of Chapter 3. By using a transformation of the form (3.14) directly on the eigenfunction series (4.27), a large amount of algebra can be saved and the nonlinear set of equations can be avoided entirely. Define the new functions $C_{jn}(t)$ and $D_{jn}(t)$ as below:

$$\text{For } j=0: \quad C_{0n}(t) = T_{0n}(t), \quad D_{0n}(t) \equiv 0$$

$$\text{For } j > 0: \quad C_{jn}(t) = -T_{jn}(t)\,\sin\epsilon_{jn}(t)$$
$$D_{jn}(t) = T_{jn}(t)\cos\epsilon_{jn}(t) \tag{4.28}$$

With these definitions, the eigenfunction expansion of $u(r,\theta,t)$ becomes:

$$u(r,\theta,t) = \sum_{n=0}^{\infty} C_{0n}(t)W_{0n}(r) + \sum_{j=1}^{\infty}\sum_{n=0}^{\infty}\left[C_{jn}(t)\cos j\theta + D_{jn}(t)\sin j\theta\right]W_{jn}(r) \tag{4.29}$$

If the eigenfunction expansion (4.29) is now substituted into the partial differential Equation (4.26) and use is made of the orthogonality condition, the result will be an infinite set of coupled linear differential equations with periodic coefficients, resembling Equations (3.15), (3.16), and (3.17). Realizing that the transformation (3.18) reduced that set of equations to a form with constant coefficients, define the new variables $A_{jn}(t)$ and $B_{jn}(t)$ by the equations:

$$\text{For } j=0: \quad A_{0n}(t) = C_{0n}(t)$$
$$\text{For } j>0: \quad A_{jn}(t) = C_{jn}(t)\cos j\Omega t + D_{jn}(t)\sin j\Omega t \tag{4.30}$$
$$B_{jn}(t) = -C_{jn}(t)\sin j\Omega t + D_{jn}(t)\cos j\Omega t$$

The inverse relations for the $j > 0$ case are:

$$C_{jn}(t) = A_{jn}(t)\cos j\Omega t - B_{jn}(t)\sin j\Omega t$$
$$D_{jn}(t) = A_{jn}(t)\sin j\Omega t + B_{jn}(t)\cos j\Omega t \qquad (4.31)$$

The expression for $u(r, \theta, t)$ thus becomes:

$$u(r,\theta,t) = \sum_{n=0}^{\infty} A_{0n}(t)W_{0n}(r) + \sum_{j=1}^{\infty}\sum_{n=0}^{\infty}\left[A_{jn}(t)\cos j(\theta - \Omega t) + B_{jn}(t)\sin j(\theta - \Omega t)\right]W_{jn}(r) \qquad (4.32)$$

Hence, if the variable Φ is defined as:

$$\Phi = \theta - \Omega t, \qquad (4.33)$$

The displacement u' relative to the coordinates r, Φ, and t is simply:

$$u'(r,\Phi,t) = \sum_{n=0}^{\infty} A_{0n}(t)W_{0n}(r) + \sum_{j=1}^{\infty}\sum_{n=0}^{\infty}\left[A_{jn}(t)\cos j\Phi + B_{jn}(t)\sin j\Phi\right]W_{jn}(r) \qquad (4.34)$$

$u'(r, \Phi, t)$ corresponds physically to the deflection of the disk as observed from a reference frame rotating with respect to the disk at constant

angular velocity Ω. The traveling load appears at a constant angular position $\Phi = 0$, $r = r_L$ in this rotating reference frame.

In order to make use of the new coordinates, the partial differential Equation (4.26) must be written in terms of r, Φ, and t rather than r, θ, and t. The following relations hold:

$$\frac{\partial u}{\partial r} = \frac{\partial u'}{\partial r}, \quad \frac{\partial^2 u}{\partial r^2} = \frac{\partial^2 u'}{\partial r^2}$$

$$\frac{\partial u}{\partial \theta} = \frac{\partial u'}{\partial \Phi}\frac{\partial \Phi}{\partial \theta} = \frac{\partial u'}{\partial \Phi}, \quad \frac{\partial^2 u}{\partial \theta^2} = \frac{\partial^2 u'}{\partial \Phi^2} \tag{4.35}$$

$$\frac{\partial u}{\partial t} = \frac{\partial u'}{\partial t} + \frac{\partial u'}{\partial \Phi}\frac{\partial \Phi}{\partial t} = \frac{\partial u'}{\partial t} - \Omega\frac{\partial u'}{\partial \Phi}$$

$$\frac{\partial^2 u}{\partial t^2} = \frac{\partial^2 u'}{\partial t^2} - 2\Omega\frac{\partial^2 u'}{\partial t \partial \Phi} + \Omega^2\frac{\partial^2 u'}{\partial \Phi^2}$$

The partial differential equation for $u'(r, \Phi, t)$ is therefore:

$$\rho\left[\frac{\partial^2 u'}{\partial t^2} - 2\Omega\frac{\partial^2 u'}{\partial t \partial \Phi} + \Omega^2\frac{\partial^2 u'}{\partial \Phi^2}\right] + \frac{Eh^2}{3(1-\sigma^2)}\left[\frac{\partial^2}{\partial r^2} + \frac{1}{r}\frac{\partial}{\partial r} + \frac{1}{r^2}\frac{\partial^2}{\partial \Phi^2}\right]^2 u'$$

$$= -\frac{1}{2h}\delta(\Phi)\frac{\delta(r-r_L)}{r_L}\left\{m_L\frac{\partial^2 u'}{\partial t^2} + c_L\frac{\partial u'}{\partial t} + k_L u'\right\} \tag{4.36}$$

To simplify the subsequent analysis, the terms in the eigenfunction expansion (4.34) corresponding to j=0 will be included in the double summation, with the index j running from 0 to ∞. Thus $B_{0n}(t)$ will be understood to be equal to zero wherever it may appear. When the

eigenfunction expansion (4. 34) is substituted into (4. 36), the resulting equation becomes:

$$\sum_{j=0}^{\infty}\sum_{n=0}^{\infty}\left\{\rho W_{jn}(r)\cos j\Phi\left[\frac{d^2A_{jn}}{dt^2}-2j\Omega\frac{dB_{jn}}{dt}+\left(p_{jn}^2-j^2\Omega^2\right)A_{jn}\right]\right.$$

$$\left.+\rho W_{jn}(r)\sin j\Phi\left[\frac{d^2B_{jn}}{dt^2}+2j\Omega\frac{dA_{jn}}{dt}+\left(p_{jn}^2-j^2\Omega^2\right)B_{jn}\right]\right\}$$

$$=-\frac{1}{2h}\delta(\Phi)\frac{\delta(r-r_L)}{r_L}\sum_{j=0}^{\infty}\sum_{n=0}^{\infty}\left\{W_{jn}(r)\cos j\Phi\left[m_L\frac{d^2A_{jn}}{dt^2}+c_L\frac{dA_{jn}}{dt}+k_LA_{jn}\right]\right.$$

$$\left.+W_{jn}(r)\sin j\Phi\left[m_L\frac{d^2B_{jn}}{dt^2}+c_L\frac{dB_{jn}}{dt}+k_LB_{jn}\right]\right\} \qquad (4.37)$$

If Equation (4. 37) is multiplied by $rW_{qv}(r)\sin q\Phi$ and integrated from 0 to 2π in Φ, and from b to a in r, the following equation is obtained:

$$\frac{d^2B}{dt^2}_{qv}+2q\Omega\frac{dA}{dt}_{qv}+\left(p_{qv}^2-q^2\Omega^2\right)B_{qv}=0 \qquad (4.38)$$

The contributions from the right-hand side of (4. 37) vanish because

$$\int_0^{2\pi}\delta(\Phi)\sin q\Phi\left\{\begin{matrix}\cos j\Phi\\ \sin j\Phi\end{matrix}\right\}d\Phi=0.$$

Similarly, if (4. 37) is multiplied by $rW_{qv}(r)\cos q\Phi$ and integrated over r and Φ, the result is:

$$\frac{d^2 A_{qv}}{dt^2} - 2q\Omega \frac{dB_{qv}}{dt} + (p_{qv}^2 - q^2\Omega^2) A_{qv}$$

$$= -\sum_{j=0}^{\infty} \sum_{n=0}^{\infty} G_{jnqv} \left[\frac{m_L}{2\rho h} \frac{d^2 A_{jn}}{dt^2} + \frac{c_L}{2\rho h} \frac{dA_{jn}}{dt} + \frac{k_L}{2\rho h} A_{jn} \right]$$

where

$$G_{jnqv} = W_{jn}(r_L) W_{qv}(r_L) \tag{4.39}$$

Equations (4.38) and (4.39) hold for $0 \leq q \leq \infty$ and $0 \leq v \leq \infty$. These equations constitute an infinite set of coupled equations for the $A_{qv}(t)$ and $B_{qv}(t)$. The important characteristic which makes these equations of use is that the coefficients of the A's and B's are all independent of time. This would not have been the case if the transformations (4.28) and (4.30) had not been utilized.

Equations (4.38) and (4.39) may be normalized by making use of the following notations:

$$\tau = p_{10} t, \quad \bar{m} = \frac{m_L}{M}, \quad \bar{k} = \frac{1}{p_{10}^2} \frac{k_L}{M}$$

$$\bar{p}_{qv} = \frac{p_{qv}}{p_{10}}, \bar{c}_L = \frac{1}{p_{10}} \frac{c_L}{M}, \quad \bar{s} = \frac{\Omega}{p_{10}}, \quad \bar{a} = \pi(b^2 - a^2) \tag{4.40}$$

Then (4.38) and (4.39) become:

$$\frac{d^2 B_{qv}}{d\tau^2} + 2q\bar{s}\frac{dA_{qv}}{d\tau} + \left(\bar{p}_{qv}^2 - q^2\bar{s}^2\right)B_{qv} = 0 \tag{4.41}$$

$$\frac{d^2 A_{qv}}{d\tau^2} - 2q\bar{s}\frac{dB_{qv}}{d\tau} + \left(\bar{p}_{qv}^2 - q^2\bar{s}^2\right)A_{qv} = -\sum_{j=0}^{\infty}\sum_{n=0}^{\infty} \bar{a}\, G_{jnqv}\left[\bar{m}\frac{d^2 A_{jn}}{d\tau^2} + \bar{c}_L\frac{dA_{jn}}{d\tau} + \bar{k}A_{jn}\right] \tag{4.42}$$

The general form of Equations (4.41) and (4.42) is very similar to that of (2.37) and (2.38) for the two degree of freedom rigid disk, and also similar to Equations (3.19), (3.20), and (3.21) for the three degree of freedom rigid disk. An eigenvalue problem of the same type as in the previous chapters may be obtained by truncating the infinite series for $u'(r, \Phi, t)$ at $j=j_1$, and $n=n_1$. Thus, the displacement $u'(r, \Phi, t)$ is approximated by a finite number of modes, as given by:

$$u'(r, \Phi, \tau) \cong \sum_{j=0}^{j_1}\sum_{n=0}^{n_1}\left[A_{jn}(\tau)\cos j\Phi + B_{jn}(\tau)\sin j\Phi\right]W_{jn}(r) \tag{4.43}$$

The infinite set of equations for the functions $A_{jn}(\tau)$ and $B_{jn}(\tau)$ is replaced by a finite set, given by (4.41) and (4.42) but with the series truncated at $j = j_1$ and $n = n_1$, and with $0 \le q \le j_1$, $0 \le v \le n_1$. The

number of equations in the truncated set is $(n_1+1)x(2j_1+1)$. This is because for q=0, $B_{0v} \equiv 0$ (refer to the discussion following Equation (4.36)), so (4.41) is identically satisfied. Thus, corresponding to q=0, there are n_1+1 equations like (4.42). For each q in the range $1 \le q \le j_1$, there are n_1+1 equations like (4.41), and n_1+1 equations like (4.42). Thus, the total number of equations is $(n_1+1)+j_1x2(n_1+1) = (n_1+1)x(2j_1+1)$. This corresponds to the number of unknowns $A_{jn}(\tau)(j=0,\ldots j_1, n=0,\ldots n_1)$ and $B_{jn}(\tau)(j=1,\ldots j_1, n=0,\ldots n_1)$.

Define the $(n_1+1)x(2j_1+1)$ component column vector $\underline{w}(\tau)$ as:

$$\underline{w}(\tau)=\left\{\begin{array}{l}\left\{\begin{array}{l}A_{00}\\A_{01}\\\vdots\\A_{0n_1}\end{array}\right\}\\\vdots\\\left\{\begin{array}{l}A_{j_10}\\\vdots\\A_{j_1n_1}\end{array}\right\}\end{array}\right\}\left[(j_1+1)x(n_1+1)A's\right]$$

$$\left.\begin{array}{l}\left\{\begin{array}{l}B_{10}\\\vdots\\B_{1n_1}\end{array}\right\}\\\vdots\\\left\{\begin{array}{l}B_{j_10}\\\vdots\\B_{j_1n_1}\end{array}\right\}\end{array}\right\}\left[j_1x(n_1+1)B's\right]$$

$$\Rightarrow (n_1+1)x(2j_1+1)\text{elements} \qquad (4.44)$$

Further, define the $2x\left[(n_1+1)x(2j_1+1)\right]$ component column vector $\underline{x}(\tau)$ as:

$$\underline{x}(\tau)=\left\{\begin{Bmatrix}\underline{w}(\tau)\end{Bmatrix}\atop\begin{Bmatrix}\frac{d\underline{w}(\tau)}{d\tau}\end{Bmatrix}\right\}$$

Then, the truncated system of equations may be written in matrix form as:

$$P\frac{d\underline{x}}{d\tau}=Q\underline{x}\ ,\quad \underline{x}(0)=\underline{f}\ , \tag{4.45}$$

where P and Q are each $\{2x[(n_1+1)x(2j_1+1)]\}x\{2x[(n_1+1)x(2j_1+1)]\}$ square matrices. The matrices P and Q may be written most conveniently as:

$$P=\begin{bmatrix} I & O \\ O & P_m \end{bmatrix}$$

$$Q=\begin{bmatrix} O & I \\ Q_k & Q_c \end{bmatrix} \tag{4.46}$$

The matrix P_m involves all of the terms with $\bar{m}$, while Q_k and Q_c contain all of the quantities involving $\bar{k}$ and $\bar{c}_L$ respectively. All of the submatrices in (4.46) are square matrices of dimension $[(n_1+1)x(2j_1+1)]$.

The matrix P_m has the form:

$$P_m = I + \begin{bmatrix} E_m & O \\ O & O \end{bmatrix} , \tag{4.47}$$

where P_m and I are each square matrices of the dimension $[(n_1+1)x(2j_1+1)]$, and E_m is a square matrix of dimension $[(n_1+1)x(j_1+1)]$, whose elements $e_m(i, j)$ are given by:

$$e_m(i, j) = \overline{a}\,\overline{m}\, G_{\alpha\beta\gamma\delta} \tag{4.48}$$

where

$$\left.\begin{aligned} \alpha &= IP\left(\frac{j-1}{n_1+1}\right) \\ \beta &= (j-1)-(n_1+1)IP\left(\frac{j-1}{n_1+1}\right) \\ \gamma &= IP\left(\frac{i-1}{n_1+1}\right) \\ \delta &= (i-1)-(n_1+1)IP\left(\frac{i-1}{n_1+1}\right) \\ 1 &\le i, j \le (n_1+1)(j_1+1) \end{aligned}\right\} \tag{4.49}$$

The constants $G_{\alpha\beta\gamma\delta}$ in (4.48) were defined in Equation (4.39). The notation "IP" appearing in Equation (4.49) stands for "Integer Part." IP(x) is defined as the greatest integer less than or equal to x.

The matrix Q_k appearing in (4.46) has the form:

$$Q_k = \begin{bmatrix} T_0 & & & & \\ & T_1 & & 0 & \\ & & \ddots & & \\ & & & T_{j_1} & \\ & & & & T_1 \\ & & & & & \ddots \\ & 0 & & & & & T_{j_1} \end{bmatrix} + \begin{bmatrix} E_k & 0 \\ 0 & 0 \end{bmatrix} \qquad (4.50)$$

where Q_k is a square matrix of dimension $[(n_1+1)x(2j_1+1)]$, E_k is a square matrix of dimension $[(n_1+1)x(j_1+1)]$, and the T_i are square diagonal matrices of dimension (n_1+1). T_i has the form:

$$T_i = \begin{bmatrix} -\bar{p}_{i0}^2 + i^{2-}\bar{s}^2 & 0 & \cdots & 0 \\ 0 & -\bar{p}_{i1}^2 + i^{2-}\bar{s}^2 & & \vdots \\ \vdots & & & \\ 0 & \cdots & & -\bar{p}_{in_1}^2 + i^{2-}\bar{s}^2 \end{bmatrix} \qquad (4.51)$$

The matrix E_k has element $e_k(i, j)$ given by:

$$e_k(i, j) = -\bar{a}\,\bar{k}\, G_{\alpha\beta\gamma\delta} \qquad (4.52)$$

where α, β, γ, and δ are given by (4.49).

The matrix Q_c appearing in Equation (4.46) has the form:

$$Q_c = \begin{bmatrix} \begin{bmatrix} & & \\ & E_c & \\ & & \end{bmatrix} \begin{bmatrix} 0 & 0 \ldots 0 \\ s_1 & 0 \ldots 0 \\ 0 & s_2 \ldots 0 \\ \vdots & \ddots \\ 0 \ldots & s_{j_1} \end{bmatrix} \\ \begin{bmatrix} 0 & -s_1 & 0 \ldots 0 \\ 0 & 0 & -s_2 \\ \vdots & & \ddots \\ 0 & 0 & -s_{j_1} \end{bmatrix} \begin{bmatrix} & & \\ & 0 & \\ & & \end{bmatrix} \end{bmatrix} \tag{4.53}$$

The matrices s_i appearing in (4.53) are square diagonal matrices of dimension (n_1+1) having the form:

$$s_i = \begin{bmatrix} 2i\bar{s} & & & \\ & 2i\bar{s} & & \\ & & \ddots & \\ & & & 2i\bar{s} \end{bmatrix} \tag{4.54}$$

The matrix E_c is a square matrix of dimension $[(n_1+1)x(j_1+1)]$ having elements $e_c(i, j)$ given by:

$$e_c(i, j) = -\bar{a}\,\bar{c}_L G_{\alpha\beta\gamma\delta} \tag{4.55}$$

With these definitions for the matrices P and Q, the matrix differential (4.45) may be solved by assuming a solution of the form:

$$\underline{x}(\tau) = e^{\lambda \tau} \underline{\Phi} \quad , \tag{4.56}$$

where $\underline{\Phi}$ is a time independent vector. The matrix Equation (4.45) then becomes:

$$(P^{-1}Q - \lambda I)\underline{\Phi} = 0 \tag{4.57}$$

For a nontrivial solution, the determinant of $(P^{-1}Q - \lambda I)$ must vanish:

$$\left| P^{-1}Q - \lambda I \right| = 0 \tag{4.58}$$

Since the dimension of P and Q is $\{2x[(n_1+1)x(2j_1+1)]\}$, the number of eigenvalues λ_i is also $\{2x[(n_1+1)x(2j_1+1)]\}$.

4.4 Low Order Approximations

Case 1: Single mode approximation.

The matrix eigenvalue problem derived in section 4.3 assumed that the series expression for $u'(r, \Phi, \tau)$ (given by Equation (4.43)) begins with $j=0$ and $n=0$. Hence, a single mode truncation of that series obtained by setting $j_1=0$ and $n_1=0$ would approximate the disk motion by the mode shape having no nodal diameters and no nodal circles. It is more helpful to consider a single mode approximation having a general number of nodal diameters and nodal circles, so assume that the deflection $u'(r, \Phi, \tau)$ is approximated by:

$$u'(r,\Phi,\tau)\cong\left[A_{j_1n_1}(\tau)\cos j_1\Phi+B_{j_1n_1}(\tau)\sin j_1\Phi\right]W_{j_1n_1}(r) \qquad (4.59)$$

Thus, the double sum in (4.43) begins and ends at $j=j_1$ and $n=n_1$. The equations for $A_{j_1n_1}(\tau)$ and $B_{j_1n_1}(\tau)$ are given by (4.41) and (4.42) with all other A_{jn} and B_{jn} vanishing. Thus, Equations (4.41) and (4.42) becomes:

$$\left[1+\Delta_1\bar{m}\right]\frac{d^2A_{j_1n_1}}{d\tau^2}+\Delta_1\bar{c}_L\frac{dA_{j_1n_1}}{d\tau}-2j_1\bar{s}\frac{dB_{j_1n_1}}{d\tau}$$
$$+\left(1+\Delta_1\bar{k}-j_1^2\bar{s}^2\right)A_{j_1n_1}=0 \qquad (4.60)$$

$$\frac{d^2B_{j_1n_1}}{d\tau^2}+2j_1\bar{s}\frac{dA_{j_1n_1}}{d\tau}+\left(1-j_1^2\bar{s}^2\right)B_{j_1n_1}=0 \qquad (4.61)$$

where

$$\Delta_1=\bar{a}G_{j_1n_1j_1n_1} \qquad (4.62)$$

The above equations have been normalized with respect to $p_{j_1n_1}$ rather than p_{10} as in (4.40), so that the comparison with Equations (2.37) and (2.38) is clearer. Note that equations (4.60) and (4.61) are identical to the equations describing the motion of the two degree of freedom rigid disk, if the following parameters are changed in (2.37) and (2.38):

$$\text{Two degree of freedom rigid disk} \quad \left\{ \begin{array}{ccc} \Delta & \rightarrow & \Delta_1 \\ \overline{c} & \rightarrow & 0 \\ \overline{s} & \rightarrow & j_1 \overline{s} \end{array} \right\} \quad \text{One mode approximation of elastic disk} \tag{4.63}$$

Hence, if the disk motion is represented by a single mode approximation of the type (4.59), the predicted response will be precisely like that discussed in Chapter 2. In particular, the stiffness instability region and terminal instability zones will be present. Further, all the figures and equations describing the behavior of the rigid disk in both the steady-state and transient cases apply for the single mode approximation here, if the relations (4.63) are kept in mind. It is interesting to note that $\overline{c}$, which is the coefficient of foundation damping for the two degree of freedom rigid disk, must vanish for the analogy to be valid. The reason is that the partial differential Equation (4.1) contains no dissipation term, and so there is no damping associated with the disk, except of course the load damping $\overline{c}_L$.

Case 2: Two mode approximation

Consider the case when the eigenfunction series is terminated at $j_1 = 1$ and $n_1 = 0$. The disk displacement $u'(r, \Phi, \tau)$ is thus approximated by:

$$\begin{aligned} u'(r, \Phi, \tau) = & A_{00}(\tau) W_{00}(r) \\ & + \left[A_{10}(\tau) \cos \Phi + B_{10}(\tau) \sin \Phi \right] W_{10}(r) \end{aligned} \tag{4.64}$$

The two modes represented in (4.64) are the mode having zero nodal diameters and zero nodal circles, and the mode with one nodal diameter and zero nodal circles. In this case, Equations (4.41) and (4.42) become:

$$\left[1+\bar{a}G_{1010}\bar{m}\right]\frac{d^2A_{10}}{d\tau^2}+\bar{a}G_{0010}\bar{m}\frac{d^2A_{00}}{d\tau^2}-2\bar{s}\frac{dB_{10}}{d\tau}+\bar{a}G_{1010}\bar{c}_L\frac{dA_{10}}{d\tau}$$
$$+\bar{a}G_{0010}\bar{c}_L\frac{dA_{00}}{d\tau}+(1+\bar{a}G_{1010}\bar{k}-\bar{s}^2)A_{10}+\bar{a}G_{0010}A_{00}=0 \tag{4.65}$$

$$\frac{d^2B_{10}}{d\tau^2}+2\bar{s}\frac{dA_{10}}{d\tau}+(1-\bar{s}^2)B_{10}=0 \tag{4.66}$$

$$\left[1+\bar{a}G_{0000}\bar{m}\right]\frac{d^2A_{00}}{d\tau^2}+\bar{a}G_{1000}\bar{m}\frac{d^2A_{10}}{d\tau^2}+\bar{a}G_{0000}\bar{c}_L\frac{dA_{00}}{d\tau}$$
$$+\bar{a}G_{1000}\bar{c}_L\frac{dA_{10}}{d\tau}+\left(\bar{p}_{00}^2+\bar{a}G_{0000}\bar{k}\right)A_{00}+\bar{a}G_{1000}A_{10}=0 \tag{4.67}$$

The equations above have much the same form as (3.19), (3.20), and (3.21) of Chapter 3, although (3.19), (3.20), and (3.21) have been arranged so that the second derivatives are uncoupled.

A general analogy such as (4.63) cannot be made in this case, since the frequencies p_{00} and p_{10} are not equal for elastic disks except in special cases. A direct analogy would be possible if the frequency p_{00} in the rigid disk problem (that is, the frequency of v(t) in Chapter 3)

were changed in the manner described in the second paragraph following Equation (3. 38). The modal coupling instability region, present in the three degree of freedom rigid disk problem, remains as an important characteristic of elastic modal interaction.

The effects of taking a larger number of modes in the eigenfunction series (4. 43) may be seen quite easily in a Frequency-Speed plot. Since the precise character of the Frequency-Speed plot depends on the specific boundary conditions of the problem, a particular example will be considered in the following section.

4. 5 Elastic Disk with Clamped Center

The free transverse vibration of an elastic disk, clamped at its center and free at the outer boundary, was investigated in a classic paper by Southwell in 1921. The boundary conditions for such a disk are given by Equations (4. 12) with b set equal to zero. Southwell was able to show that the determinental equations giving the eigenfrequencies and eigenfunctions of modes having one or more nodal diameters reduce to the same forms as those for a completely free disk. This is helpful analytically, because the Y_j and K_j functions appearing in Equation (4. 11) then do not appear for $j \geq 1$. The expressions for these eigenfunctions, as well as comprehensive tables of eigenfrequencies and receptance data for forced vibration problems, may be found in the monograph by

McLeod and Bishop.[2] The eigenfunctions $W_{jn}(r)$, for $j \geq 1$, are:

$$W_{jn}(r)=N_7(\kappa_{jn}a)J_j(\kappa_{jn}r)-N_5(\kappa_{jn}a)I_j(\kappa_{jn}r) \tag{4.68}$$

where

$$N_7(\kappa_{jn}a)=\left[\frac{j(j-1)(1-\sigma)}{a^2}+\kappa_{jn}^2\right]I_j(\kappa_{jn}a)-\frac{\kappa_{jn}(1-\sigma)}{a}I_{j+1}(\kappa_{jn}a)$$

$$N_5(\kappa_{jn}a)=\left[\frac{j(j-1)(1-\sigma)}{a^2}-\kappa_{jn}^2\right]J_j(\kappa_{jn}a)+\frac{\kappa_{jn}(1-\sigma)}{a}J_{j+1}(\kappa_{jn}a)$$

One exception to (4.68) occurs when $j=1$ and $n=0$, which is a special case to be discussed shortly. The radial eigenfunctions given by (4.68) are not properly normalized as required by Equation (4.18). That is, the functions $W_{jn}(r)$ must be scaled so that:

$$\pi\int_0^a \overline{W}_{jn}^2(r)rdr = 1 \tag{4.69}$$

The normalized eigenfunction $\overline{W}_{jn}(r)$ in (4.69) is then related to the eigenfunction of (4.68) by:

$$\overline{W}_{jn}(r)=\frac{W_{jn}(r)}{\left[\pi\int_0^a W_{jn}^2(r)rdr\right]^{\frac{1}{2}}} \tag{4.70}$$

The integral necessary in the denominator of (4.70) may be evaluated in closed form as:

$$\int_0^a W_{jn}^2(r)\,r\,dr = N_7^2(\kappa_{jn}a)\,\mathcal{J}_1 - 2N_7(\kappa_{jn}a)N_5(\kappa_{jn}a)\,\mathcal{J}_2 + N_5^2(\kappa_{jn}a)\,\mathcal{J}_3 \qquad (4.71)$$

where

$$\mathcal{J}_1 = \frac{1}{2}a^2\left[J_{j-1}^2(\kappa_{jn}a) - \frac{2j}{\kappa_{jn}a}J_{j-1}(\kappa_{jn}a)J_j(\kappa_{jn}a) + J_j^2(\kappa_{jn}a)\right]$$

$$\mathcal{J}_2 = \frac{a}{2\kappa_{jn}}\left[J_j(\kappa_{jn}a)I_{j-1}(\kappa_{jn}a) - I_j(\kappa_{jn}a)J_{j-1}(\kappa_{jn}a)\right]$$

$$\mathcal{J}_3 = -\frac{1}{2}a^2\left[I_{j-1}^2(\kappa_{jn}a) - \frac{2j}{\kappa_{jn}a}I_{j-1}(\kappa_{jn}a)I_j(\kappa_{jn}a) - I_j^2(\kappa_{jn}a)\right]$$

For the modes having zero nodal diameters, the eigenfunctions $W_{0n}(r)$ are clearly different from those for a completely free disk. McLeod and Bishop give the eigenfunctions for the disk with a fixed center as:

$$W_{0n}(r) = \left[Y_1(\kappa_{0n}a) - \frac{2}{\pi}K_1(\kappa_{0n}a)\right]\left[I_0(\kappa_{0n}r) - J_0(\kappa_{0n}r)\right] + \left[J_1(\kappa_{0n}a) - I_1(\kappa_{0n}a)\right]\left[Y_0(\kappa_{0n}r) + \frac{2}{\pi}K_0(\kappa_{0n}r)\right] \qquad (4.72)$$

Once again, these eigenfunctions must be normalized so that Equation (4.18) is valid, reducing in this case to:

$$2\pi\int_0^a \overline{W}_{0n}^2(r)\,r\,dr = 1 \qquad (4.73)$$

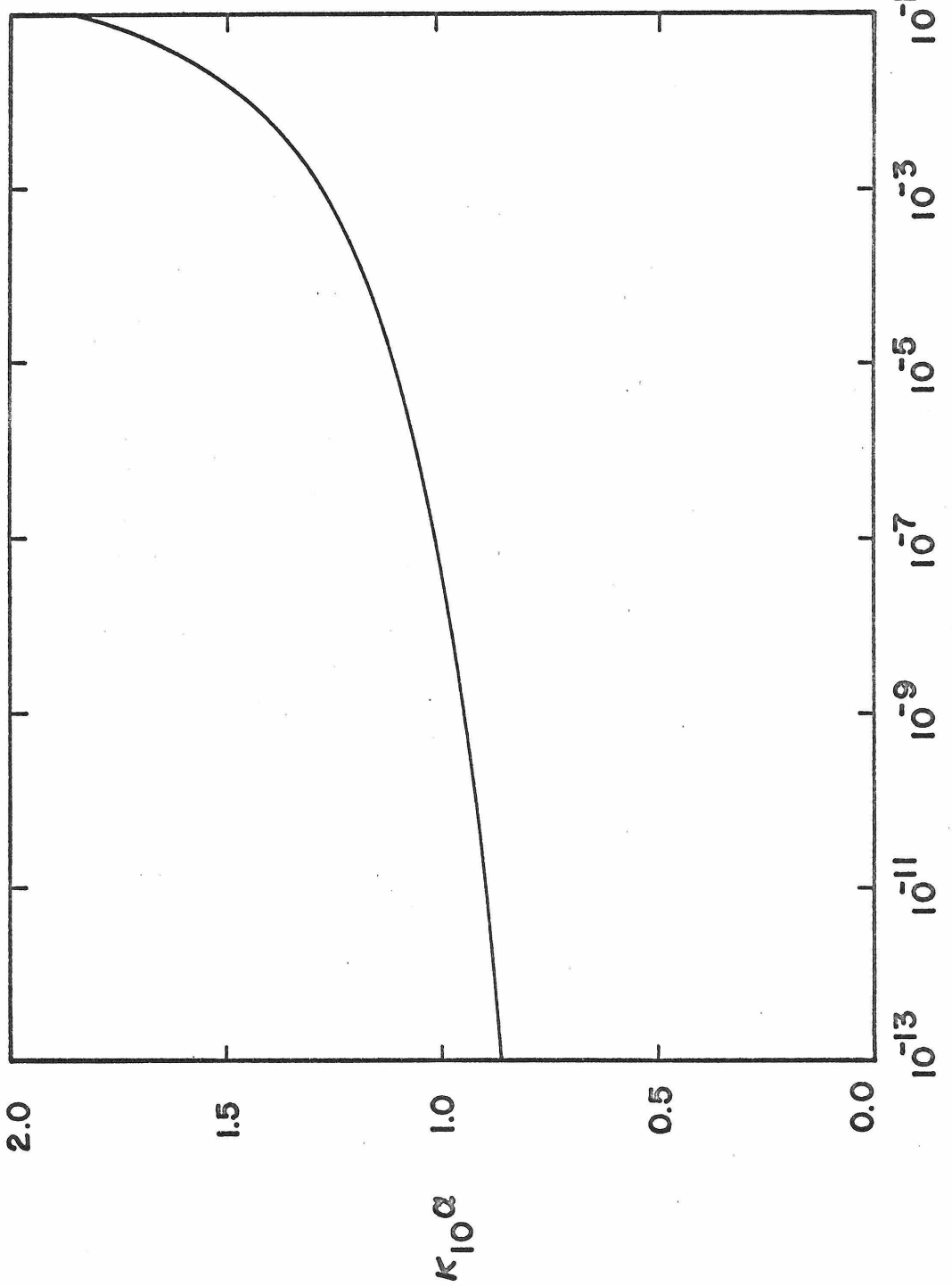

Fig.32: Behavior of K_{10} as a function of b/a .

The factor of 2 which does not appear in (4.69) is due to the integration over θ. The normalized eigenfunctions $\overline{W}_{on}(r)$ are related to those of (4.72) by:

$$\overline{W}_{0n}(r)=\frac{W_{0n}(r)}{\left[2\pi\int_0^a W_{0n}^2(r)rdr\right]^{\frac{1}{2}}} \qquad (4.74)$$

Because of the appearance of $Y_0(r)$ and $K_0(r)$ in (4.72), the integral appearing in (4.74) is most easily evaluated numerically.

As was pointed out earlier in this section, the assumption that the disk is clamped at its center (that is, b=0 in Equations (4.12)) eliminates the Y_j and K_j functions from the eigenfunctions $W_{jn}(r)$ for $j \geq 1$. This simplifies the analysis considerably, but introduces another difficulty which is undesirable from a physical standpoint. The problem, which has been discussed in detail by Southwell, [1] is that as the inner clamping radius b tends toward zero, the eigenvalue κ_{10} (and therefore the frequency p_{10}) tends toward zero as well. For very small but nonvanishing values of b, κ_{10} behaves as is shown in Figure 32. Clearly, most physically meaningful problems lie somewhere in the range of nonvanishing κ_{10}. In order to approximate the physical problem, Southwell introduces the approximate eigenfunction $\Psi_{10}(r,\theta)$ to accompany the eigenvalue κ_{10}, where:

$$\Psi_{10}(r,\theta) = (1+\zeta r) r \sin(\theta - \varepsilon_{10})$$
$$= W_{10}(r)\sin(\theta - \varepsilon_{10}) \tag{4.75}$$

The function $\Psi_{10}(r,\theta)$ satisfies the partial differential Equation (4.2) when κ_{10} vanishes, and satisfies the boundary conditions, provided that ζ is infinitesimal but satisfies the relation:

$$1+\zeta\left[\log r+1\right]\Big|_{r=b} = 0 \tag{4.76}$$

The choice of b/a is relatively arbitrary, and will affect the shape as well as the frequency of the mode having one nodal diameter and zero nodal circles. From Figure 32 a value of $b/a=10^{-7}$ was selected as a representative figure. This value of b/a lies in a relatively flat portion of the curve, and has a corresponding value of $\kappa_{10}a \cong 1.015$. The value of ζ from Equation (4.76) is 0.078. The eigenfunction $W_{10}(r)$ must also be normalized according to (4.18), giving:

$$\overline{W}_{10}(r) = \frac{W_{10}(r)}{\left[\pi \int_b^a W_{10}^2(r) r dr\right]^{\frac{1}{2}}} \tag{4.77}$$

The integral appearing in the denominator of (4.77) can be evaluated analytically in this case.

Combining the results of Southwell, and McLeod and Bishop, the eigenvalues $\kappa_{jn}a$ are given in Table 4.1 below.

j = Number of Nodal Diameters

n=Number of Nodal Circles	0	1	2	3	4	5
0	1.95	1.015	2.29	3.50	4.64	5.75
1	4.73	4.53	5.96	7.28	8.57	9.82
2	7.79	7.73	9.20	10.58	11.93	13.25

Table 4.1 Frequency Parameters $K_{jn}a$

The frequencies p_{jn} are related to the eigenvalues K_{jn} by the Equation (4.14). That is the p_{jn} are proportional to K_{jn}^2. Normalized with respect to p_{10}, as indicated in (4.40), the normalized natural frequencies $\bar{p}_{jn}$ are given in Table 4.2 below.

j = Number of Nodal Diameters

n=Number of Nodal Circles	0	1	2	3	4	5
0	3.69	1.00	5.10	11.9	21.0	32.2
1	21.8	20.0	34.6	51.5	71.4	93.7
2	58.9	58.0	82.5	109	138	171

Table 4.2 Normalized Natural Frequencies $\bar{p}_{jn}$

The critical speed of the mode with j nodal diameters and n nodal circles was defined earlier as p_{jn}/j. The normalized critical speeds are given by $\frac{1}{p_{10}} \frac{p_{jn}}{j}$, summarized in Table 4.3 below.

j=Number of Nodal Diameters

n=Number of Nodal Circles	0	1	2	3	4	5
0		1.00	2.55	3.95	5.25	6.45
1		20.0	17.3	17.2	17.9	18.7
2		58.0	41.2	36.4	34.5	34.2

Table 4.3 Normalized Critical Speeds

These results are summarized in Figure 31, which is the Frequency-Speed plot for the centrally-clamped elastic disk. The only modes with branches which appear in Figure 31 are the lowest six modes, having 0 nodal circles and 0 to 5 nodal diameters.

In order to follow the conventions established by Southwell, McLeod and Bishop, and others, the radial coordinate r has not yet been normalized. It is somewhat more convenient to define $\bar{r}$ as r/a, reducing integrals of the type in the denominator of (4.70) to the form:

$$\pi \int_0^a W_{jn}^2(r) r dr = \pi a^2 \int_0^1 W_{jn}(\bar{r}) \bar{r} \, d\bar{r} \qquad (4.78)$$

The factor πa^2 will then cancel $\bar{a}$ as it appears in Equations (4.42), (4.48), (4.52), and (4.55), so that only dimensionless quantities are present throughout. This added normalization will be used in the following discussions in order to represent a wider range of problems with the same number of parameters.

To set up the eigenvalue problem (4.58) for the disk with an attached moving spring and mass, it is first necessary to compute the matrices P and Q. The parameters which distinguish one disk problem from another, aside from the frequencies $\overline{p}_{jn}$, are the eigenfunctions $\overline{W}_{jn}(\overline{r})$. These enter through the constants G_{jnqv} given in Equation (4.39), which are:

$$G_{jnqv} = \overline{W}_{jn}(\overline{r}_L)\overline{W}_{qv}(\overline{r}_L) \tag{4.79}$$

Hence, having determined the eigenfrequencies and modal shapes for the free vibration of the disk alone, the constants G_{jnqv} are evaluated at the load radius $\overline{r}_L$. These constants are independent of the load speed Ω. The load mass, stiffness, and damping parameters are then used in computing the submatrices P_m, Q_k, and Q_c, from which P and Q are determined. The matrix P is then inverted, and the eigenvalues of the matrix $P^{-1}Q$ are found by the use of standard numerical techniques.

As an example of the Frequency-Speed behavior of a centrally-clamped elastic disk, consider the results shown in Figures 33a, b, c, and d. These figures correspond respectively to one, two, three, and six mode approximations with the normalized load parameters in each case given by: $\overline{r}_L = \frac{r_L}{a} = 0.5$, $\overline{k} = 1.0$, $\overline{m} = 0.1$, and $\overline{c}_L = 0.0$.

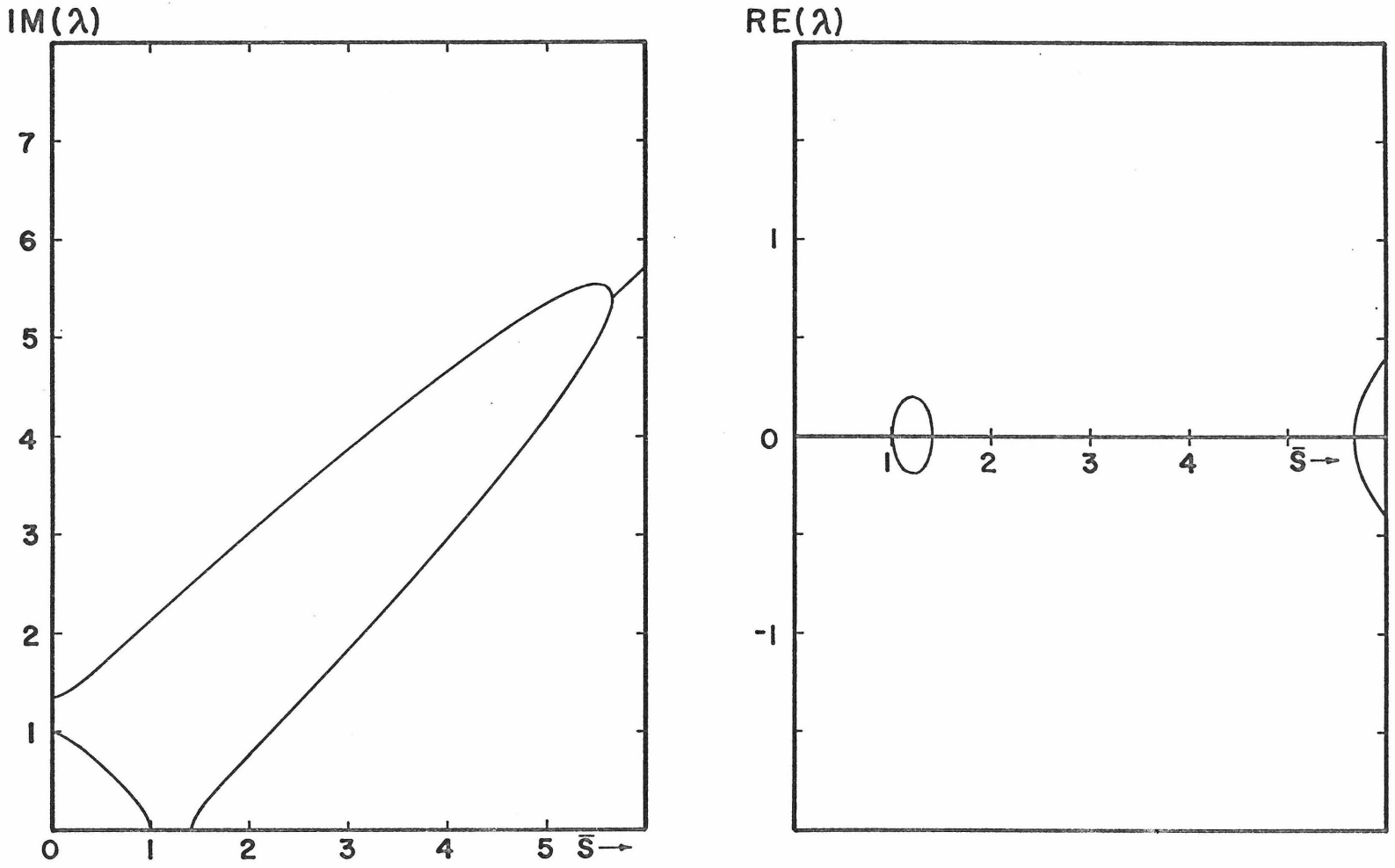

Fig. 33a: Single mode approximation. ($\bar{m}$=0.1, $\bar{k}$=1.0, $\bar{r}_L$=0.5, $\bar{c}_L$=0.0).

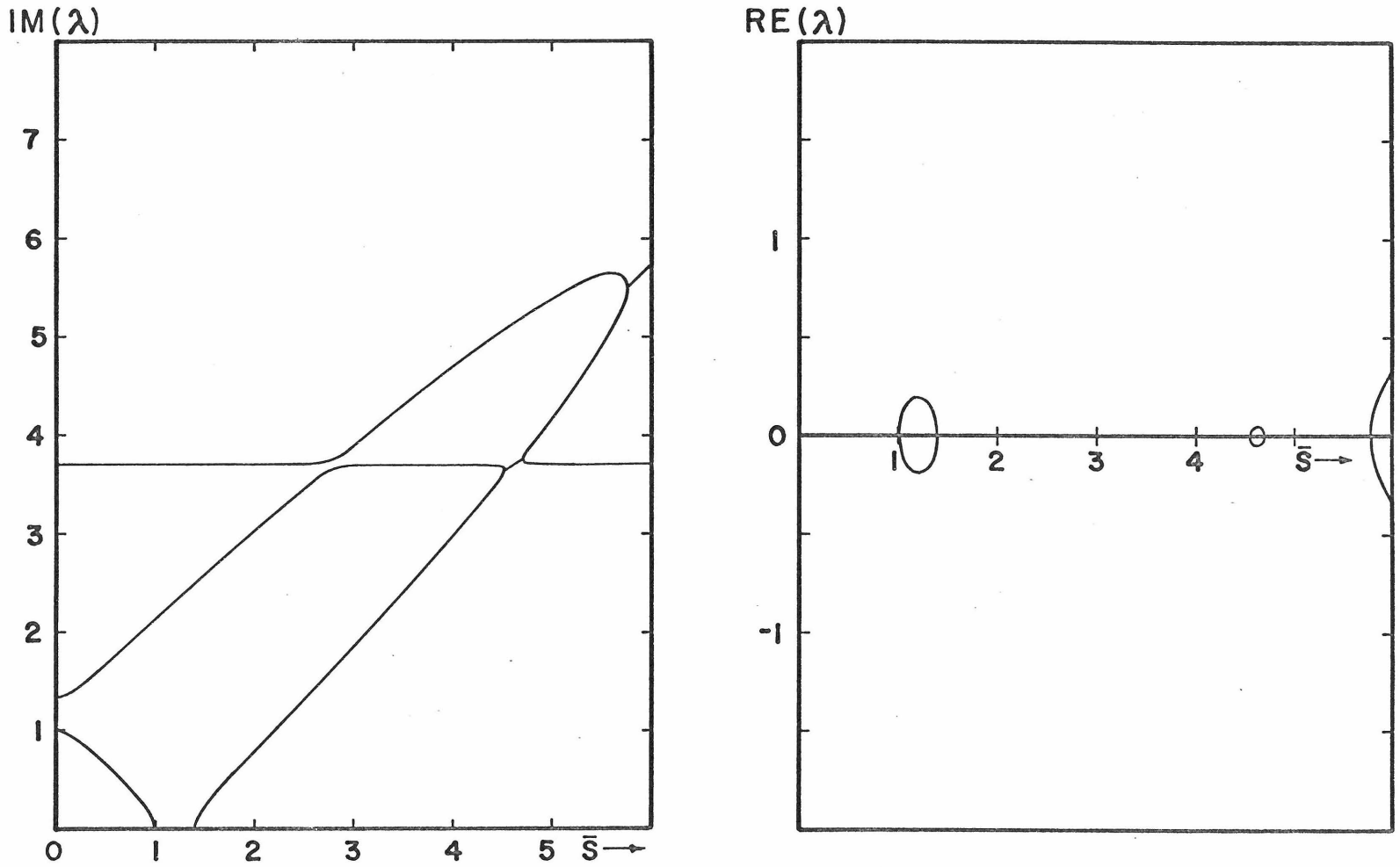

Fig. 33b: Two mode approximation (m=0.1, k=1.0, r_L=0.5, c_L=0.0).

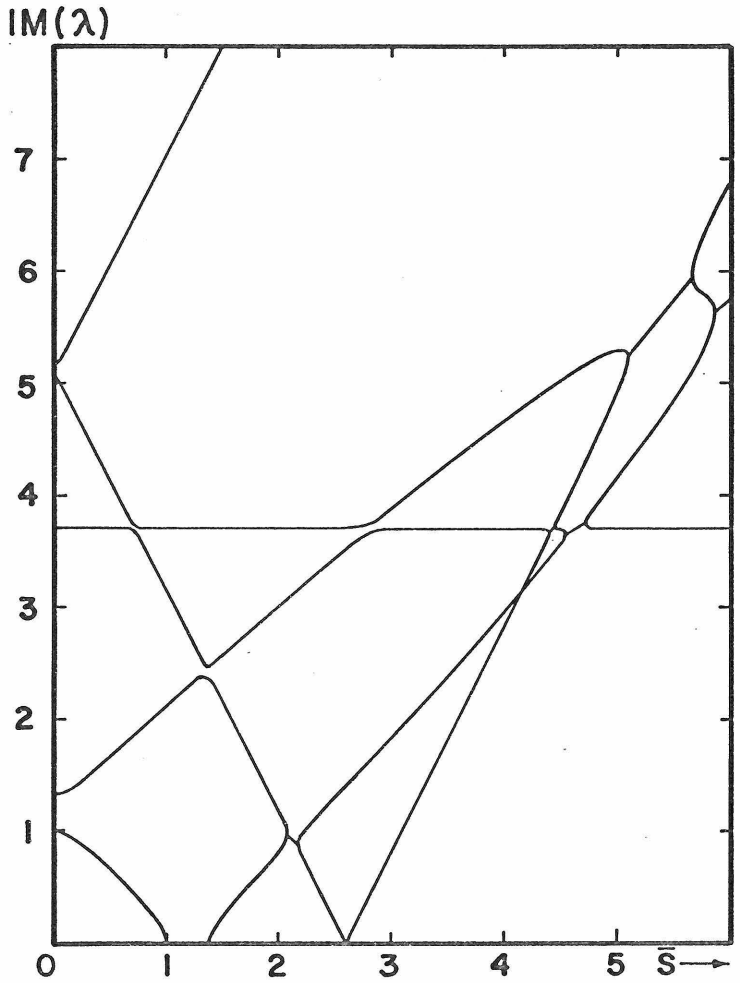

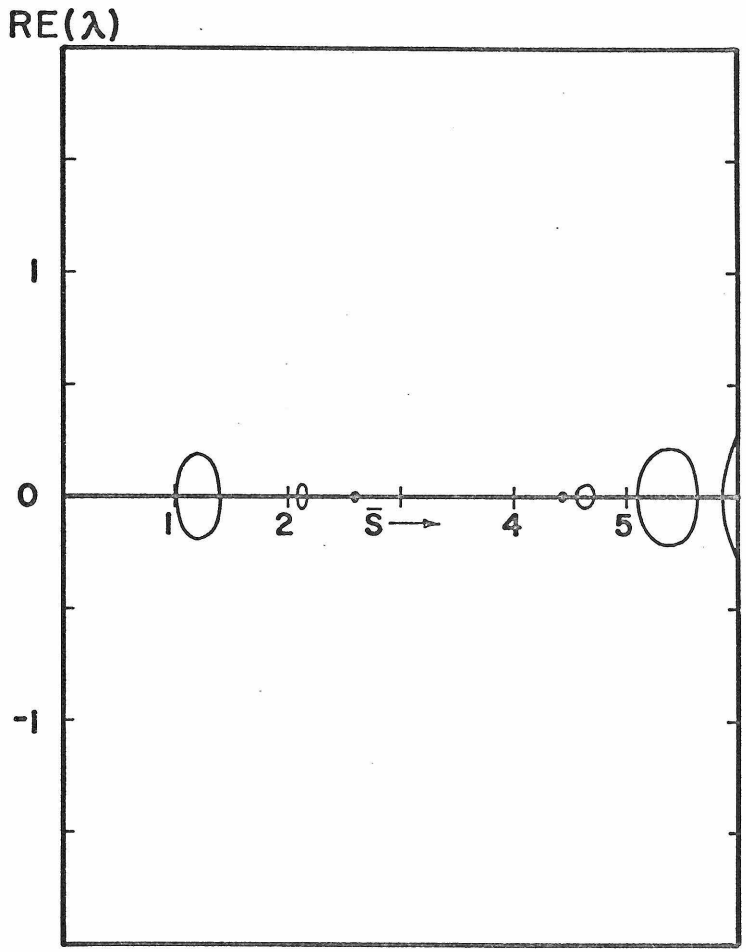

Fig. 33c: Three mode approximation ($\bar{m}$=0.1, $\bar{k}$=1.0, $\bar{r}_L$=0.5, $\bar{c}_L$=0.0).

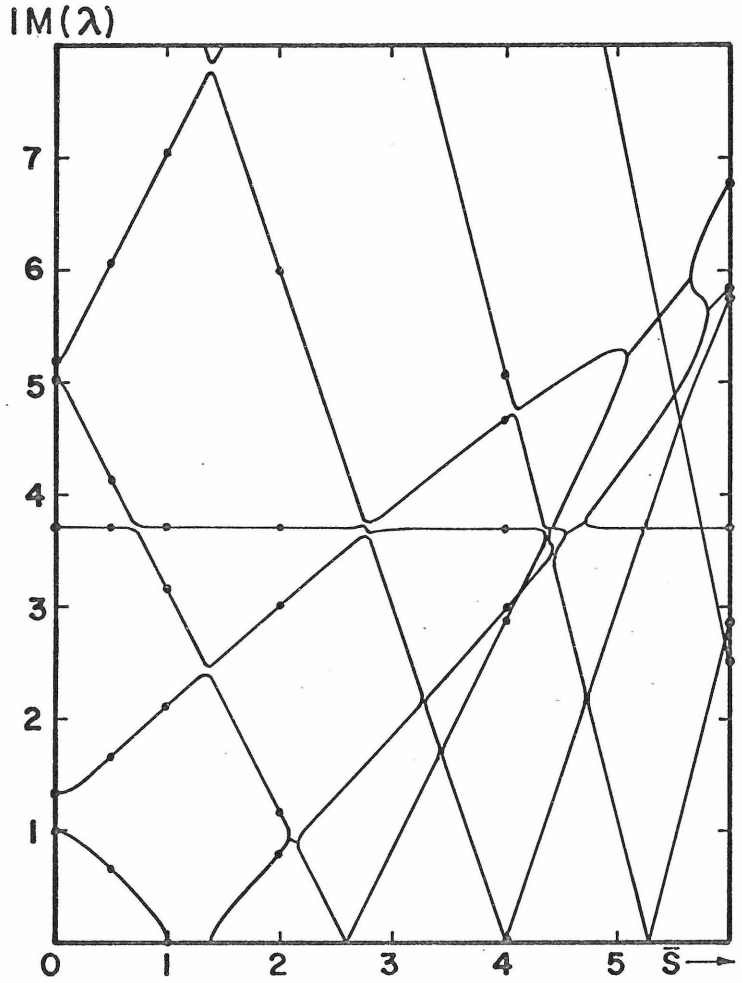

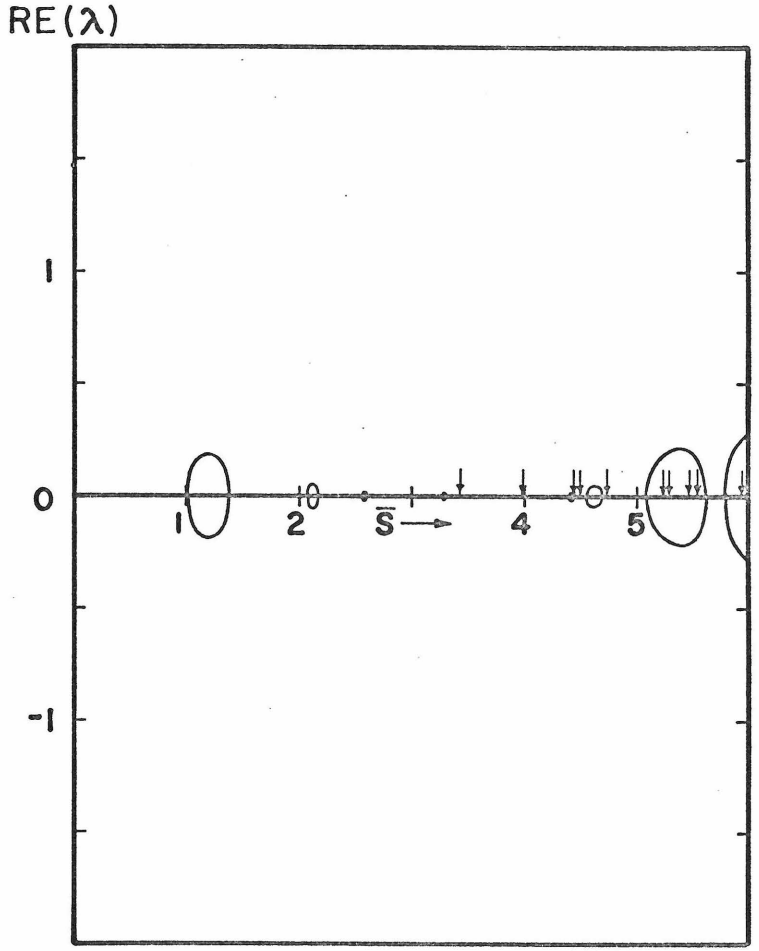

Fig. 33d: Six mode approximation ($\bar{m}$=0.1, $\bar{k}$=1.0, $\bar{r}_L$=0.5, $\bar{c}_L$=0.0).

The one mode approximation of Figure 33a assumes that the deflection of the disk is given by Equation (4.59) with $j_1 = 1$ and $n_1 = 0$. This is the mode with one nodal diameter and zero nodal circles. In a one mode approximation such as this, it is easier to use the relation (4.63) in Equation (2.47) to obtain the eigenvalues exactly rather than to solve the eigenvalue problem (4.58) numerically. For the parameters of Figure 33a. the constant $\Delta_1 = \bar{a} G_{1010} \cong 0.967$, so that $\Delta_1 \bar{m} \cong 0.0967$ and $\Delta_1 \bar{k} \cong 0.967$. The width of the stiffness instability region may be calculated from Equation (2.64) of Chapter 2, with the substitution (4.63), as $1 < \bar{s} < 1.40$, and the terminal velocity $\bar{s}^*$ may be estimated from Figure 8 as $\bar{s}^* \cong 5.7$. Because the stiffness instability region and terminal velocity are so easily predicted from the one mode approximation and the results of Chapter 2, it will be of particular interest to note how these regions change as more modes are taken into account.

If the mode having zero nodal diameters and zero nodal circles is included, then the disk displacement will be of the type (4.64). The result of this two mode approximation is shown in the Frequency-Speed diagram in Figure 33b. This figure was obtained by solving the eigenvalue problem (4.58), with $n_1 = 0$ and $j_1 = 1$. The matrices P and Q are 6x6 matrices in this case, and the 6 eigenvalues were obtained for 240 discrete values of $\bar{s}$ (that is, the step size in $\bar{s}$ was

0.025). Figure 33b shows the expected modal coupling instability region at the intersection of the j=0, n=0 branch with the reflected branch of the j=1, n=0 mode. This instability region occurs for speeds in the range $4.55 < \bar{s} < 4.75$. The stiffness instability region appears to be essentially unchanged from the one mode approximation, but the terminal velocity $\bar{s}^*$ appears to be increased somewhat to about $\bar{s}^* \cong 5.75$. If Figures 33a and 33b are superposed, the two mode approximation differs only in the immediate neighborhood of the coupling zones, and near the terminal velocity $\bar{s}^*$.

Figure 33c shows a three mode approximation, formed by adding the mode with two nodal diameters and zero nodal circles (j=2, n=0) to the approximation. Thus, in (4.43) $j_1=2$ and $n_1=0$. The matrices P and Q in the eigenvalue problem (4.58) are now 10x10, and Figure 33c was obtained by solving the eigenvalue problem at 240 discrete values of $\bar{s}$. There are now four new regions of instability in addition to the three regions of Figure 33b. One is a stiffness instability region for the j=2, n=0 mode which occurs immediately above the critical speed of that mode, in the region $2.55 < \bar{s} < 2.60$. If the j=2, n=0 mode is used in a one mode approximation, the stiffness instability region may be approximated by Equation (2.64), using the substitutions (4.63). That is,

$$1 < 4\frac{\Omega^2}{p_{20}^2} < 1 + \bar{a} G_{2020} \frac{1}{p_{20}^2} \frac{k}{M} \tag{4.80}$$

This equation may be rewritten as:

$$\bar{p}_{20}^2 < 4\bar{s}^2 < \bar{p}_{20}^2 + \bar{a} G_{2020} \bar{k} \tag{4.81}$$

Substituting the appropriate values into Equation (4.81), the stiffness instability region for the mode with two nodal diameters and zero nodal circles is found to be $2.55 < \bar{s} < 2.58$. This compares well with the three mode result, the accuracy of which is limited by the discrete step size in $\bar{s}$ of 0.025.

The other three new regions of instability are all due to modal coupling, and all have the same property in common. If that part of the forward branch which lies beyond the critical speed of a particular mode is denoted as the reflected branch, then it can be seen in Figure 33c that the modal coupling instability regions occur where reflected branches intersect nonreflected branches. Additionally, there is no apparent modal coupling instability at the intersection of two non-reflected branches, or at the intersection of two reflected branches. These properties appear to be valid in every case which has been studied to date.

As more modes are added, the resulting Frequency-Speed plot becomes more complicated until all the six modes shown in Figure 31

are used. The addition of modes which do not have branches appearing in the region being investigated ($0 \leq \bar{s} \leq 6$, $0 \leq \mathrm{Im}\{\lambda\} \leq 8$) have no noticable affect on this region when they are added to the approximation. Figure 33d shows the result of the six mode approximation obtained for $j_1=5$ and $n_1=0$ in Equation (4.43). The matrices P and Q for this case are each 22x22. With the step size in $\bar{s}$ of 0.025, only two new regions of instability were found. However, when finer divisions were used in $\bar{s}$, it was confirmed that modal coupling instability regions occur only when reflected branches intersect nonreflected branches. Those modal coupling instability regions which have width in $\bar{s}$ of less than 0.025 are indicated by small arrows on the $\bar{s}$ axis of the Re $\{\lambda\}$ plot. The stiffness instability regions which occur immediately above the critical speed of each mode narrows for higher modes. This is to be expected, since a one mode approximation using the mode with j nodal diameters and n nodal circles predicts a stiffness instability zone in the region:

$$\bar{p}_{jn}^2 < j^2 \bar{s}^2 < \bar{p}_{jn}^2 + \bar{a} G_{jnjn} \bar{k} \qquad (4.82)$$

Thus, as j increases, the width of the stiffness instability region is expected to decrease.

The points which are superposed on the $\mathrm{Im}\{\lambda\}$ plot at speeds $\bar{s}$=0.0, 0.5, 1.0, 2.0, 4.0, and 6.0 are the results of a twelve mode approximation

with $j_1=5$ and $n_1=1$. In this case, it is necessary to find the eigenvalues of a 44x44 matrix at each speed $\bar{s}$. As can be seen in Figure 33d, there are no significant differences between the six mode approximation curves and the points at which twelve modes were included.

The discussion above indicates a method for approximately determining the regions of instability of an undamped disk-spring-mass system without actually solving the eigenvalue problem. It is necessary to know only the Frequency-Speed diagram for the disk alone (Figure 31), and to make use of the one-mode approximation technique. To illustrate, suppose that the load parameters are $\bar{m}=0.5$, $\bar{k}=1.0$, and $\bar{r}_L=0.5$. It is first necessary to calculate $\bar{a}G_{1010}$, which in this case is equal to 0.967. The width of the stiffness instability region above the first critical speed may be calculated from (4.82) as $1<\bar{s}<1.40$. (The same as in Figure 33 since $\bar{k}$ has not been changed). From Figure 8 of Chapter 2, replacing $\Delta\bar{m}$ by $\bar{a}G_{1010}\bar{m}$ as indicated in (4.63), the terminal velocity of the mode j=1, n=0 is approximately $\bar{s}^*\cong 2.75$. From the Frequency-Speed plot of the disk alone, it can be seen that the only modal coupling instability region at speeds less than 2.75 is expected at the intersection of a reflected mode branch with a nonreflected branch at $\bar{s}\cong 2.1$. The width of this region cannot be easily estimated, however.

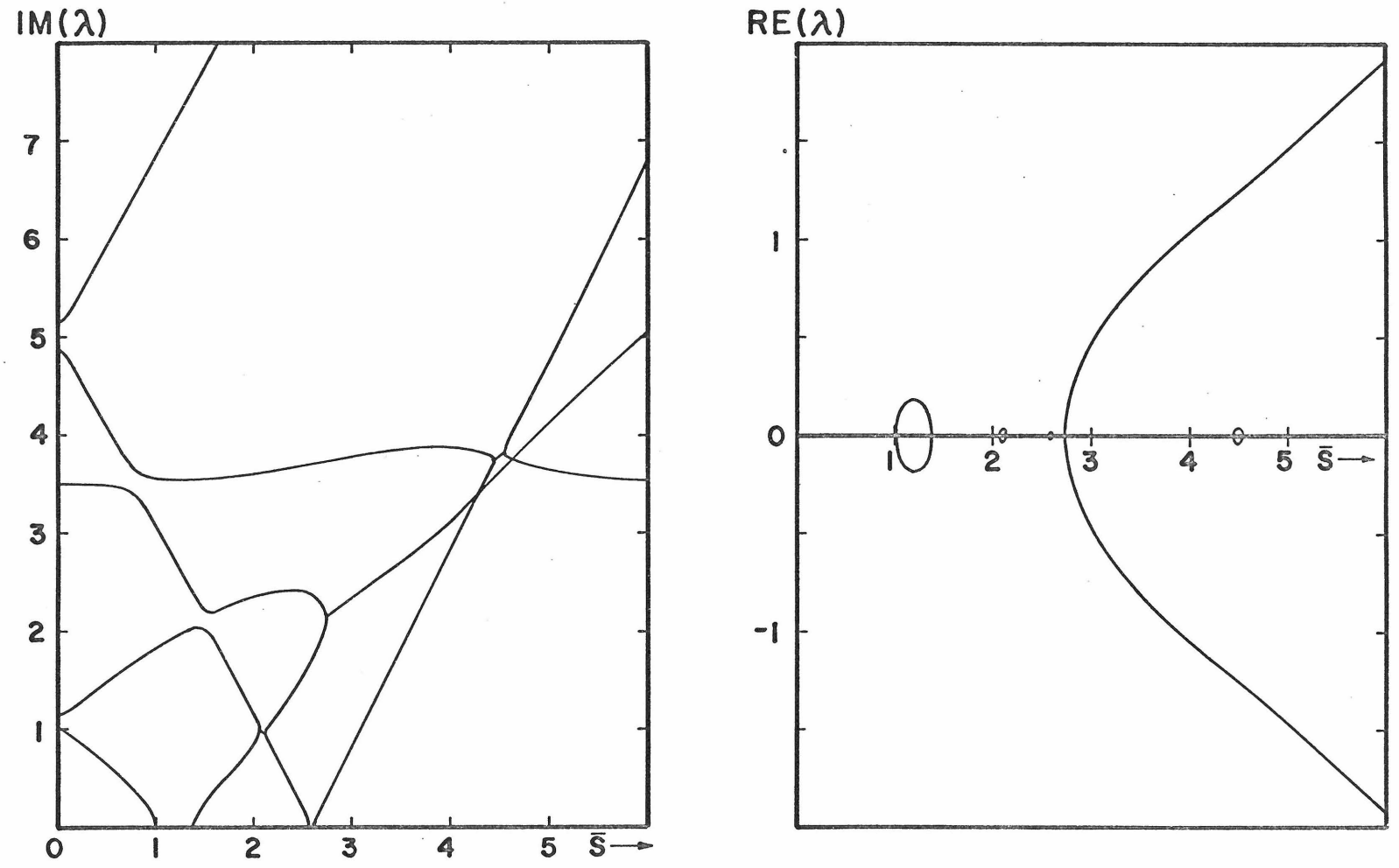

Fig. 34: Three mode approximation ($\bar{m}$=0.5, $\bar{k}$=1.0, $\bar{r}_L$=0.5, $\bar{c}_L$=0.0)

There is another stiffness instability region lying below $\bar{s} = 2.75$, immediately above the second critical speed. The width of this region can be calculated from (4.81) if the constant G_{2020} is known. Since $\bar{r}_L$ and $\bar{k}$ are the same as in Figure 33, the width of this region is the same as in that case, $2.55 < \bar{s} < 2.58$. The results of a three mode approximation for this set of parameters is shown in Figure 34. The instability regions appear as expected from the discussion above. Including more modes in the approximation will not yield any significant new instability zones, since all such zones will lie at speeds greater than the terminal velocity $\bar{s}^* \cong 2.75$.

4.6 Influence of Load Damping

The addition of load damping has the same effect in elastic disk problems as it had in the rigid disk problems of the previous chapters as shown in Figure 35. Below the first critical speed the amplitude of the motion will decay due to the negative $\mathrm{Re}\{\lambda\}$ contribution. However, above the first critical speed, $\bar{s} = 1$, a positive branch of $\mathrm{Re}\{\lambda\}$ appears, indicating unstable behavior beyond that point. When a viscous type dissipation is included in the partial differential equation for the disk, the tendency is to stabilize the system in a fashion analogous to that of the foundation damping in Chapter 2. Including this type of disk dissipation, or some other form of dissipation within the disk, along with load damping, appears to merit further study.

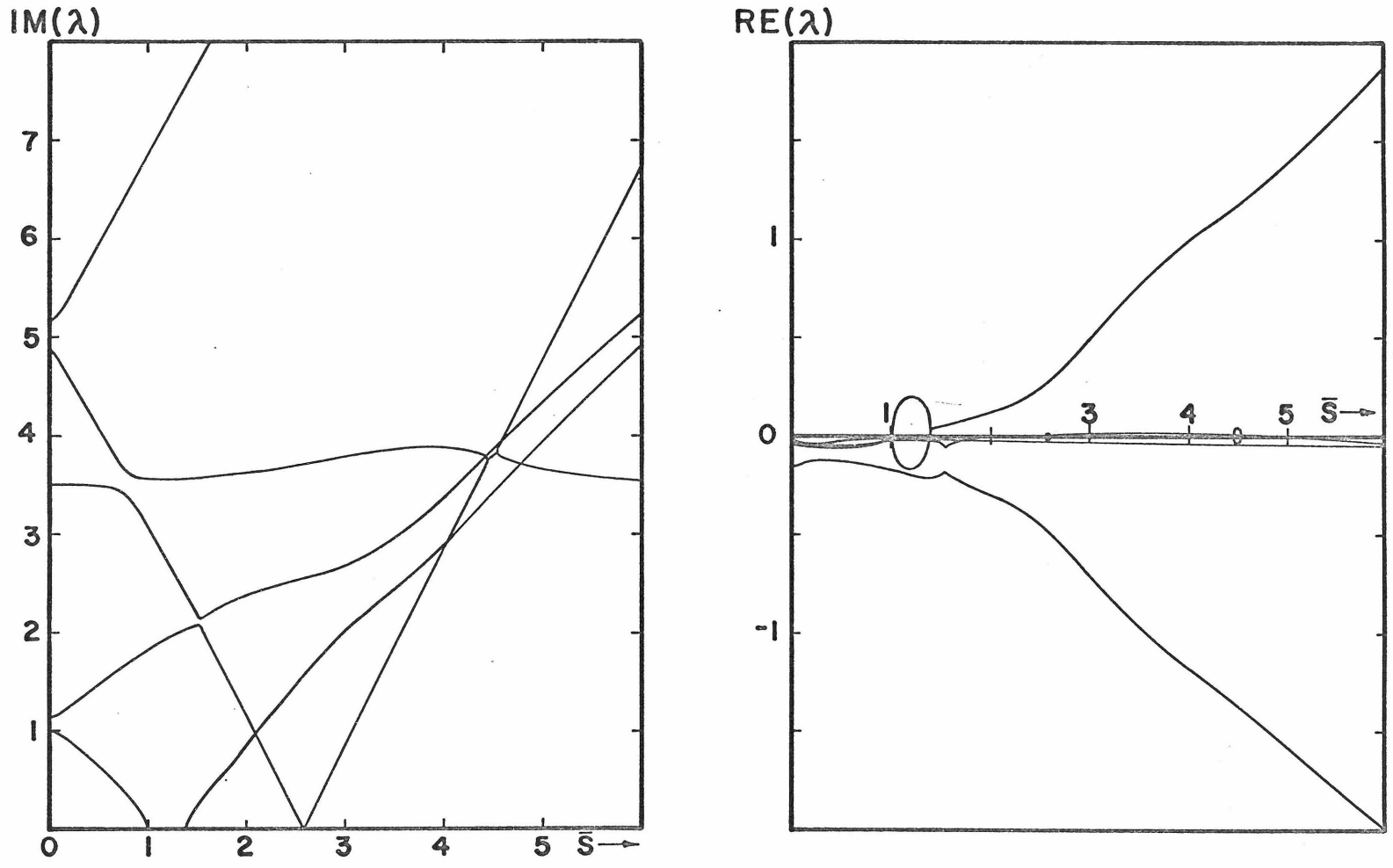

Fig. 35: Three mode approximation, damped ($\bar{m}$=0.5, $\bar{k}$=1.0, $\bar{r}_L$=0.5, $\bar{c}_L$=0.5)

4.7 Modal Participation

The nature of the motion of the disk-spring-mass system on any of the branches of the Frequency-Speed figures may be analyzed by the modal participation technique, directly analogous to the discussion in section 3.5 of Chapter 3. Any eigenvector $\underline{y}_i$ of the disk-spring-mass system may be written as a linear combination of the eigenvectors describing the motion of the disk alone, denoted by $\underline{x}_i$. The modes having zero nodal diameters correspond to the vertical motion v(t) of Chapter 3, and each such mode has two eigenvalues and eigenvectors associated with it. Modes having j nodal diameters ($j > 0$) can be decomposed into forward and backward waves, each of which has two associated eigenvectors. Thus, in the six mode approximation of Figure 33d, for example, there would be two eigenvectors corresponding to the mode with $j=0$, $n=0$, and four eigenvectors for each mode with j nodal diameters ($1 \leq j \leq 5$). These 22 vectors, describing the motion of the disk alone, form an orthonormal basis in which an eigenvector $\underline{y}_i$ of the disk-spring-mass system may be decomposed. Modal participation factors may then be defined as in Chapter 3. For the six mode case of Figure 33d, there are 11 modal participation factors. These measure the participation of the mode with zero nodal diameters and zero nodal circles, denoted by $\delta_v(0, 0)$, the participation of the backward waves of each mode with j nodal diameters ($1 \leq j \leq 5$),

$\bar{s}$	0.00	0.25	0.50	0.75	1.00	2.00	3.00	4.00	5.00	6.00
δ_v (0, 0)	0.046	0.040	0.059	0.167	0.001	0.015	0.050	0.015	0.077	0.004
δ_b (1, 0)	0.027	0.020	0.019	0.019	0.001	0.067	0.201	0.034	0.572	0.618
δ_b (2, 0)	0.706	0.028	0.011	0.005	0.000	0.007	0.025	0.003	0.022	0.003
δ_b (3, 0)	0.005	0.003	0.002	0.001	0.000	0.002	0.007	0.001	0.006	0.001
δ_b (4, 0)	0.002	0.001	0.000	0.000	0.000	0.001	0.003	0.000	0.002	0.000
δ_b (5, 0)	0.000	0.000	0.000	0.000	0.000	0.000	0.001	0.000	0.001	0.000
δ_f (1, 0)	0.027	0.015	0.010	0.007	0.000	0.342	0.268	0.295	0.426	0.039
δ_f (2, 0)	0.706	0.998	0.998	0.986	1.000	0.937	0.941	0.955	0.696	0.785
δ_f (3, 0)	0.005	0.003	0.002	0.001	0.000	0.002	0.009	0.000	0.007	0.004
δ_f (4, 0)	0.002	0.001	0.000	0.000	0.000	0.001	0.003	0.000	0.001	0.000
δ_f (5, 0)	0.000	0.000	0.000	0.000	0.000	0.000	0.001	0.000	0.002	0.000

Table 4.4 - Typical Modal Participation Factors for Six Mode Approximation

denoted by $\delta_b(j, 0)$, and the participation of the forward waves of each mode with j nodal diameters ($1 \leq j \leq 5$), denoted by $\delta_f(j, 0)$.

Table 4.4 lists the 11 modal participation factors at certain discrete speeds $\bar{s}$ along a particular branch of Figure 33d. The branch chosen is the one which most nearly follows the forward branch of the mode with 2 nodal diameters and 0 nodal circles in the case of the disk alone. This is not a continuous branch in Figure 33d, but the one on which $\delta_f(2, 0)$ is expected to predominate (the branch begins at $\mathrm{Im}\{\lambda\} \cong 5.07$, reaches a critical speed at $\bar{s} \cong 2.55$, and has the value $\mathrm{Im}\{\lambda\} \cong 6.85$ when $\bar{s} = 6.0$).

Table 4.4 indicates that $\delta_f(2, 0)$ does generally predominate along this branch, but also shows the presence of other modes at various speeds on the branch. When $\bar{s} = 0$, the modal participation factors $\delta_b(j, 0)$ and $\delta_f(j, 0)$ are equal for each j, indicating that the forward and backward waves superpose equally for each mode. This does not mean that there is a nodal diameter, however, since there is more than one mode present. The frequency of 5.07 on this branch at $\bar{s} = 0$ is lower than that of the j=2, n=0 mode natural frequency of 5.10 because the natural frequency of the attached spring and mass alone is equal to $\sqrt{10} \cong 3.16$.

As the load speed $\bar{s}$ increases, $\delta_f(2, 0)$ begins to predominate, until at $\bar{s} = 0.75$ a significant contribution from $\delta_v(0, 0)$ appears. Referring

to Figure 33d, it can be seen that this is to be expected, since this point is in close proximity to the branch for j=0, n=0. At $\bar{s}$=1.0, the mode shape is nearly the same as for the undisturbed disk. The frequency of the j=2, n=0 mode of the disk alone is very close to $\sqrt{10}$ at this point, and therefore the attached mass and spring, which have nearly the same frequency, do not affect this mode of the disk at this particular speed. As the speed continues to increase, significant contributions are noted from the wave components with j=1 and n=0. These contributions are especially noticable at $\bar{s}$=5.0, which is nearly within the modal coupling instability region which occurs for $5.10 < \bar{s} < 5.65$. In this way, the modal participation factors indicate the amount of coupling which is taking place.

4.8 Discussion

The conventional eigenfunction expansion technique, when used with the transformations developed in the earlier chapters, results in an infinite system of differential equations with constant coefficients. Hence, if an approximate solution is sought by truncating the eigenfunction series, an ordinary eigenvalue problem is obtained. The solutions to the eigenvalue problem indicate that the dynamic behavior of the elastic disk is much the same as the rigid disk behavior, for which exact solutions have been obtained.

V. ELASTIC DISK ON AN ELASTIC FOUNDATION

5.1 Introduction

In the previous chapters, the dynamic behavior of rigid and elastic disks with moving massive loads was studied. In this chapter, an interesting special case of an elastic disk on an elastic (Winkler) foundation is investigated which exhibits rigid body motions as the lower normal modes, and elastic deformations as the higher normal modes. When the elastic foundation modulus k is small (i. e., a soft foundation), the rigid body modes have a much lower natural frequency than the modes of elastic deformation, and the disk behaves like the rigid disk of Chapter 3. For larger values of k (i. e., firm foundations), modal interaction becomes more important, and the Frequency-Speed plots resemble those of Chapter 4.

5.2 Free Vibration of an Elastic Disk on an Elastic (Winkler) Foundation

If an elastic foundation is used to support a circular elastic disk, the partial differential Equation (4. 2) becomes:

$$\rho \frac{\partial^2 u}{\partial t^2} + \frac{Eh^2}{3(1-\sigma^2)}\left[\frac{\partial^2}{\partial r^2} + \frac{1}{r}\frac{\partial}{\partial r} + \frac{1}{r^2}\frac{\partial^2}{\partial \theta^2}\right]^2 u + \frac{k}{2h}u = 0 \qquad (5.1)$$

where k is the foundation modulus. Using the separation of variables technique as in Chapter 4, let:

$$u(r, \theta, t) = T(t)\Psi(r, \theta) \tag{5.2}$$

Substituting (5.2) into (5.1) gives:

$$\frac{d^2T}{dt^2} + p^2T = 0 \tag{5.3}$$

$$\left[\frac{\partial^2}{\partial r^2} + \frac{1}{r}\frac{\partial}{\partial r} + \frac{1}{r^2}\frac{\partial^2}{\partial \theta^2}\right]^2 \Psi - \kappa^4 \Psi = 0 \tag{5.4}$$

where

$$\kappa^4 = \frac{3\rho(1-\sigma^2)}{Eh^2}\left[p^2 - \frac{k}{2\rho h}\right] \tag{5.5}$$

Equations (5.3) and (5.4) are identical to those of Chapter 4, (4.4) and (4.5), except that the relation between κ and the frequency p is modified by the foundation modulus term. The solution procedure from this point on is identical to Chapter 4. If the separation of variables technique is applied to (5.4) by letting $\Psi(r, \theta) = W(r)\Theta(\theta)$, the result is:

$$\Theta(\theta) = \sin(j\theta - \epsilon)$$

$$W(r) = \alpha J_j(\kappa r) + \beta Y_j(\kappa r) + \gamma I_j(\kappa r) + \delta K_j(\kappa r) \tag{5.6}$$

The eigenvalues κ_{jn} are found by substituting the expression for $u(r, \theta, t)$ into the four boundary conditions of the problem, leading to a

homogeneous set of four linear algebraic equations for the constants $\alpha, \beta, \gamma,$ and δ. Since the presence of the elastic foundation does not affect the boundary conditions of the problem, this set of equations is identical to the set obtained when no foundation is present. Therefore, the eigenvalues κ_{jn} and the eigenfunctions $\Psi_{jn}(r, \theta)$ are precisely the same as those for the disk with no foundation and with the same boundary conditions. The frequencies of vibration p_{jn} are different, of course, from (5.5):

$$p_{jn}^2 = \frac{Eh^2\kappa_{jn}^4}{3\rho(1-\sigma^2)} + \frac{k}{2\rho h} = p'^2_{jn} + \frac{k}{2\rho h} \tag{5.8}$$

where p'_{jn} is the frequency of vibration of the corresponding mode for the disk with no elastic foundation. For fixed foundation modulus k, the greatest change in frequency occurs for the lowest modes (when p'_{jn} is smallest).

The wave speeds associated with modes having one or more nodal diameters are changed as well, and are given by

$$\frac{1}{j}p_{jn} = \frac{1}{j}\left[p'^2_{jn} + \frac{k}{2\rho h}\right]^{\frac{1}{2}} \tag{5.9}$$

The preceding results are of particular interest for the case of a disk with a free outer boundary as well as a free center. The boundary conditions in this case are given by the last two equations of (4.12), applied at r=0 as well as at r=a. The eigenvalues κ_{jn} and eigenfunctions $\Psi_{jn}(r,\theta)$ have been given by McLeod and Bishop [2] for the problem with no elastic foundation. The eigenvalues $\kappa_{jn}a$ are tabulated below:

j=Number of Nodal Diameters

n=Number of Nodal Circles	0	1	2	3	4	5
0	0	0	2.29	3.50	4.64	5.75
1	3.01	4.53	5.96	7.28	8.57	9.82
2	6.20	7.73	9.20	10.58	11.93	13.25

Table 5.1 Eigenvalues $\kappa_{jn}a$

For the disk with no foundation, the zero values of $\kappa_{00}a$ and $\kappa_{10}a$ signify respectively rigid body translational motion, and rigid body rotational motion about a nodal diameter. The frequencies of these motions, p_{00} and p_{10} given by (4.14), are zero because the disk is free to rotate and translate with the prescribed free boundary conditions.

When an elastic foundation is present, the frequencies p_{00} and p_{10} are not zero, but are given by (5.8) as:

$$p_{00}^2 = p_{10}^2 = \frac{k}{2\rho h} \tag{5.9}$$

Thus, the presence of the elastic foundation gives rise to oscillatory motions with frequency $\sqrt{\frac{k}{2\rho h}}$ as the lowest modes of the disk. Note from (5.8) that if k is small (i.e., a soft foundation) the frequencies of the lowest modes p_{00} and p_{10} will be much lower than the frequencies of the higher modes. Further, the critical speed of the mode j=1, n=0 is given by (5.9) as $\sqrt{\frac{k}{2\rho h}}$. Thus, the critical speed for this mode can be made much lower than the critical speeds of the higher modes if k is small.

The radical eigenfunctions $W_{00}(r)$ and $W_{10}(r)$ are not given by (5.6) since $\kappa_{00} = \kappa_{10} = 0$. Instead, for these modes the separation of variables technique leads to:

$$\frac{d^2 W_{j0}}{dr^2} + \frac{1}{r}\frac{dW_{j0}}{dr} - \frac{j^2}{r^2} W_{j0} = 0 \tag{5.10}$$

where j=0 or 1. The solutions to this equation which satisfy the particular boundary conditions, and the corresponding spatial eigenfunctions are:

$$\begin{aligned} W_{00}(r) &= 1 \Rightarrow \Psi_{00}(r,\theta) = 1 \\ W_{10}(r) &= r \Rightarrow \Psi_{10}(r,\theta) = r\sin(\theta - \varepsilon_{10}) \end{aligned} \tag{5.11}$$

Thus, the lowest two normal modes of the disk have the form:

$$u_{00}(r,\theta,t) = F_{00}\sin(p_{00}t - t_{00})$$
$$u_{10}(r,\theta,t) = F_{10}\sin(p_{10}t - t_{10})r\sin(\theta - \epsilon_{10}) \tag{5.12}$$

where $p_{00} = p_{10} = \left[\frac{k}{2\rho h}\right]^{\frac{1}{2}}$. These modes are clearly rigid body modes directly analogous to those of Chapter 3, and as such they involve no elastic distortion of the disk as do the higher modes.

The radial eigenfunctions $W_{jn}(r)$ for higher modes having one or more nodal diameters are given by McLeod and Bishop [2], and are the same as those in (4.68) of Chapter 4. The eigenfunctions for the symmetric modes, $W_{0n}(r)$, for $n \geq 1$, are:

$$W_{0n}(r) = J_1(\kappa_{0n}a)I_0(\kappa_{0n}r) - I_1(\kappa_{0n}a)J_0(\kappa_{0n}r) \tag{5.13}$$

Before these eigenfunctions are used in the analysis of the moving mass and spring, the functions $W_{jn}(r)$ $(j>0)$ must be normalized according to (4.70), and the functions $W_{0n}(r)$ must be normalized according to (4.74). The general solution to the free vibration problem for arbitrary initial conditions may then be written as a linear combination of all the normal modes:

$$u(r,\theta,t) = \sum_{j=0}^{\infty}\sum_{n=0}^{\infty} T_{jn}(t)\Psi_{jn}(r,\theta) \tag{5.14}$$

$$= \sum_{j=0}^{\infty}\sum_{n=0}^{\infty} T_{jn}(t)\sin(j\theta - \epsilon_{jn})\overline{W}_{jn}(r) \tag{5.15}$$

The time dependent terms $T_{jn}(t)$ may be written in either real or complex form as:

$$T_{jn}(t) = F_{jn}\sin(p_{jn}t - t_{jn}), \quad [F_{jn}, t_{jn} \text{ real}]$$
$$= E_{jn}e^{ip_{jn}t} + \tilde{E}_{jn}e^{-ip_{jn}t} \tag{5.16}$$

where $\tilde{E}_{jn}$ is the complex conjugate of E_{jn}.

It should be clear from the preceding discussion that it is not possible to make one Frequency-Speed diagram to cover all ranges of the foundation parameter k. For example, if k is chosen so that $k/2\rho h = \frac{1}{100}p_{20}^2$, then the frequencies p_{00} and p_{10} will be one-tenth of the frequency of the next highest mode, p_{20}. Thus, a Frequency-Speed diagram of the same scale as Figure 20 would indicate only the branches shown in that figure, with none of the higher modes appearing. On the other hand, if k is larger, then the branches of the higher modes will lie in much closer proximity to the rigid body mode branches, and branch intersections will occur at lower speeds.

5.3 Effects of a Moving Spring and Mass

If a moving spring and mass is included in the system in the same fashion as in previous chapters, the partial differential Equation (5.1) becomes:

$$\rho\frac{\partial^2 u}{\partial t^2}+\frac{Eh^2}{3(1-\sigma^2)}\left[\frac{\partial^2}{\partial r^2}+\frac{1}{r}\frac{\partial}{\partial r}+\frac{1}{r^2}\frac{\partial^2}{\partial\theta^2}\right]^2 u+\frac{k}{2h}u$$

$$=-\frac{1}{2h}\delta(\theta-\Omega t)\frac{\delta(r-r_L)}{r_L}\left\{m_L\left[\frac{\partial^2 u}{\partial t^2}+2\Omega\frac{\partial^2}{\partial t\partial\theta}+\Omega^2\frac{\partial^2 u}{\partial\theta^2}\right]\right.$$

$$\left.+c_L\left[\frac{\partial u}{\partial t}+\Omega\frac{\partial u}{\partial\theta}\right]+k_L u\right\} \qquad (5.16)$$

The solution procedure follows the same pattern in this case as in Chapter 4. The displacement $u(r, \theta, t)$ is expanded in an infinite series of the eigenfunctions of the homogeneous problem, in the form:

$$u(r,\theta,t)=\sum_{j=0}^{\infty}\sum_{n=0}^{\infty}T_{jn}(t)\sin\left[j\theta-\varepsilon_{jn}(t)\right]W_{jn}(r) \qquad (5.17)$$

The transformations (4.28) and (4.30) are utilized so that the series (5.17) becomes:

$$u'(r,\Phi,t)=\sum_{j=0}^{\infty}\sum_{n=0}^{\infty}\left[A_{jn}(t)\cos j\Phi+B_{jn}(t)\sin j\Phi\right]W_{jn}(r) \qquad (5.18)$$

where $\Phi=\theta-\Omega t$. The partial differential Equation (5.16) is written in terms of r, Φ, and t, so the equation for u' has the form:

$$\left.\rho\left[\frac{\partial^2 u'}{\partial t^2}-2\Omega\frac{\partial^2 u'}{\partial t\partial\Phi}+\Omega^2\frac{\partial^2 u'}{\partial\Phi^2}\right]+\frac{Eh^2}{3(1-\sigma^2)}\left[\frac{\partial^2}{\partial r^2}+\frac{1}{r}\frac{\partial}{\partial r}+\frac{1}{r^2}\frac{\partial^2}{\partial\Phi^2}\right]^2 u'+\frac{k}{2h}u'\right\} \qquad (5.19)$$

$$= -\frac{1}{2h}\,\delta(\Phi)\,\frac{\delta(r-r_L)}{r_L}\left\{m_L\frac{\partial^2 u'}{\partial t^2}+c_L\frac{\partial u'}{\partial t}+k_L u'\right\} \qquad (5.19)\ \text{cont.}$$

The series (5.18) is substituted into (5.19), and the orthogonality relations for the trigonometric functions and for the $\overline{W}_{jn}(r)$ functions are used to arrive at the set of Equations (4.38) and (4.39). If the eigenfunction expansion (5.18) is truncated at $j=j_1$ and $n=n_1$, the number of equations in the set is equal to the number of unknown functions. Since the equation set is linear and homogeneous, and has constant coefficients, the set may be expressed as a matrix differential equation of the type:

$$P\frac{d\underline{x}}{dt} = Q\underline{x}\,, \quad \underline{x}(0)=\underline{f} \qquad (5.20)$$

The vector $\underline{x}$ appearing above has the same definition as in Chapter 4, as do the matrices P and Q. These quantities are all defined following Equation (4.44). Premultiplying (5.20) by P^{-1}, and assuming a solution of the form $\underline{x}=e^{\lambda t}\underline{\Phi}$, where $\underline{\Phi}$ is a time independent vector, results in:

$$(P^{-1}Q-\lambda I)\underline{\Phi}=0 \qquad (5.21)$$

For a nontrivial solution, the determinant of $(P^{-1}Q-\lambda I)$ must vanish:

$$|P^{-1}Q-\lambda I|=0 \qquad (5.22)$$

5.4 Two Mode Approximation

If the series expansion (5.18) is truncated at j=1 and n=0, the disk motion will be approximated by the rigid body modes (5.11) alone. The equations resulting from this two mode approximation were given explicitly in Chapter 4 by Equations (4.65), (4.66), and (4.67). The constants $\bar{a}G_{\alpha\beta\gamma\delta}$ appearing in those equations may be easily shown to be:

$$\bar{a}G_{0000}=1, \quad \bar{a}G_{1010}=\left(\frac{2r_L}{a}\right)^2$$
$$\bar{a}G_{1000}=\bar{a}G_{0010}=\frac{2r_L}{a} \tag{5.23}$$

If the second derivative terms appearing in (4.65) and (4.67) are uncoupled, the equations are identical to (3.19), (3.20), and (3.21) of Chapter 3, providing that following identifications are made:

$$A_{00}(\tau)=ar_L\sqrt{\pi}\,\bar{v}(\tau)$$
$$A_{10}(\tau)=\frac{a^2\sqrt{\pi}}{2}\,A(\tau) \tag{5.23}$$
$$B_{10}(\tau)=\frac{a^2\sqrt{\pi}}{2}\,B(\tau)$$

The equations in Chapter 3 were investigated quite fully, and thus the two mode approximation here may be understood simply by applying the results of Chapter 3.

A two mode approximation such as this will provide a good estimate of the low frequency and low speed portion of the Frequency-Speed

diagram only if the foundation modulus is small. In that case the frequencies and critical velocity of the rigid body modes will be substantially less than those of the modes with elastic deformation, and therefore the lower regions of instability discussed in Chapter 3 will occur before appreciable coupling with elastic modes takes place. Since the behavior of the rigid body modes alone is well understood from Chapter 3, it is of somewhat greater interest to examine a particular case in which the elastic modes are more significant.

5.5 Firm Elastic Foundation

As the foundation modulus k becomes larger, the frequency and critical speed of the rigid body modes increase and lie in closer proximity to the modes of elastic deformation. The Frequency-Speed diagram for such a case is shown in Figure 36. Clearly, the forward traveling branches of the modes of elastic deformation will have some influence on the Frequency-Speed diagram for the disk-spring-mass system.

As an example, consider the case with load parameters $\bar{r}_L = 0.5$, $\bar{m} = 1.0$, and $\bar{k} = 2.0$. The two mode approximation is shown as the undamped branch in Figure 23. A five mode approximation, formed with $j_1 = 4$ and $n_1 = 0$, gives the Frequency-Speed diagram shown in Figure 37. The expected modal coupling is evident in this figure, although the particular choice of parameters is such that all new areas

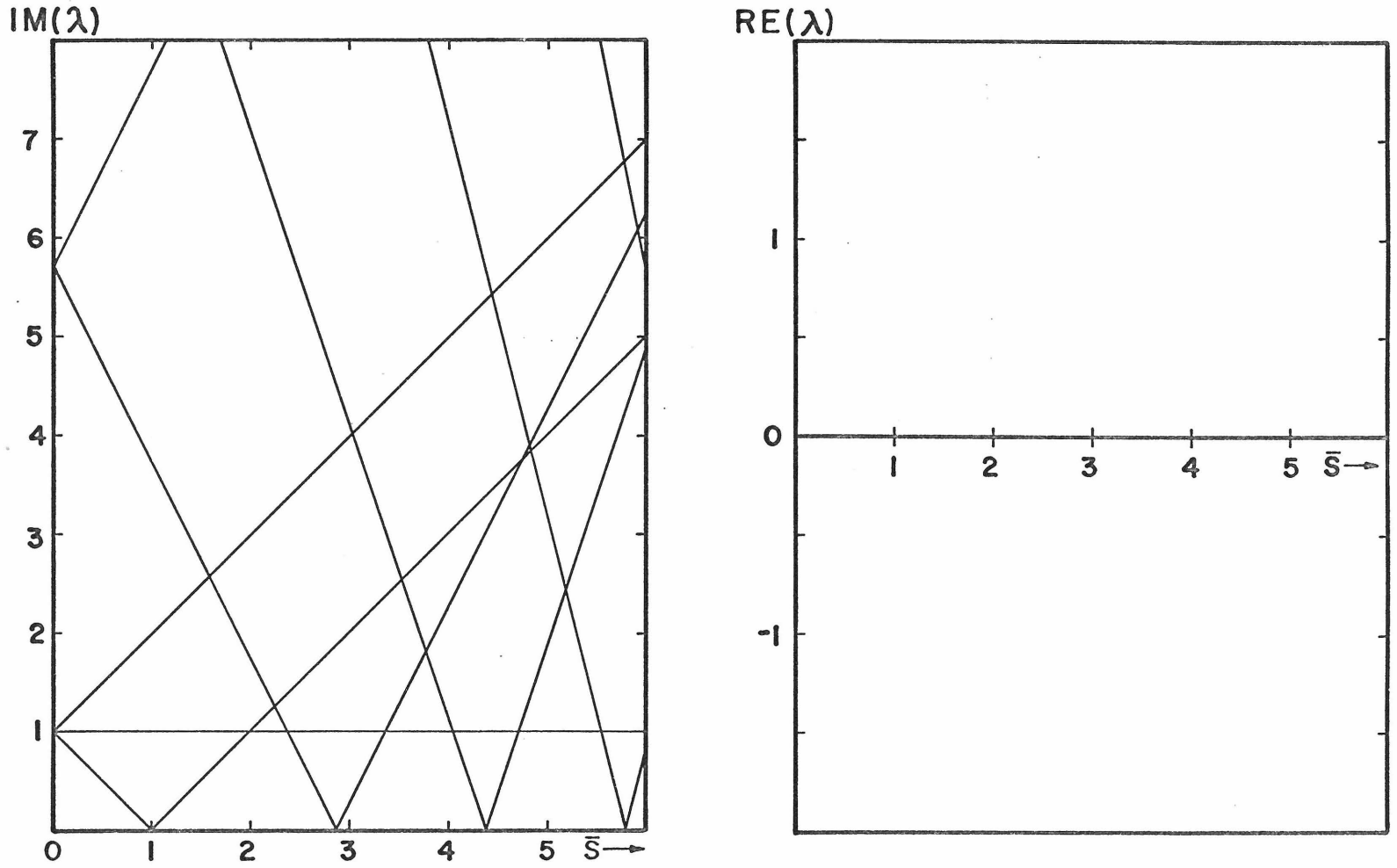

Fig. 36: Frequency-speed diagram for elastic disk on elastic foundation.

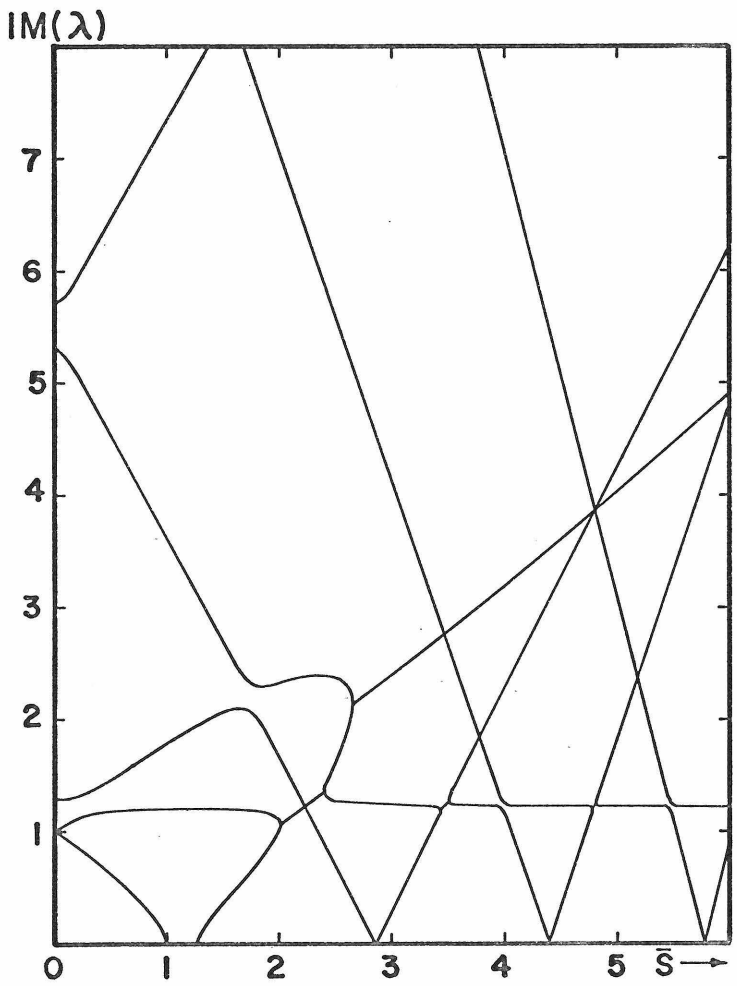

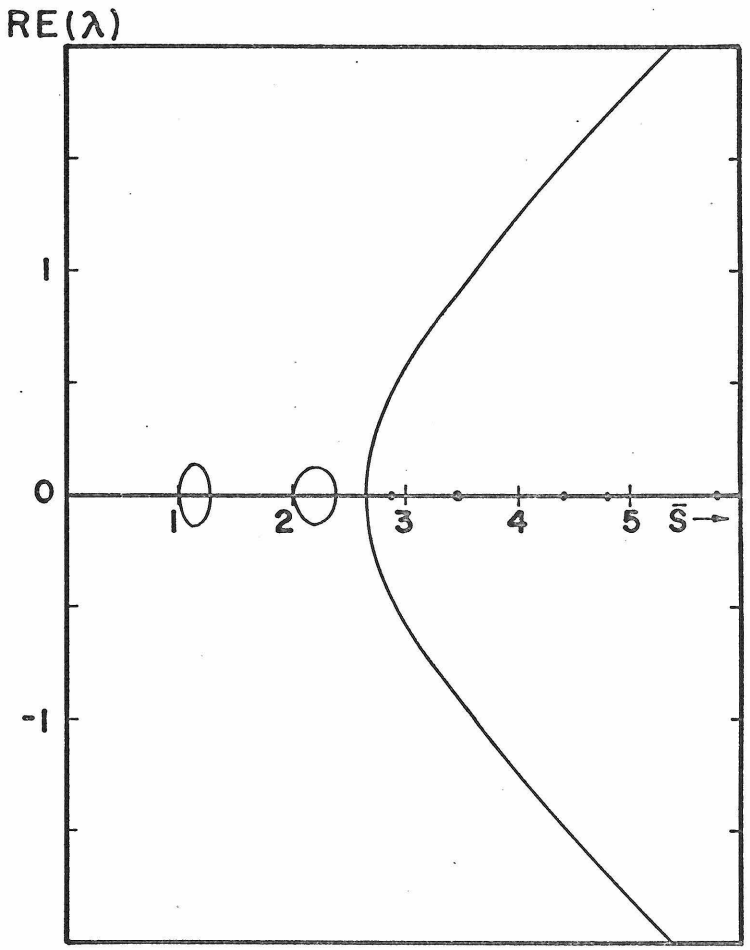

Fig. 37: Five mode approximation ($\bar{m}$=1.0, $\bar{k}$=2.0, $\bar{r}_L$=0.5, $\bar{c}_L$=0.0).

of instability lie above the terminal velocity of the rigid body modes. The most interesting feature of Figure 37 is that it incorporates the basic features of the three degree of freedom rigid disk problem along with the complicated modal interactions found in elastic disk problems. Specifically, there is no apparent change in the boundaries of the instability regions predicted by the rigid disk theory, although new areas of instability occur because of the presence of higher modes. The shape of the disk along any of the branches will include some elastic deformation, as a modal participation analysis will show, because of the effects of modal coupling.

5.6 Discussion

The case of a free elastic disk, supported by an elastic foundation, provides an interesting example by which the results of the previous chapters may be combined. The techniques developed in the previous chapters apply here as well, and indicate that the elastic disk behaves in much the same way as the rigid disk, and that modal coupling occurs between rigid and elastic modes as well.

VI. SUMMARY AND CONCLUSIONS

An analytical technique is developed to investigate the dynamic response of circular disks subjected to moving loads with inertia and stiffness. In Chapters 2 and 3, nonlinear equations of motion are derived for cases of elastically supported rigid disks with moving mass-spring loads. Although the equations are nonlinear and have time-dependent coefficients as well, exact solutions are obtained by applying two relatively simple transformations. These transformations allow the nonlinear equations to be written as a set of coupled linear differential equations with constant coefficients. By this method, the problem is reduced to solving an ordinary eigenvalue problem.

When the load position, mass, and stiffness are specified, the eigenvalues are plotted as a function of load speed, called a "frequency-speed" diagram. The frequency-speed diagrams provide information on stability and transient response as well as the frequencies of steady-state oscillations. In regions where all the eigenvalues are pure imaginary, the imaginary parts correspond to the frequency components in the motion of the moving mass. The motion of the disk may be found by inverting the transformations used to obtain the eigenvalue problem. This in general results in motions which may be very

complicated. In other regions, one or more eigenvalues have positive real parts, corresponding to motions of both the disk and moving mass which are unbounded in time. Such regions are denoted as unstable, although the stability will in fact be dependent on initial conditions.

Three distinct areas of instability appear in the rigid disk problems. A stiffness instability region occurs immediately above the critical speed of the disk, and is caused by the load stiffness. At higher speeds, in the three degree of freedom disk of Chapter 3, a region of instability due to modal coupling appears. Finally, beyond a certain terminal velocity, there will always be an eigenvalue with a positive real part. This causes unstable behavior beyond this limiting speed.

In Chapters 4 and 5, the dynamic response of circular elastic disks subjected to moving mass-spring loads is investigated. The conventional eigenfunction expansion technique is utilized, reducing the partial differential equation to a system of coupled ordinary differential equations. As is generally the case when this technique is applied to moving mass problems, the system of coupled equations involves the complication of time-dependent periodic coefficients. It is shown, however, that when the transformations developed in Chapters 2 and 3 are employed, the resulting system of coupled differential equations

reduce to a set with constant coefficients. Thus, if the eigenfunction series is truncated, the system of equations may be rewritten as an eigenvalue problem.

If a one mode approximation is made, the resulting set of equations is identical to the set describing the behavior of the two degree of freedom rigid disk of Chapter 2. Similarly, if a two mode approximation is made, the equations have the same form as for the three degree of freedom rigid disk of Chapter 3. In particular, the stiffness instability region, modal coupling instability region, and terminal instability zone appear for elastic disks as well. As more modes are considered in the approximation, the regions of instability predicted by the one and two mode approximations do not appear to change significantly. However, new regions of instability appear. The number of modes necessary to adequately represent the frequency-speed diagram depends on the particular load parameters involved.

Areas for Further Investigation

The results of this analysis indicate several major areas for possible future investigations. These are:

1. Dynamic response of rigid disks with foundation damping and load damping simultaneously applied. Above critical speed, these appear to have opposing effects in influencing the terminal instability zone.

2. Investigation of more complicated loading systems. For example, inclusion of another spring between the mass and disk may cause new areas of dynamic instability.

3. Investigation of multiple loading systems. The presence of more than one mass-spring system may also influence stability boundaries.

4. Investigation of the response of other structures subjected to similar loading systems. The methods developed here are quite likely applicable to other structures with circular symmetry, such as circular rings or cylinders. Similar methods may prove helpful in the analysis of beams and plates subjected to moving massive loads, although the boundary conditions in such problems generally do not allow the direct application of the transformations presented here.

REFERENCES

1. Southwell, R. V., "On the Free Transverse Vibrations of a Uniform Circular Disk Clamped at its Centre; and on the Effects of Rotation", Proceedings of the Royal Society (London), Vol. 101, 1921, pp. 133-153.

2. McLeod, A. J., and Bishop, R. E. D., "The Forced Vibration of Circular Flat Plates", Mechanical Engineering Science Monograph, No. 1, March, 1965.

3. Weiner, R. S., "Transient Motion of Circular Elastic Plates Subjected to Impulsive and Moving Loads", Bell Systems Technical Journal, December, 1965, pp. 2405-2431.

4. Tobias, S. A., and Arnold, R. N., "The Influence of Dynamical Imperfection on the Vibration of Rotating Disks", Proceedings of the Institution of Mechanical Engineers, Vol. 171, 1957, pp. 669-690.

5. Tobias, S. A., "Free Undamped Non-Linear Vibrations of Imperfect Circular Disks", Proceedings of the Institution of Mechanical Engineers, Vol. 171, 1957, pp. 691-701.

6. Williams, C. J. H., and Tobias, S. A., "Forced Undamped Non-Linear Vibrations of Imperfect Circular Disks", Journal of Mechanical Engineering Science, Vol. 5, No. 4, 1963, pp325-335.

7. Todhunter, I. and Pearson, K., A History of the Theory of Elasticity and of the Strength of Materials, Cambridge University Press, London, Vol. I, 1886, Vol. II, 1893.

8. Reference 7, Vol. I, pp. 762-770.

9. Reference 7, Vol. I, pp. 690-698.

10. Reference 7, Vol. II, Part I, pp. 254-263.

11. Inglis, C. E., A Mathematical Treatise on Vibrations in Railway Bridges, Cambridge University Press, London, 1934.

12. Piszczek, K., "Possibility of Dynamic Stability Loss under Moving Concentrated Loads", Archiwum Mechaniki Stosowanej, Warsaw, Vol. 10, 1959, pp. 195-210.

13. Bolotin, V. V., Dynamic Stability of Elastic Systems, Holden-Day, San Francisco, 1964, pp. 139-141.

14. Raske, T. F., and Joung, K. S., "Dynamic Response of Elastic Bodies to an Oscillating Point Mass", Journal of the Acoustical Society of America, Vol. 47, No. 5 (Part 2), 1970, pp. 1375-1380.

15. McLachlan, N. W., Ordinary Non-Linear Differential Equations in Engineering and Physical Sciences, Oxford University Press, London, 1958, Chapter VII.

16. Stanisic, M. M., Hardin, J. C., and Lou, Y. C., "On the Response of the Plate to a Multi-masses Moving System", Acta Mechanica, Vol. 5, 1968, pp. 37-53.

17. Singhvi, G. M., and Feeser, L. J., "Response of Stiffened Plates to Moving Sprung Mass Loads", Shock and Vibration Bulletin, No. 39, 1968.

18. Veletsos, A. S., and Huang, T., "Analysis of Dynamic Response of Highway Bridges", Journal of the Engineering Mechanics Division, Proceedings of the American Society of Civil Engineers, October, 1970, pp. 593-620.

19. Timoshenko, S. P., and Woinowsky-Krieger, S., Theory of Plates and Shells, McGraw-Hill, 1959.